Chromatographic purification of biological macromolecules by their capture on hydrophilic surfaces with the aid of non-ionic polymers

Dissertation

zur Erlangung des akademischen Grades

Doktoringenieur
(Dr.-Ing.)

von

Pável Alejandro Marichal-Gallardo, M.Sc.

geboren am

05. Mai 1987 in Coatzacoalcos, México

genehmigt durch die Fakultät für Verfahrens- und Systemtechnik
der Otto-von-Guericke-Universität Magdeburg

Promotionskommission:

Prof. Dr.-Ing. Andreas Seidel-Morgenstern   (Vorsitz)

Dr. rer. nat. Egbert Müller   (Gutachter)

Prof. Dr. Michael W. Wolff   (Gutachter)

Prof. Dr.-Ing. Udo Reichl   (Gutachter)

Repetitio est mater studiorum

This page intentionally left blank

Declaration

I hereby declare that I prepared the work submitted without inadmissible assistance and without the use of any aids other than those indicated. Facts or ideas taken from other sources, either directly or indirectly have been marked as such.

In particular, I did not use the services of a commercial graduation consultation. Further I have not made payments to third parties either directly or indirectly for any work connected with the contents of the submitted dissertation.

The work has not been submitted as a dissertation either in Germany or abroad in the same or similar form and has also not been published as a whole.

Ich erkläre hiermit, dass ich die vorliegende Arbeit ohne unzulässige Hilfe Dritter und ohne Benutzung anderer als der angegebenen Hilfsmittel angefertigt habe. Die aus fremden Quellen direkt oder indirekt übernommenen Gedanken sind als solche kenntlich gemacht.

Insbesondere habe ich nicht die Hilfe einer kommerziellen Promotionsberatung in Anspruch genommen. Dritte haben von mir weder unmittelbar noch mittelbar geldwerte Leistungen für Arbeiten erhalten, die im Zusammenhang mit dem Inhalt der vorgelegten Dissertation stehen.

Die Arbeit wurde bisher weder im Inland noch im Ausland in gleicher oder ähnlicher Form als Dissertation eingereicht und ist als Ganzes auch noch nicht veröffentlicht.

(Place, Date/*Ort, Datum*) _____

(Signature/*Unterschrift*) _____

Abstract

Chromatographic purification of biological macromolecules by their capture on hydrophilic surfaces with the aid of non-ionic polymers

Viral vaccines are considered to be amongst the most successful achievements in health science. Also, the use of viral vectors for gene therapies has shown the promise to become the next medical revolution for combating a wide variety of currently untreatable diseases. The wide range of viruses and their production methods make it extremely difficult to standardize viral vaccine manufacturing. Purification processes require several steps and are typically tailored to each particular virus species and how it is produced, making process development time-consuming and potentially delaying time to market. Even for the same product, purification processes might differ almost in their totality between a small laboratory and a commercial manufacturing facility. Due to scalability, costs, efficiency, and capacity constraints, industrial purification methods are mostly limited to chromatography and filtration operations.

This work presents the development of steric exclusion chromatography (SXC) as a new platform purification method for large biomolecules such as virus particles. In SXC, an unpurified sample is mixed with a non-ionic polymer — in this case polyethylene glycol (PEG) — and fed onto a device made of a porous hydrophilic stationary phase. The target product is captured without a direct chemical interaction by a thermodynamic effect caused by the presence of the PEG. Smaller impurities such as media components and proteins are unaffected by the PEG and washed away. The bigger the target product, the lesser size and/or concentration of PEG is needed for its capture. Finally, the purified product is recovered by flushing the device with a solution not containing PEG.

SXC was used for the purification of 14 different cell-based virus strains and serotypes — influenza virus, yellow fever virus, adeno-associated virus (AAV), and Modified Vaccinia Ankara (MVA) — with a wide variety of sizes (20–250 nm) and from several production processes. Likewise, extracellular vesicles (EVs) of 160–230 nm from Madin-Darby canine kidney (MDCK), baby hamster kidney (BHK), and human embryonic kidney (HEK) cells were purified.

A number of stationary phases were tested, including hydroxylated monoliths (1–2 µm pore size), cellulose membranes (1–1.2 µm pore size), and 3D-printed cellulose monoliths (400–500 µm pore size). Devices packed with regenerated cellulose membranes of 1.0 µm pore size were the most efficient in terms of product yield as were concentrations of 8–10% PEG-6000 for sample loading.

Four different strains of influenza virus produced in suspension MDCK cells in batch systems showed product recoveries >98%. The highest measured productivity for influenza virus A/Puerto Rico/8/34 H1N1 in terms of the hemagglutinin protein antigen was around 69 000 µg per square meter per hour (4600 monovalent doses per square meter per hour).

In the case of yellow fever virus, two strains used for commercial vaccine manufacture were produced separately in adherent Vero cells. Virtually full yield of infectious titer was observed and residual DNA and protein levels were below regulatory requirements. As many as 6×10^9 plaque forming units (equivalent to more than 100 000 vaccine doses) were purified from around one liter of cell culture with a productivity of more than 5 million doses per square meter per hour.

For adeno-associated virus (AAV), several wild-type and recombinant variants were produced in adherent HEK cells by triple transfection and purified from both cell lysates and cell supernatants; no product losses were detected during SXC and the purified AAV (up to 2×10^{14} viral genomes per liter) successfully induced either gene expression or gene knockdown in transduced cells both *in vitro* and *ex vivo*.

Exploratory results with Modified Vaccinia Ankara (MVA) virus produced in avian cells showed virtually full yield with a $TCID_{50}$ titer of 3.7×10^9 virions. The virus, however, seemed susceptible to aggregation upon addition of PEG as evidenced by particle size distribution analysis. Adding sucrose or sorbitol (8% of either) to the PEG-conditioned virus seemed to lower the amount of aggregates observed compared to the PEG-conditioned sample without stabilizers. Regardless, the SXC-purified MVA virus showed a distinct monomer peak of around 220 nm without visible aggregation.

It was observed that EVs from the host cells were often co-purified with the target virus particles. This was attributed to the very similar characteristics between both. Preliminary results for the capture of EVs present in cell supernatants showed particle recoveries of around 40% and concentrations close to 8×10^{10} particles per mL. Further studies should continue to evaluate SXC for the preparative purification of EVs.

Clearance of protein and DNA with SXC were typically >85% and >75%, respectively, depending on the virus and the experimental setup (e.g., placing a DNA digestion step before SXC). In all cases, it was advantageous to have a nuclease treatment before SXC to achieve lower amounts of residual DNA.

SXC with 3D-printed cellulose monoliths with channel diameters of 400 µm and 500 µm was inefficient in terms of product yield (around 40% for influenza A virus) compared to the 1.0 µm regenerated cellulose membranes, however, their use is interesting for future work, e.g., as an alternative to expanded-bed chromatography.

The ability to load and recover the product at physiological pH and conductivity as well as the conformation stabilizing properties of PEG are relevant advantages during the purification of labile biopharmaceuticals. The high product recoveries achieved so far with SXC make it possible to allow for subsequent polishing operations for improving

purity without risking unacceptably low process yields. The narrow operational range of SXC permits the purification of viruses with a high probability of success (e.g., testing 8% PEG-6000 as a starting point) and the low cost of the membranes allows single-use operation (which avoids expensive and time-consuming cleaning and sanitization steps). Scale-up of SXC is simple, as it requires only a linear increase in membrane surface, and the use of devices of up to 20 square meters would enable industrial-scale virus purification.

As a capture step, SXC seems to be comparable or better than most chromatography methods available in terms of product yield, ease of use, and scalability. However, estimating capacities is challenging since there is no direct chemical bond involved. Recovery was highly dependent on certain quality attributes of the starting material, such as residual cell debris and/or aggregated product.

The results shown here are the basis for further optimization and application of this technology and they indicate that membrane-based SXC has the potential for becoming a platform technology for both viral vaccine and gene therapy applications.

Zusammenfassung

Chromatographic purification of biological macromolecules by their capture on hydrophilic surfaces with the aid of non-ionic polymers

Virale Impfstoffe gelten als eine der größten Errungenschaften der Gesundheitswissenschaften. Die Nutzung viraler Vektoren für die Gentherapie zur Heilung momentan unheilbarer Krankheiten hat das Potential zu einer neuen Revolution in den Medizinwissenschaften zu führen Die große Anzahl an verschiedenen Viren sowie deren Herstellungsmethoden erschweren eine standardisierte Produktion viraler Impfstoffe jedoch in hohem Maße. Aufreinigungsverfahren erfordern mehrere Schritte und sind typischerweise spezifisch auf die Virusart und das Herstellungsverfahren zugeschnitten. Dies führt zu zeitaufwendigen Verfahrensentwicklungen und potentiell verzögerten Markteinführungen. Aufreinigungsverfahren im Labormaßstab und in kommerziellen Produktionsstätten können für das gleiche Produkt gänzlich unterschiedlich sein. Aufgrund der Skalierbarkeit, der Kosten, der Effizienz und der Kapazitätseinschränkungen beschränken sich industrielle Aufreinigungsmethoden auf Chromatographie- und Filtrationsverfahren.

Die vorliegende Arbeit behandelt die Entwicklung einer Steric Exclusion Chromatographie (SXC)-Methode als Plattformtechnologie für die Aufreinigung großer Biomoleküle wie zum Beispiel Viruspartikeln. Bei SCX-Methoden wird eine unaufgereinigte Probe mit nicht-ionischen Polymern, in diesem Fall Polyethylenglycol (PEG), gemischt und in Vorrichtungen mit einer porösen, hydrophilen stationären Phase injiziert. Das Zielprodukt wird hierbei ohne chemische Bindung durch einen thermodynamischen Effekt, welcher durch PEG hervorgerufen wird, erfasst. Kleine Verunreinigungen wie Medienbestandteile und Proteine bleiben von PEG unberührt und werden ausgewaschen. Je größer das Zielprodukt ist, umso geringer ist die für die Aufreinigung benötigte PEG-Menge ,bzw. umso geringer ist die erforderliche PEG-Größe.

SCX wurde in dieser Arbeit für die Aufreinigung von 14 verschiedenen, zellbasierenden Virenstämme und Serotypen — Influenzavirus, Gelbfiebervirus, Adeno-assoziiertes Virus (AAV) und modifiziertes Vaccinia Ankara (MVA) — einer Vielzahl an Größen (20–250 nm) und von unterschiedlichen Produktionsverfahren angewandt. Ebenso extrazelluläre Vesikel (EVs) von 160–230 nm aus Madin-Darby-Hundenieren (MDCK), Baby-Hamster-Nieren (BHK) und humanen embryonalen Nierenzellen (HEK) wurden aufgereinigt.

Eine Anzahl an stationären Phasen, u. A. hydroxilierte Monolithen (1–2 µm Porengröße), Zellulosemembrane (1–1.2 µm Porengröße) und 3D-gedruckte Zellulosemonolithen

(Porengröße 400–500 µm) wurden getestet. Vorrichtungen mit regenerierten Zellulose-membranen mit einer Progengröße von 1 µm erwiesen sich am effizienten mit Bezug auf Produktausbeute und PEG-6000 Konzentrationen von 8–10% für die Probenladung.

Produktrückgewinnungsraten für vier unterschiedliche, in MDCK-Suspensionszellen mit Reaktorsystemen produzierte, Influenzavirusstämme lagen bei über 98%. Die größte gemessen Produktivität für den Influenzavirusstamm A/Puerto Rico/8/34 H1N1 mit Bezug auf Hemagglutinin-Antikörper lag bei ungefähr 69 000 µg pro Quadratmeter und Stunde (4600 monovalente Dosen pro Quadratmeter und Stunde).

Des Weiteren wurden zwei für kommerzielle Impfstoffproduktion verwendete Gelb-fieberstämme getrennt in adherenten Vero-Zellen produziert. Eine praktisch komplette Produktausbeute der infektiösen Titer wurde erzielt und verbleibende DNA- und Pro-teinkonzentrationen lagen unter den vorgeschriebenen regulatorischen Anforderungen. Bis zu 6×10^9 Plaque-formende Einheiten (100 000 Impfstoffdosen entsprechend) wur-den pro Liter Zellkultur aufgereinigt mit einer Produktivität von 5 Millionen Dosen pro Quadratmeter und Stunde.

Mehrere Wildtypen und rekombinante Varianten von Adeno-assoziierten Viren (AAV) wurden in adherenten HEK-Zellkulturen mittels dreifach Transfektion produziert und sowohl von Zelllysaten wie von Zellüberstanden aufgereinigt. Hierfür wurden bei SCX keine Produktverluste detektiert und der aufgereinigte AAV induzierte die Genexpression oder Gen-Knockdown in transduzierten Zellen, sowohl *in vitro* wie *ex vivo*.

Bei explorative Versuchen konnte für, in aviären Zellen produzierten, Modified-Vaccinia-Ankara-Virus (MVA) eine praktisch komplette Produktausbeute mit $TCID_{50}$ Titern von 3.7×10^9 Virionen erzielt werden. Jedoch war der Virus anfällig für, mittels Partikelgrößenverteilung festgestellte, Aggregationen bei PEG-Zugabe. Die Zugabe von Sorbitol oder Sukrose von je 8% zu den PEG-konditionierten Virusproben verringerte scheinbar die Menge an Aggregaten im Vergleich zu PEG-konditionierten Virusproben ohne Stabilisatoren.

Es konnte festgestellt werden, dass extrazelluläre Vesikel (EVs) oft zusammen mit den Zielproduktviruspartikeln von Wirtszellen aufgereinigt wurden. Dies ist auf deren sehr ähnliche Charakteristika zurückzuführen. Erste Resultate für das Abfangen von EVs von Zellüberständen zeigten eine Partikelausbeute von 40% und Konzentrationen von bis zu 8×10^{10} Partikeln pro mL. Weitere Studien sollten sich mit Evaluierung von SXC für die präparative Aufreinigung von EVs auseinandersetzen.

Protein- und DNA-Abscheidungen mittels SXC lagen typischerweise bei $> 85\%$ beziehungsweise $> 75\%$, abhängig von Virus und Experiment, z.B. bei Vorschaltung eines DNA-Verdauschritts. Bei allen Fällen erwies es sich als vorteilhaft eine Nucleasebehand-lung vor SXC durchzuführen um geringere Rest-DNA-Mengen zu erzeugen.

SXC mit 3D-gedruckte Zellulosemonolithen (Porengrößen von 400 und 500 µm) erweist sich als ineffizient mit Bezug auf die Produktausbeute (ungefähr 40% für Influenza A Viren)

verglichen mit 1.0 µm regenerierten Zellulosemembranen. Die 3D-gedruckten Monolithen stellen dennoch eine interessante Alternative für die Zukunft dar, z.B. für Expansionsbett-Chromatographie.

Die Fähigkeit der Produktladung und Rückgewinnung bei physiologischen pH-Werten und Konduktivitäten sowie die konformationsstabilisierende Eigenschaften von PEG sind wesentliche Vorteile für die Aufreinigung von labilen Biopharmazeutika. Die mittels SXC bisher erzielten hohen Produktrückgewinnungsraten ermöglichen nachfolgende Polierschritte um den Reinheitsgrad zu erhöhen ohne dabei nicht-akzeptierbare niedrige Prozessausbeuten zu riskieren. Die engen Operationsbereiche von SXC ermöglicht die Aufreinigung von Viren mit einer großen Erfolgswahrscheinlichkeit (z.B. 8% PEG-6000 als Ausgangpunkt) und die geringen Kosten der Membrane erlauben Single-Use Einsätze, welche zeit- und kostenintensives Reinigungs- und Sanitisation-Schritte vermeidet.

Das Scale-up von SXC ist einfach, da es nur lineare Steigerungen der Membranoberflächen erfordert, und der Einsatz von Geräten auf bis zu 20 Quadratmetern ermöglicht Virusaufreinigungen im industriellen Maßstab.

Als Auffangschritt erscheint SXC bezüglich Produktausbeute, Benutzerfreundlichkeit und Skalierbarkeit vergleichbar oder besser als die meisten verfügbaren Chromatographiemethoden. Die Abschätzung von Kapazitäten ist jedoch eine Herausforderung, da keine direkten chemischen Bindungen entstehen. Produktrückgewinnungsraten sind stark abhängig von bestimmen Qualitätsattributen des Ausgangsmaterials, w.z.B. Restzellrückständen und/oder aggregierten Produkten.

Die hier beschriebenen Ergebnisse sind die Grundlage für eine weitere Optimierung und Anwendung dieser Technologie und sie zeigen, dass die membran-basierende SXC das Potential hat zu einer Plattformtechnologie für virale Impfstoffe und Genetherapieanwendungen zu werden.

Acknowledgements

The **Acknowledgments** section is empty in the electronic PDF version of this dissertation according to paragraph 4.1.1. of the *Regulations for the submission of depositary copies to the library of the Otto von Guericke University Magdeburg within the framework of doctoral and habilitation procedures* as of 5th November 2019, which partially states that "[. . .]. The document does not include a CV, acknowledgments or further personal data. [. . .]".

More information:

https://www.ub.ovgu.de/ub_media/Service/Formulare/Pflichtexemplarrichtlinie_englisch-p-934.PDF

Table of Contents

List of Acronyms

AAV   adeno-associated virus

Ad   adenovirus

AEC   anion exchange chromatography

aHA   hemagglutination activity

ATF   alternating tangential flow

BCG   Bacillus Calmette-Guérin

BHK   baby hamster kidney

BSA   bovine serum albumin

CAR   chimeric antigen receptor

CDC   Centers for Disease Control and Prevention

CFP   cyan fluorescent protein

CHO   chinese hamster ovary

CMV   cytomegalovirus

CPSF6   cleavage and polyadenylation specificity factor subunit 6

CV   column volumes

DBC   dynamic binding capacity

$DBC_{10\%}$ dynamic binding capacity at 10% breakthrough

$DBC_{5\%}$ dynamic binding capacity at 5% breakthrough

DCS   differential centrifugal sedimentation

ddPCR   Droplet Digital™ polymerase chain reaction (PCR)

DLS	dynamic light scattering
DMEM	Dulbecco's Modified Eagle Medium
DSP	downstream processing
EBC	equilibrium binding capacity
ECACC	European Collection of Animal Cell Cultures
ELISA	enzyme-linked immunosorbent assay
EM	electron microscopy
EMA	European Medicines Agency
EMBL	European Molecular Biology Laboratory
EVs	extracellular vesicles
FASP	filter aided sample preparation
FCS	fetal calf serum
FDA	U.S. Food & Drug Administration
FFU	focusing forming units
FT	flow-through
GMEM	Glasgow Minimum Essential Medium
HA	hemagglutinin
HAU	hemagglutination units
HEK	human embryonic kidney
HIC	hydrophobic interaction chromatography
hpi	hours post infection
HPV	human papillomavirus
IEC	ion exchange chromatography
IgG	immunoglobulin G
IgM	immunoglobulin M
IPV	inactivated polio vaccine
ITR	inverted terminal repeat
LC	liquid chromatography
LOD	limit of detection
LOQ	limit of quantitation
LRV	logarithmic reduction value
LS	light scattering
LV	lentivirus

MDCK	Madin-Darby canine kidney
MDCK$_{adh}$	adherent MDCK
MDCK$_{sus}$	suspension MDCK
MDM	monocyte-derived macrophages
MEM	Minimum Essential Medium
MMCO	molecular mass cut-off
MOI	multiplicity of infection
MVA	Modified Vaccinia Ankara
MVBs	multivesicular bodies
NA	neuraminidase
NISBC	National Institute for Biological Standards and Control
NP	nucleoprotein
NS	non-silencing
NTA	nanoparticle tracking analysis
OPV	oral polio vaccine
OTAT	Office of Tissues and Advanced Therapies
PBS	phosphate buffered saline
PCR	polymerase chain reaction
PDB	Protein Data Bank
PEG	polyethylene glycol
PES	polyethersulfone
PFU	plaque forming units
PS	porcine kidney stable epithelial
PSD	particle size distribution
PVC	polyvinyl chloride
qRT-PCR	quantitative real-time PCR
rAAV	recombinant adeno-associated virus
RC	regenerated cellulose
rcf	relative centrifugal force
rpm	revolutions per minute
RSD	relative standard deviation
RV	reduction value

SCMA	sulfated cellulose membrane adsorber
SD	standard deviation
SE	standard deviation of the mean
SEC	size exclusion chromatography
SEM	scanning electron microscopy
shRNA	short hairpin RNA
SIB	Swiss Institute of Bioinformatics
SRID	single radial immunodiffusion
STED	stimulated emission depletion
STR	stirred tank reactor
SXC	steric exclusion chromatography
$TCID_{50}$	tissue culture 50% infective dose
TEM	transmission electron microscopy
USP	upstream processing
VEGF	vascular endothelial growth factor
vg	viral genomes
VLPs	virus-like particles
vp	virus particles
WHO	World Health Organization
YF	yellow fever
YFP	yellow fluorescent protein
YFV	yellow fever virus

List of Symbols

Roman Letters

$[A]$	kg L^{-1}	concentration of component A
$[A]_{in}$	kg L^{-1}	concentration of component A at inlet
C_L	kg L	concentration of ligand
$[A]_{out}$	kg L^{-1}	concentration of component A at outlet
d	m	diameter
DBC_x	kg m^{-2}	dynamic binding capacity at x% breakthrough (Equation 2.10), p. 36
d_h	m	hydrodynamic diameter
d_p	m	mean size particle diameter
E	–	number of elutions
F	–	number of fractions
K_b	M^{-1}	binding constant for the binding equilibrium (Equation 1.2 and 1.6), pp. 20, 21
K_{ex}	M^{-1}	exchange binding constant (Equation 1.6), p. 21
K_L	M^{-1}	binding constant of ligand (co-solvent)
K_W	M^{-1}	binding constant of water
L	mol	ligand (co-solvent)
LRV	–	logarithmic reduction value (Equation 2.9), p. 36
m_A	mol kg^{-1}	molal concentration of component A
M_r	Da	molecular mass
n	–	number of binding sites
n_{rep}	–	number of replicates

P	mol	protein
$[Prod]$	$\mathrm{kg\,L^{-1}}$	concentration of target product
$\dot{Q}$	$\mathrm{m^3\ h^{-1}}$	volumetric flow rate
q_A	kg	mass of component A
q_A^{in}	kg	mass of component A at inlet
q_A^{out}	kg	mass of component A at outlet (all chromatography fractions)
q_A^{elut}	kg	mass of component A in eluate
q_{Prod}^{elut}	kg	mass of target product in eluate (Equation 2.4), p. 35
q_{Prod}^{in}	kg	mass of target product at inlet
R	$\mathrm{J\ mol^{-1}\ K^{-1}}$	gas constant
r_h	m	hydrodynamic radius
RV	%	percentile reduction value (Equation 2.9), p. 36
S	$\mathrm{m^2}$	surface area
S_{col}	$\mathrm{m^2}$	geometric membrane surface area of column
s		standard deviation
$s\left(\bar{x}\right)$		standard deviation of the mean (or standard error, SE); (Equation 2.11), p. 37
T	K	temperature
t_r	h	residence time
t_{sxc}	h	duration of steric exclusion chromatography
u	$\mathrm{cm\ h^{-1}}$	superficial mobile phase velocity
V	$\mathrm{m^3}$	volume
$V_{b,x\%}^{\mathrm{in}}$	$\mathrm{m^3}$	volume of feed at x% breakthrough
V_{out}	$\mathrm{m^3}$	volume at outlet
W	mol	water
$\bar{x}$		mean

Greek Letters

$\chi_{A,Prod}$	$\mathrm{kg_A\,dose^{-1}}$ $\mathrm{kg_A\,kg_{Prod}^{-1}}$	purity ratio of component A to target product (Equation 2.7), p. 35
ΔG_b^0	$\mathrm{J\ mol^{-1}}$	free energy of binding (Equation 1.4 and 1.7), pp. 20, 21
ΔG_L^0	$\mathrm{J\ mol^{-1}}$	free energy of binding of ligand (co-solvent) to a protein site
ΔG_W^0	$\mathrm{J\ mol^{-1}}$	free energy of binding of water to a protein site

ΔP	Pa	pressure drop
η	Pa s	mobile phase viscosity
Γ_{23}	$\mathrm{mol\,mol^{-1}}$	preferential interaction parameter in the Casassa and Eisenberg notation (Equation 1.8), p. 21
μ_A	$\mathrm{J\,mol^{-1}}$	chemical potential of component A
φ	$\mathrm{doses\,m^{-2}\,h^{-1}}$ $\mathrm{kg}_{Prod}\,\mathrm{m^{-2}\,h^{-1}}$	productivity of the SXC step for target product (Equation 2.6), p. 35
ρ	$\mathrm{kg\ m^{-3}}$	density of mobile phase
ρ_p	$\mathrm{kg\ m^{-3}}$	particle density
υ_b	$-$	binding isotherm (Equation 1.3), p. 20
$\bar{\upsilon}$	$\mathrm{mol\,mol^{-1}}$	preferential interaction parameter in the Scatchard notation (Equation 1.8), p. 21
ξ_{Prod}	%	percentile yield of target product (Equation 2.5), p. 35
ζ_A	%	percentile recovery of component A (Equation 2.2), p. 35

Theoretical Background

Viral vaccines are considered to be one of the most successful achievements in health science thanks to all the diseases they help prevent. Also, the use of viral vectors for gene therapies has shown the promise to become the next medical revolution for combating a wide variety of currently untreatable diseases.

Vaccines — and in the future gene therapies as well — need to be available to a large part of the population at affordable prices, which represents a huge manufacturing burden. The wide range of viruses and their production methods make it extremely difficult to standardize virus manufacturing. Moreover, in order to ensure their safety and potency, virus products have to be purified to extremely high standards. All these are considerable challenges for the process engineer.

Downstream processing (DSP) refers to the recovery and the purification of biological products. These purification processes require several steps and most of the time are tailored to each particular virus species and how it is produced, making process development time-consuming and potentially delaying time to market. Even for the same product, purification processes might differ almost completely between a small laboratory and a commercial manufacturing facility. Due to scalability, robustness, costs, efficiency, and capacity constraints, chromatography is one of the few purification methods than can be used at industrial scales. However, traditional bead-based chromatography was originally developed for protein purification and is extremely inefficient for virus particles. Wolff & Reichl [1] and Gagnon [2] provide a thorough literature review on the DSP of viruses. The authors show that efficient purification methods for viruses are scarce — even more so the ones available for industrial manufacturing — and that there is a lack of platform technologies.

There are currently severe shortages in the industrial supply of viruses for human

use, both for regular supply and for pandemic emergencies.[3, 4]. In order to meet the current and future demands of viral gene therapy and vaccine products, new more efficient purification technologies are urgently needed.

This work is focused on the purification of several cell culture-based viruses — and to a lesser extent, extracellular vesicles (EVs) — with a new approach to a method called steric exclusion chromatography (SXC), where widely available and low-cost disposable membranes are used instead of monolithic stationary phases.

Membrane-based SXC has the potential of becoming a capture platform for virus particles and to help alleviate the current and future challenges related to industrial virus purification in order to increase availability of vaccines and gene therapies to the general population.

The sections in this Chapter describe the main characteristics and relevance of the target products purified in this work, together with the basics of SXC.

Section 1.1 introduces viral vaccines and gives a brief description of influenza virus (A and B) and yellow fever virus (YFV). Section 1.2 introduces gene therapies and describes adeno-associated virus (AAV) and vaccinia (MVA) virus; EVs are also briefly discussed.

Section 1.3 introduces the concept of "molecular crowding", which causes the interaction mechanisms behind SXC, which is further described in Section 1.4.

1.1   Viral vaccines

Vaccines have begun their fourth century and their evolution has been directly related to the development of bioprocess technologies. The oldest written record is from the practice of variolation as described in a medical book from 1695 by Zhang Lu, where human pox was used as against smallpox in imperial China even before Jennerian vaccination. Variolation was also practiced in India, Persia, Turkey, and Africa [5].

Smallpox was once the scourge of mankind, a highly contagious disease that affected all levels of society [6]. Even for survivors, the disease could have devastating sequelae. Smallpox showed an average death rate of about 30%, but the case-fatality rate in infants was even higher: around 80% in London and 98% in Berlin in the 1800s. Smallpox was commonly referred to as *variola*, a term introduced by Bishop Marius of Avenches in Switzerland in AD 570; the term derives from *varus*, meaning "mark on the skin". The term *small pockes* (*pocke*=sac) or *smallpox* was used at first in the 15th century in England in order to distinguish the disease from syphilis, at that time known as the great pox [5, 7].

Credited with initiating a safer approach in vaccine development, Jenner invented a Latin name for cowpox, *variolae vaccinae* (smallpox of the cow) and published his results at his own expense in a monograph titled *An Inquiry into the Causes and Effects of the Variola Vaccinae*. The terms "cowpox inoculation" and "vaccine inoculation" were first used to describe Jenner's procedure. The word *vaccination* was first employed in 1800 by Richard Dunning with Jenner's approval [5].

The eradication of smallpox was certified on May 8 of 1980 by the World Health Assembly [5].

Table 1.1 shows an overview on the development of human vaccines. The first vaccines were live attenuated organisms that had complex complex upstream processing (USP) cultivations and minimal DSP. Jenner used patients with cowpox as production system for the smallpox vaccine.

Since its introduction, until 1879 (83 years), Jenner's vaccine was the only available. Pasteur then described immunization by attenuated chicken cholera and also immunized sheep and cattle against anthrax (1881). Pasteur additionally used rabbits as bioreactors for the rabies vaccine [5]. Another important bioreactor system used until today is the hen egg. Ernest Goodpasture discovered in 1931 that this could be used as a production system. For instance, the manufacture of influenza and yellow fever (YF) vaccines still relies heavily on egg-based production [8].

A major breakthrough in vaccine production was made by Enders, who successfully propagated polio virus *in vitro* with non-neural human cells, maintaining the cultures in roller tubes for long periods of time changing the medium several times a week. They were able to induce paralysis in mice by injecting the cell culture fluids intracerebrally into

Table 1.1

Development of human vaccines. Modified from Ref. [5]

	Live attenuated	Killed whole organisms	Purified proteins of organisms or polysaccharides	Reassortants	Genetically engineered
18th century	Smallpox				
19th century	Rabies	Typhoid			
		Cholera			
		Plague			
Early 20th century	BCG (Tuberculosis)	Pertussis (whole cell)			
	Yellow fever (YF)	Influenza	Diphtheria		
		Rickettsia	Tetanus		
Late 20th century	Polio (OPV)	Influenza	Pneumococcus	Influenza (killed + live)	Hepatitis B recombinant
					Cholera toxin
					Pertussis toxin
	Measles	Polio (IPV)	Meningococcus		
	Mumps	Rabies (new)	Hepatitis B (plasma derived)		
	Rubella (cold adapted)	Anthrax			
	Adenovirus	Japanese encephalitis	*H. influenzae*		
	Typhoid Ty12a	Hepatitis A	Typhoid (Vi)		
	Varicella (chickenpox)	Tick-borne encephalitis	Pertussis (acellular)		
	Cholera CVD103	*E. coli* (+cholera toxin B)	*H. influenzae*, meningococcus (protein conjugated)		
21st century	Zoster (shingles)		Pneumococcal conjugate	Rotavirus	Human papillomavirus (HPV)

BCG=Bacillus Calmette-Guérin; IPV=inactivated polio vaccine; OPV=oral polio vaccine

Table 1.2

Human viral vaccines. Modified from Ref. [9].

Year	Vaccine	Cell substrate
1795	Smallpox (Jenner)	Calf lymph
1885	Rabies (Pasteur)	Rabbit central nervous system
1937–1940	Influenza, yellow fever	Embryonated eggs (Woodroof and Goodpasture)
1953	Polio	non-neural cell culture (Enders, Weller, and Robbins)
1963–1965	Measles	Chick embryo fibroblast
1967	FMDV	BHK21 (McPhearson and Stocker)
1968	Rubella	Human diploid cells (W138, Hayflick and Morhead)
1981	Polio (killed)	Vero cell line (continuous)
1985	Polio (live)	Vero cell line (continuous)

the animals. The first publication detailing these results appeared in early 1949 and the scientists noticed soon after that types 1 and 3 polio grew similarly in cell culture systems. Shortly afterwards, Salk developed an inactivated polio vaccine (IPV) produced in primary monkey kidney cells, which are related to the now widely used Vero continuous cell line. In a relatively short time, cell culture of viruses became a convenient technology that would cover several fields including: quantitative assays, diagnostic tests, cell transformations, and of course, vaccine manufacturing [5].

Although several modern vaccines are quite complex, ranging from conjugates, carbohydrates, virus-like particles (VLPs), recombinant viruses, etc., many are still legacy products done with whole viruses (Table 1.2) [9].

1.1.1 Influenza virus

Influenza is a highly contagious acute respiratory disease that was first described by Hippocrates in 412 BC [10].

Influenza viruses are members of the *Orthomyxoviridae* family, and they are divided into types A, B, and C, based on antigenic characteristics of the nucleoprotein (NP) and matrix (M) protein antigens. Influenza A viruses are further subtyped on the basis of the major membrane glycoproteins, hemagglutinin (HA) and neuraminidase (NA). Individual strains are designated according to the site of origin, isolate number, year of isolation, and subtype (e.g., influenza A/Hiroshima/52/2005 [H3N2]). So far, 18 HA subtypes and 11 NA subtypes have been identified [11].

Influenza A and B viruses are major human pathogens and the most extensively studied. Type A and type B viruses are morphologically similar. The virions contain negative sense RNA and are irregularly shaped spherical particles, measure 80–120 nm in diameter, and have a lipid envelope from the surface of which the HA and NA glycoproteins project (10 to 14 nm nm long).

The influenza virus was first isolated in 1933. The first demonstrably effective influenza vaccine was tested on 800 retarded male subjects in a state colony in Pennsylvania [12] and reported in 1936 [13]. The first influenza vaccine was licensed in 1945 and was given only to military personnel. After the pandemic of 1957–1958, seasonal influenza vaccines were recommended for the non-military population by the U.S. Public Health Service. The strategy of immunizing only high-risk groups became the standard policy globally, except in the United States, where the decision was made to recommend annual vaccinations to all people over 6 months of age.

The first live-attenuated influenza vaccine was available in 2003 and before then, influenza vaccines were administered intramuscularly and had been produced from inactivated, purified influenza viruses propagated in embryonated eggs. In 2007, the European Medicines Agency (EMA) approved a vaccine produced in MDCK mammalian cells [10].
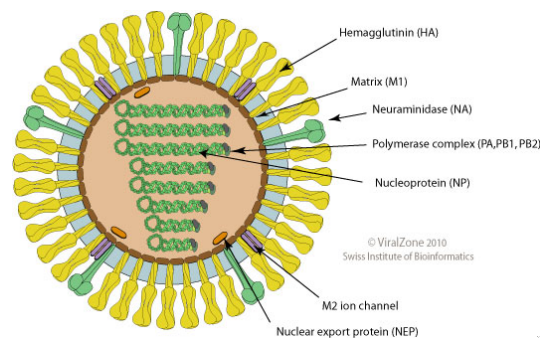
Figure 1.1. The influenza A virion, about 80–120 nm in diameter. Source: ViralZone; www.expasy.org/viralzone, Swiss Institute of Bioinformatics.

Influenza outbreaks are recorded virtually every year and vary widely in extent and severity. The factors that result in the beginning and termination of an outbreak are not fully understood. Outbreaks peak over a 2–3 week period, last for 2–3 months generally, and often subside as quickly as they began [14]. The attack rates are highly variable between outbreaks but most commonly range in 10–20% of the general population [14].

Seasonal epidemics are the consequence of "antigenic drift" caused by the lack of a proofreading function of the influenza RNA polymerase, which results in misincorporation of nucleotides.

On the other hand, pandemics are the result of "antigenic shift", which is an abrupt, major change in the influenza viruses that infect humans, with most people not having immunity against them. A pandemic is a widespread epidemic that may affect continents or the entire planet. At least 10 pandemics have been confirmed since the first one in 1580 [15]. During the pandemic of 1918 (Spanish flu) at the end of the first world war, one-third of the world's population became infected and it caused as many as 50 million deaths [16]. The impact of the Spanish flu was many times greater than the bubonic plague in Medieval Europe and is by far the biggest outbreak of infectious disease ever recorded [17].

Unfortunately, there is neither periodicity to the occurrence of pandemics nor basis for predicting when and where an outbreak might occur. Only influenza A viruses undergo both antigenic shift and drift, while influenza B viruses only change gradually by antigenic drift.

The Centers for Disease Control and Prevention (CDC) estimates that, from October 1, 2018 to May 4, 2019, there have been 37.4–42.9 million flu illnesses, 531 000–647 000 flu hospitalizations and 36 400–61 200 flu deaths in the U.S. alone [18].

One disadvantage with egg-based immunization is egg allergy, which has an estimated prevalence of 0.5–2.5%; the allergens include ovalbumin and ovomucoid. This risk is eliminated when using mammalian cell-based systems [19]. Yet another disadvantage of the egg-based system is that chickens potentially carry viruses such as Rous sarcoma virus, avian leukosis virus, and reticuloendotheliosis, which can potentially be introduced into the manufacturing process [19].

Most importantly, there is the issue of preparedness: from 2004 to 2014, the annual output of seasonal vaccine doubled to around 450 million doses; in the event of a pandemic, this can be ramped up to give a total potential capacity of around 850 million doses. Unfortunately, that number is not even close to the billions of doses that would be needed in a short time in case of a pandemic [4].

Influenza is also responsible for a considerable burden in public health spending. It is estimated that interpandemic outbreaks of influenza currently incur annual costs of more than 12 billion in the U.S. The estimated annual costs if a new pandemic were to happen, would range from 71 to 167 billion for attack rates of 15–35% [14]. Bresee et al. [11] note

Table 1.3

Regulatory specifications for whole-virion inactivated influenza vaccines. Modified from Ref. [26].

Characteristic	EP (cell culture)[a]	EP (egg-derived culture)[a]	WHO[b]
HA antigen	>15 µg per strain[c]	15 µg per strain	15 µg per strain
DNA	<10 ng		<10 ng[d]
Protein	<6 × HA antigen content <100 µg per strain	<6 × HA antigen content <100 µg per strain	<100 µg per strain <300 µg per dose
Endotoxins	<25 IU	<100 IU	To be tested
Sterility	To be tested	To be tested	To be tested
Formaldehyde	<2 g L^{-1}	<0.2 g L$^{-1,f}$	<0.1%[e]
β-propiolactone		<0.1%[e]	<0.1%[e]
Ovalbumin		<1 µg	<5 µg
BSA (from serum)	<50 ng		
Residual infectivity	Amplification test in cell culture over two passages	Amplification test in fertilized eggs over two passages	To be tested in in fertilized eggs or cell culture, respectively

HA=hemagglutinin;

[a] European Pharmacopoeia Commission, 2012; Ref. [27]
[b] World Health Organization (WHO) Technical Report Series, 2005; Ref. [28]
[c] unless clinical evidence supports the use of a different amount
[d] for virus grown in cell culture
[e] at any time during inactivation

that: "Few other infectious diseases have adversely affected the health and economies of global populations as consistently and extensively as influenza."

The majority of influenza infections occur in infants, children, and the elderly [10]. Around 90% of all influenza-related deaths are among seniors >65 years. People aged >80 years are at approximately 11 times higher risk than people aged 65–69 years [20].

The best way to prevent influenza illness is vaccination. Most commercially influenza vaccines are either trivalent or quadrivalent formulations from viruses propagated in chicken eggs. The efforts to develop universal influenza vaccines are discussed elsewhere [21–24]. Most vaccines manufactured since the 1970s are not whole-virus but rather subvirion, sometimes referred as "split". Splitting of influenza vaccines by disrupting the viral envelope also adds assurance of viral inactivation (typically done chemically). A variety of detergents are used for splitting, such as deoxycholate, tri-N-butyl phosphate, polysorbate 80, and Triton X-100. A third class of influenza vaccines are called "subunit" [25], where the viral membrane proteins are separated from the core. These vaccines do not contain any internal parts of the virus, only the HA and NA proteins.

Bresee et al. [11] give a detailed description of all approved influenza vaccines for the 2016-2017 season. The regulatory requirements for inactivated influenza vaccines are listed in Table 1.3.

1.1.2 Yellow fever virus

Yellow fever (YF) is an acute viral hemorrhagic disease transmitted by infected mosquitoes. The "yellow" in the name refers to the jaundice that affects some patients. A small proportion of patients who contract the virus develop severe symptoms and approximately half of those die within 7 to 10 days [29].

Its etiologic agent, YFV, is a 38 nm sized positive-sense ssRNA virus (Figure 1.2) from the Flaviviridae family transmitted to humans by infected mosquitos of genera *Haemagogus* (in jungle areas) and *Aedes* (urban areas). The genome of the 17D-204 substrain contains 10 862 nucleotides.

YFV is thought to have evolved in Africa around 3000 years ago and it was imported into the Western hemisphere by the slave trade of the 16th century. YF was once a scourge of human kind with the first recorded outbreak in Mayan manuscripts in the year 1648 and serious epidemics spreading as far as Europe and North America in the 18th and 19th centuries. The last YF outbreak in the U.S. was in New Orleans in 1905 [5].

Today, the disease is endemic in 32 countries in Africa and 13 countries in Central and South America [30]. YFV can cause devastating epidemics and is regarded as a reemerging disease of considerable importance.

There are no antiviral drugs for any flavivirus infection, but since the late 1930s a highly efficient YF vaccine is available that confers lifelong immunity according to the current understanding of many advisory committees [31]. The vaccine provides effective immunity within 10 days for 80–100% of people vaccinated, and within 30 days for more than 99% of people vaccinated.

The currently commercially available YF vaccines consist of a live-attenuated virus (strain 17D) propagated in embryonated hens' eggs. More than 500 million doses of the vaccine have been administered worldwide, and it has a very high efficacy and safety record. A critical property of the 17D vaccine is its inability to disseminate from the
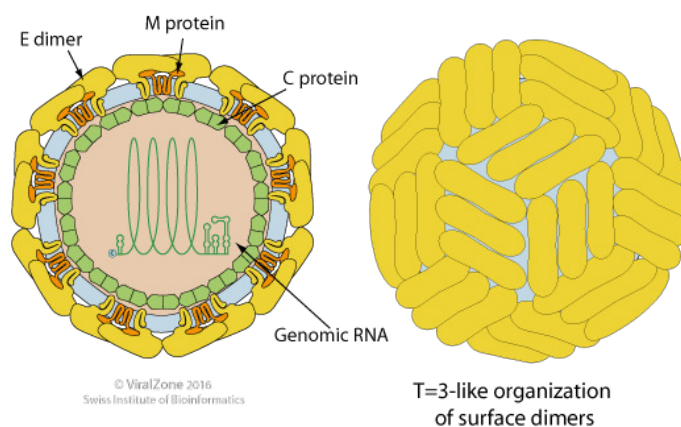
Figure 1.2. The Flaviviridae virion, about 50 nm in diameter. Source: ViralZone; www.expasy.org/viralzone, Swiss Institute of Bioinformatics.

midgut to other tissues in the mosquito, so it won't be transmissible from the mosquito to vertebrate hosts. Regardless of its high safety record, concerns with a new rare but severe type of viscerotropic disease identified in 2001 [8], shortage of vaccine supply in recent epidemics in Brazil and Africa, rapid urbanization, and waning immunization coverage [32] have pushed the development for alternative approaches to egg-based manufacturing and the live-attenuated vaccine platform. One of such alternatives is YFV production in adherent Vero cells, a continuous cell line derived from African green monkeys, widely accepted for production of human viral vaccines [33, 34]. The use of cell-based systems for virus production is usually accompanied by purification techniques that offer both high resolution and throughput, in particular chromatography processes. For instance, recent purification efforts for YFV produced in cell culture include capture steps with anion exchange membrane adsorbers (ion exchange chromatography (IEC)) [33].

Virus stability, however, is a serious concern since YFV is thermolabile (the vaccine is available as a lyophilized powder). Even for the good and promising results using IEC for the capture of YFV, the process has to be modified to minimize infectivity losses. Additionally, the specificity of process parameters during IEC most certainly does not allow to use it as a platform for purification of other *Flavivirus* types.

1.2   Viral gene therapies

Around 50 years ago, scientists first considered the idea that genetic disorders could be potentially eliminated by correcting defective genes and so the concept of human gene therapy emerged with the first clinical trial in 1989 [35].

Gene therapy is the use of a vector to transfer genetic material to a cell, where the nucleic acid will induce a beneficial therapeutic effect by the expression of the gene(s) themselves or by affecting the expression of other genes [36].

Despite initial clinical setbacks [37], gene therapy gained momentum thanks to the hope that it would eventually replace pharmaceuticals. Although at first only monogenic diseases were targeted, cancer treatment became a logical extension of the gene therapy concept. Cancer is a genetic disease. In contemporary industrialized countries, it is the leading cause of death, so it comes as no surprise that today, cancer gene therapy represents the major portion of research and clinical effort in the gene therapy field (with solid tumors as the primary target) [38]. The potential uses for gene therapy are varied, though, as evidenced by data from human clinical trials (see Figure 1.3) [39]. The first gene therapy was approved in Europe in 2012 (Glybera®) with an approximate cost of 1.11 million euros per patient [35]. On May 24th 2019, at the time of writing of this work, Novartis announced the approval of Zolgensma®, a pedriatric gene therapy against spinal muscular atrophy [40]. This treatment is the first and only gene therapy for this disease and has a cost of 2.1 million US dollars, becoming the world's most expensive drug.

A gene therapy vector can be: 1) naked nucleic acid, 2) nucleic acid combined with additional agents such as lipids (see Section 1.2.3) and proteins, 3) or a modified virus
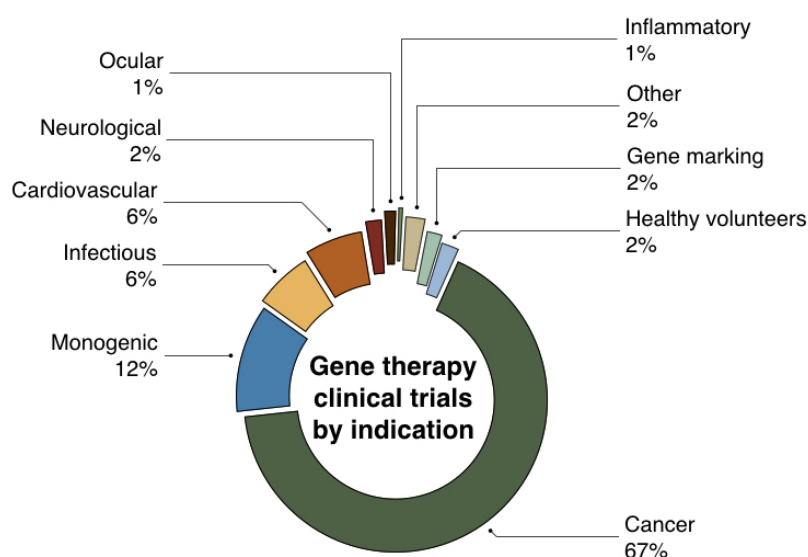
Figure 1.3. Gene therapy human clinical trials by target disease category as of December 2018. Data from The Journal of Gene Medicine [39].

containing therapeutic genes. An overview of the most common viral gene therapy vectors is shown in Table 1.4.

For safety reasons, a vector should not be able to able to replicate outside the producer cell system, e.g., MVA is propagated in avian cell and cannot reproduce in human cells.

Gene therapy gained notoriety because there are certain disorders than cannot be treated successfully with conventional pharmaceuticals. The first target field for gene therapy were inherited diseases, where repairing defective gene function is much more attractive than endlessly treating for symptoms. Gene therapy is a complex field where the therapies can be targeted to particular cells and tissues by vector design, vector choice (Table 1.4), or delivery method. These therapies can be used to treat metabolic diseases (e.g., cystic fibrosis, hemophilia), cancer (e.g., inducing cell death and raised immune response), vascular disease (e.g., expression of vascular endothelial growth factor (VEGF)), and inflammatory disorders (e.g., arthritis).

Gene delivery can also be done *ex vivo* where the transfer can be combined with traditional tissue engineering approaches. This strategy can be used to improve tissue regeneration by the expression of therapeutic genes. In fact, the first gene transfer clinical trials for cartilage repair and osteoarthritis have been finished [41].

As observed from Figure 1.3, most gene therapy trials are directed at cancer. Some of these treatments are for the so called "suicide gene therapy" in which cancer cells are reprogrammed for destruction and to achieve tumor regression. For example, oral cancer is a particularly good target for gene therapy since the treatment can be injected directly to the lesions [42].

Unfortunately, a lot of severe setbacks in the progress to market of several gene therapies were due to the assumption that small-scale operations were scaleable and appropriate for commercial manufacturing [36]. Clayton et al. point out that using freeze-thaw cycles to release AAV from the cells and using density gradient centrifugation for purification are barely adequate options for large-scale manufacturing [36].

In the same regard, the use of cell therapies has hugely developed in the past 10 years. Cellular therapy products include cancer vaccines, immunotherapies, and stem cells (hematopoetic and embryonic) [43].

As of 31 May, 2019, there were 17 approved cellular and gene therapies products by the Office of Tissues and Advanced Therapies (OTAT) from the U.S. Food & Drug Administration (FDA) [44]. For example, a chimeric antigen receptor (CAR)-T cell therapy for acute lymphoblastic leukemia was approved in 2017 which is engineered with a lentiviral vector [45]. Additional developments with CAR-T cells are in the way for the treatment of cutaneous T cell lymphomas as well [46]. The engineering of CAR-T is one of the most important clinical uses of lentiviral vectors at the moment [47]. Despite their huge success, also non-CAR immunotherapeutic approaches for malignancies are reported [48]. The

Table 1.4

Characteristics of most common viral vectors used in gene therapy. Modified from Ref. [52].

		Adenovirus (Ad)	Adeno-associated virus (AAV)	Retrovirus/ Lentivirus (LV)	Vaccinia virus	Herpesvirus	Alphavirus
Virus particle properties	Genome	dsDNA	ssDNA	ssRNA(+)	dsDNA	dsDNA	ssRNA(+)
	Capsid	Icosahedral	Icosahedral	Icosahedral	Complex	Icosahedral	Icosahedral
	Coat	Naked	Naked	Enveloped	Enveloped	Enveloped	Enveloped
	Polymerase	Negative	Negative	Positive	Positive	Negative	Negative
	Virion diameter	70–90 nm	18–26 nm	80–130 nm	170–200× 300–450 nm	150–200 nm	60-70 nm
	Family	Adenoviridae	Parvoviridae	Retroviridae	Poxviridae	Herpesviridae	Togaviridae
	Genome size	39 kb	5 kb	3–9 kb	130-280 kb	120–200 kb	12 kb
Gene therapy properties	Infection/ tropism	Dividing and non-dividing cells	Dividing and non-dividing cells	Dividing cells[a]	Dividing and non-dividing cells	Dividing and non-dividing cells	Dividing and non-dividing cells
	Host genome interaction	Non-integrating	Non-integrating[b]	Integrating	Non-integrating	Non-integrating	Non-integrating
	Transgene expression	Transient	Potential long lasting	Long lasting	Transient	Potential long lasting	Transient
	Packing capacity	7.5 kb	4.5 kb	8 kb	25 kb	>30 kb	7.5 kb

[a] LV can also infect non-dividing cells

[b] AAV can integrate with low frequency into chromosome 19

use of stem cells for the treatment of inflammatory disorders and other ailments such as stroke are described [49–51].

Although cell therapies are not directly relevant to this work, CAR-T cell therapies heavily rely on lentiviral vectors, whose manufacturing processes face the same drawbacks of traditional purification methods as many other viruses, i.e., loss of biological activity and low product recoveries [1].

1.2.1 Adeno-associated virus

Belonging to the Parvoviridae family, AAV was first discovered in 1965 as a co-infecting agent of Adenovirus, hence its name. On its own, AAV is replication-defective and in order to replicate in the cell, it requires either the presence of a helper virus — e.g., herpes virus or adenovirus (Ad) — or some form of genotoxic stress.

AAV is a made of a non-enveloped, icosahedral protein shell of around 22 nm (Figure 1.4) comprised of three structural proteins VP1, VP2, and VP3. There are many serotypes, each with its own capsid and host-cell receptors with particular tropisms (Table 1.5). AAV is a single-stranded DNA virus with a 4.7 kb genome (Table 1.4). In the absence of helper virus, AAV-2 can set up latency by integration into chromosome 19q13.4, making it the only mammalian DNA virus known to be capable of site-specific integration [53].

AAV is currently one of the most frequently used viral vectors for gene therapy. The fact that AAV is not pathogenic, inhibited initially its broad use as a gene vector. It has, however, been used extensively in clinical trials for several ailments including Parkinsons's
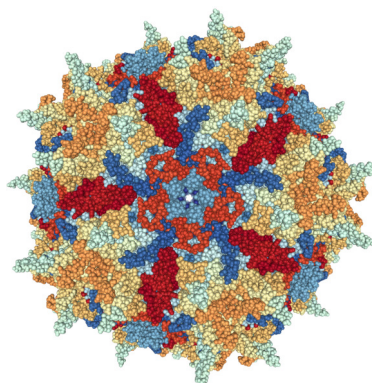
Figure 1.4. The adeno-associated virus capsid, about 22 nm in diameter. Protein Data Bank entry: 1LP3.

Table 1.5
Adeno-associated virus (AAV) wild-type serotypes and their tropisms. Adapted from Ref. [54]. The serotypes marked with an asterisk (*) were purified in this work.

Serotype	Skeletal muscle	CNS/Retina	Heart	Lung	Liver
AAV-1*	×	×	×	×	
AAV-2*	×	×			×
AAV-3		×	×		×
AAV-4		×	×		
AAV-5		×		×	
AAV-6*	×		×	×	×
AAV-7	×	×			×
AAV-8*	×	×			×
AAV-9	×	×	×	×	×
AAV-10		×		×	

disease, hemophilia B, muscular dystrophy, heart failure, prostate cancer, vision loss, and epilepsy, to name a few [53, 55, 56].

Prior exposure of natural AAV variants leads to anti-AAV neutralizing antibodies. In fact, 80–90% of the population is seropositive to AAV-2, but the discovery of new serotypes suggests that preexisting immunity is not a significant barrier to therapy [53]. Santiago-Ortiz et al. provide an extremely detailed account of AAV vectors used in models of cancer [57].

Transfection of plasmid DNA into eukaryotic cells was the first and still remains the most commonly used method for production of recombinant adeno-associated virus (rAAV) in both development laboratories and for clinical grade manufacturing. The triple transfection (or two-helper) method is widely used; typically up to 80% of cells are transfected and the virus titer peaks at 48–72 hours. This transient strategy uses either adherent or the less commonly used suspension HEK293 cells. The first plasmid has the transgene of interest flanked by inverted terminal repeat (ITR) sequences, which have essential elements for genome replication and packaging. The second plasmid contains the rep (for the expression of viral enzymes) and cap (for the expression of structural proteins) genes. Finally, the adenoviral helper plasmid expresses the genome replication helper functions [58, 59].

The recovery of AAV is done typically from cell lysates although in some cases AAV has been recovered from cell supernatant. After clarification steps that usually comprise centrifugation and filtration, the main purification steps are done. Among them, density gradient ultracentrifugation is the most used in research environments. Both iodixanol and $CsCl_2$ can be used, but iodixanol is preferred over its higher particle yields [60]. More recently, a universal affinity resin (POROS CaptureSelect AAVX) based on camelid antibodies has shown high selectivity for a broad range of naturally occurring and synthetic AAV serotypes [61]. Empty capsids present in the product are not desirable and are often separated from packed capsids with IEC [62, 63].

The amount of viral vectors needed for extensive preclinical studies (e.g., toxicology, safety, dose) often reach 10^{15}–10^{16} particles. Although the manufacturing of these amounts is technically feasible and has been done in the past, it represents a monumental task when using the current production and purification systems. For example, generating 10^{16} AAV particles would require more than 500 cell factories, which is not a viable option for most facilities. Clément and Grieger [58] report a list of institutions and AAV manufacturing facilities and their production methods.

Challenges with the production of rAAV are the scalability of current systems, speed, and lack of adequate manufacturing facilities with a regular product output.

1.2.2 Vaccinia virus

Smallpox is caused by two closely related viruses, variola minor and variola major, that can be distinguished from each other by PCR analysis. Both viruses are similar clinically, but variola minor is associated with milder symptoms and far fewer deaths (1% compared to 20–30%) [64].

Variola virus belongs to the family Poxviridae, genus *Orthopoxvirus*, which includes vaccinia, monkeypox, cowpox, camelpox, and ectromelia (mousepox). The poxvirus genome is the largest of all viruses than infect humans and is contained in an ovoid brick-shaped structure (Figure 1.5) with approximate dimensions of 170–200×300–450 nm, consisting of a single dsDNA molecule of nearly 200 kb. In contrast to most other DNA viruses, variola virus multiplies in the cell cytoplasm rather than in the cell nucleus [7].

MVA is a live, non-replicating form of vaccinia virus that was developed in Germany in the 1950s and 1960s. It was originated from a Turkish vaccine strain and was derived by more than 500 serial passages in primary chick embryo fibroblasts, which resulted in the loss of around 15% of its genome and its ability to replicate in most mammalian cells.

MVA virus has been used as a third generation vaccinia vaccine (attenuated vaccines), as vector vaccine against other infectious targets [65] and cancer [66], and as a gene therapy vector [67].

IMVAMUNE is an MVA-based vaccine developed by Bavarian Nordic available as a frozen liquid suspension with at least 5×10^7 tissue culture 50% infective dose (TCID$_{50}$) formulated in 10 mM Tris, 140 mM NaCl, pH 7.4 [64].
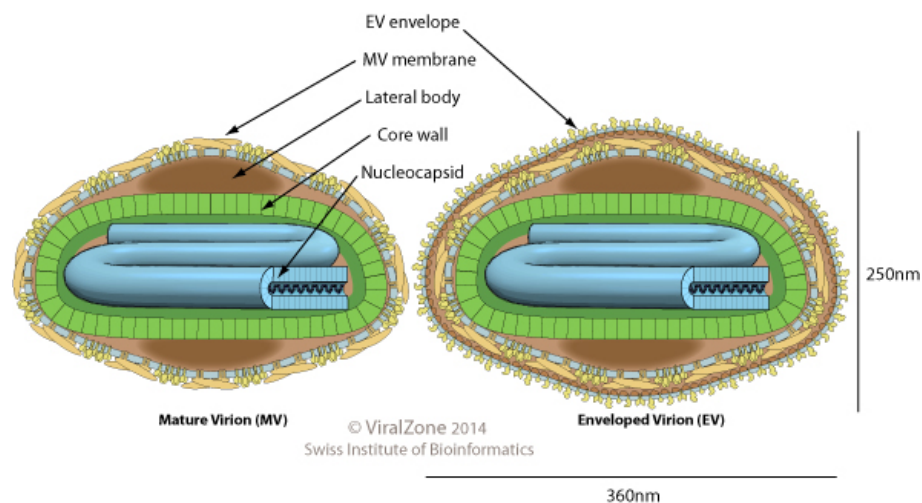
Figure 1.5. The Poxviridae virion, 220–450 nm long and 140–260 nm wide. Source: ViralZone; www.expasy.org/viralzone, Swiss Institute of Bioinformatics.

1.2.3 Extracellular vesicles

EVs are lipid bilayers than can be found in all body fluids and are secreted by almost all cell types. EVs have gained significant attention in several areas of biology. Since their discovery over 30 years ago, it has become clear that EVs are regulators of the cellular niche and that they can be used as biomarkers [68–75] and therapeutic delivery vehicles [76–83].

EVs can be separated in subpopulations based on their size and origin mechanisms. Exosomes are around 30–120 nm in diameter and are released into the extracellular space when intracellular multivesicular bodies (MVBs) fuse with the plasma membrane. Ectosomes (100–1000 nm) and apoptotic blebs (1–5 µm) are vesicles shed directly from the cell membrane. Exosomes perform diverse cellular functions including antigen presentation, intercellular communication, and transfer of proteins and nucleic acids [84].

Effective isolation of EVs remains challenging. Typical strategies include precipitation with PEG [79, 85], pseudo-affinity chromatography [86], immunoaffinity capture [84], density gradient ultracentrifugation [84, 87], and size exclusion chromatography (SEC) [88]. Semicontinuous multi-column approaches have also been reported [89]. A comparison between purification methods are discussed by Xu et al. [90]. Typical recoveries are 1–10 µg per mL of culture supernatant [91].

The therapeutic potential of exosomes has to be matched to the appropriate technologies to produce them. Unfortunately, centrifugation methods are time consuming and SEC is not well suited for processing large sample volumes.
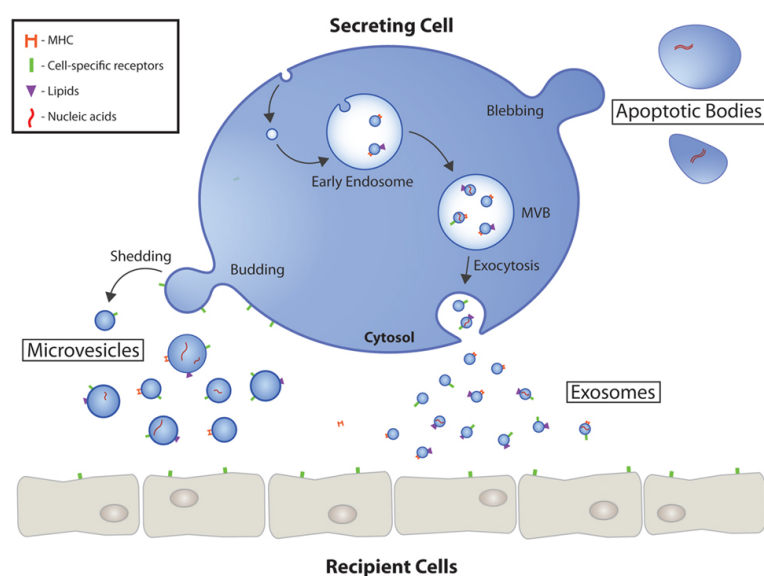
Figure 1.6. Classification and origin of extracellular vesicles. Reproduced with permission from Ref. [92].

1.3 Molecular crowding and the Schellman paradox

This section explains molecular crowding, which causes the interaction mechanisms behind SXC. With this theoretical basis, the technical execution of SXC is further described in Section 1.4.

The theory described below is based mainly on a thorough description by Timasheff [93] and supported by several other authors cited where appropriate.

Biological solutions typically contain a high total concentration of soluble macro-molecules. Take, for instance, the interior of a *Escherichia coli* cell, where the total concentration of protein and DNA is in the range of 300–400 $g\,L^{-1}$. Sometimes, a single species at high concentration predominates, such as the hemoglobin protein inside red blood cells at around 350 $g\,L^{-1}$. This can also be observed in the extracellular matrix of tissues such as cartilage. Such media are referred as "crowded" rather than "concentrated" because, taken together, the macromolecules occupy a significant fraction of the total volume (20–30%) [94]. There is no molecular crowding in concentrations of 1–10 $g\,L^{-1}$ or less.

Crowding generates thermodynamic consequences on the properties of the system known as "excluded volume effects". These phenomena manifest themselves in several ways: affecting macromolecular equilibria, modulating the conformation and stability of biological macromolecules, and altering the rates of chemical reactions, protein folding, and macromolecular association, to name a few.

The interactions of proteins with weakly-binding ligands such as protein salting-out and crystallizing agents (e.g., ammonium sulfate), precipitants (e.g., PEG), denaturants (e.g., urea), stabilizers (e.g., sucrose), and solubilizers (e.g., polyols) have been of interest for around a century. The underlying interaction mechanisms were first described around 50 years ago with the theory of multicomponent solution thermodynamics. This theory explained systems with three components (water, protein, and ligand) in terms of the *preferential interaction parameter* or *thermodynamic binding* by Schellman [95, 96]. Strongly binding ligands like enzymes work at low concentrations ($<10^3$ M). For weakly acting ligands to have any effect, they must be used at high concentrations (0.5–1.0 M). Because of their high concentration, they can occupy as much as 30–40% of the solvent volume and thus are also called *co-solvents*. In three component analysis, preferential binding is given by positive binding stoichiometries and preferential exclusion by negative binding stoichiometries.

Consider a protein (P) immersed in a mixture with solvent (water, W) and co-solvent (weakly-binding ligand, L) at equilibrium:

$$P + L \rightleftarrows PL \tag{1.1}$$

with a binding constant:

$$K_b = [\text{PL}]/[\text{P}][\text{L}] \tag{1.2}$$

Classical binding theory predicts that the protein will be indifferent to whether it is in contact with either solvent or co-solvent molecules. For n equivalent sites, the binding isotherm is:

$$v_b = n\frac{K_b C_\text{L}}{1 + K_b C_\text{L}} \tag{1.3}$$

The free energy of binding is therefore given by:

$$\Delta G_b^0 = -nRT \ln\left(1 + K_b[\text{L}]\right) \tag{1.4}$$

If the system is indeed indifferent to whether the protein is in contact with either water or co-solvent, the departure of water from binding sites at the protein should be accompanied by a free energy change opposite in sign and equal in magnitude to the co-solvent takes its place ($\Delta G_b^0 = 0$). Treating such binding equilibriums with weakly interacting ligands can lead to puzzling results [93]. An example is depicted in Figure 1.7 as a Scatchard plot.

Thus, at any point in its surface, the "protein interacts with identical free energy with water or co-solvent" [93], say PEG, meaning that the solvent composition on the protein surface is the same as in the bulk solvent. Dialysis experiments at equilibrium, however, show different co-solvent concentrations inside the dialysis bag and the bulk solvent. The classical binding theory contradicts these experimental observations. This is known as "the Schellman paradox" [93].

Schellman resolved this paradox by the principle of exchange. As observed by dialysis equilibrium giving a preferential exclusion value, if the co-solvent is not at the protein surface, it is clear that the empty ligand site has to be occupied instead by water. The
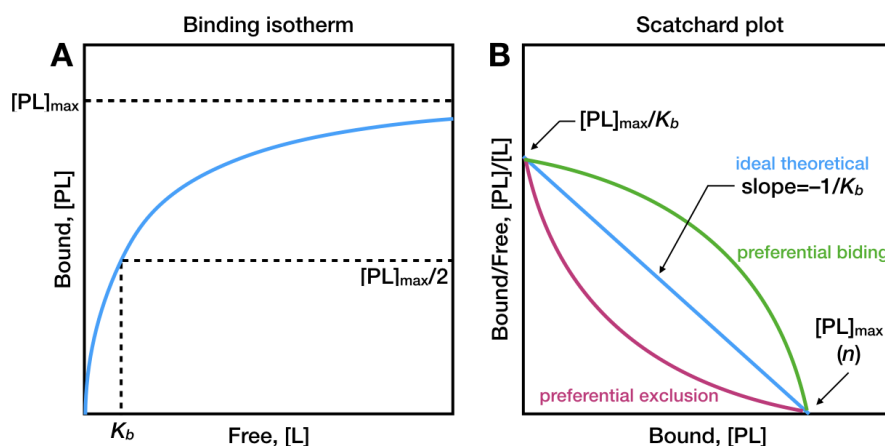
Figure 1.7. Binding isotherm and Scatchard plot. Weakly-binding ligands (co-solvents) deviate from ideal theoretical behavior and show curved responses in a Scatchard plot. For example, PEG displays preferential exclusion on protein surfaces (the protein becomes preferentially hydrated).

exchange of water at the site implies a change of free energy opposite in sign and equal in value to that of the co-solvent. This concludes that classical binding theory is incomplete and that water must be introduced explicitly into the stoichiometry:

$$P \cdot nH_2O + L \rightleftharpoons PL + nH_2O \tag{1.5}$$

The binding constant K_b is treated then as a relation between the binding constant of ligand (K_L) and the binding constant of water (K_W) and can be expressed as an exchange constant:

$$K_b = K_L/K_W \equiv K_{ex} \tag{1.6}$$

K_{ex} can be determined by dialysis equilibrium. The equation above pictures a hypothetical equilibrium on the protein site where either water or co-solvent binds. In this site exchange, ΔG_b^0 is:

$$\Delta G_b^0 = \Delta G_L^0 - \Delta G_W^0 \tag{1.7}$$

If $K_L > K_W$ (ΔG_L^0 more negative than ΔG_W^0), there is an excess of the ligand on the protein surface compared to the ligand concentration in the bulk solvent. This is defined as "preferential binding (of ligand)". On the other hand, when $K_W > K_L$, there is a lack of ligand on the protein surface and, based on the exchange concept, water molecules bind to those sites, so the protein becomes preferentially hydrated, i.e., "preferential exclusion (of ligand)". The derivation of the modified thermodynamic expressions are reported by Timasheff [93].

Schellman observes that the preferential binding/interaction is solely a thermodynamic measure of the relative interaction of the protein in aqueous solution with a third component (the ligand). If the interactions are strong, the typical definition of binding explained at the beginning applies, but with weakly-binding ligands the latter definition is used. Schellman defines the preferential interaction parameter as follows (Casassa and Eisenberg notation [97]):

$$\Gamma_{23} = \left(\frac{\partial m_3}{\partial m_2} \right)_{\mu_3} \tag{1.8}$$

where m is the molal concentration and μ the chemical potential. The numbers represent the system components in the Scatchard notation (1 for water, 2 for the protein, and 3 for the co-solvent). The preferential interaction parameter has also been expressed as $\bar{v}$ in the Scatchard notation [98] and stands for the reciprocal perturbation of the chemical potentials of protein and ligand, which means that "a molecule does not have to be in contact with a macromolecule to be bound to it" [93, 95] (there is no direct chemical bond/molecular contact). Γ_{23} can be interpreted as the amount of co-solvent molecules that have to be either added or subtracted from the protein solution to restore its chemical potential.

Table 1.6

Excipients commonly used in vaccine drug product and their expected impact [105].

Excipient	Examples	Impact on formulation
Salts	Ammonium sulfate, sodium chloride, calcium chloride, magnesium chloride, potassium chloride	Tonicity modifier
Buffers	Succinate, sodium phosphate, potassium phosphate, histidine, tris, HEPES	pH
Sugars and polyols	Cyclodextrin, sucrose, sorbitol, trehalose, mannitol, lactose, glycerol	Stabilizing effect
Amino acids	Arginine, proline, glycine, aspartic acid, glutamic acid	Stabilizing effect, bulking agents, aggregation modifiers
Surfactants (detergents)	Sodium lauryl sulfate, poloxamer 188/407, polysorbate (Tween) 20/80	Air surface interfaces, mitigation of surface adsorption
Antioxidants	Methionine, gluthathione, ascorbic acid	Prevention of oxidation
Polymers	Dextran, polyethylene glycol (PEG)	Bulking agents, freeze-point depressors
Preservatives	Methylparabens, chlorobutanol, 2-phenoxyethanol, m-cresol	Antimicrobials

These definitions above explain the consequences of molecular crowding [99]. PEG for example, is preferentially excluded from the surface of proteins and promotes their preferential hydration (negative value of Γ_{23}). Preferential hydration due to steric exclusion has some general rules. Notably, the co-solvents can stabilize the native structures of proteins. This occurs because co-solvents create a thermodynamically unfavorable situation that is relieved by reducing the surface area contact between protein and co-solvent by 1) shifting folding-unfolding equilibrium and 2) by molecular association. The magnitude of the change is proportional to solute size so bigger molecules are more affected than smaller ones.

Regarding shifting folding-unfolding equilibrium, it is common that aqueous sugar systems induce protein preferential hydration, leading to their structural stabilization [100, 101]. Similar observations have been made for glycerol and polyalcohols, leading to the use of several such molecules as excipients (Table 1.6) in virtually all biopharmaceutical formulations, and very often combined with freeze-drying. For example, in 2004, 46% of all biologics approved by the FDA were freeze-dried; in 2013, four out of the six top selling biologics were freeze-dried [102, 103]. Around 20% of freeze-dried reference materials were virus lysates, and 14% were live viruses [104].

On the other hand, molecular association relates to the known effect of PEG as a precipitant [96, 106–110] and has been widely applied for the purification of macromolecules, notably virus particles and VLPs [111–116]. PEG is a non-ionic polymer highly soluble in water by extensive hydrogen bonding.

1.4   Steric exclusion chromatography (SXC)

SXC is a separation method that exploits the effects of molecular crowding and weakly binding co-solvents on large biomolecules. To the authors' knowledge, the first report was published in 2012 by Lee et al. [117], where the authors used hydroxylated monoliths to purify large proteins (immunoglobulin G (IgG), immunoglobulin M (IgM)) and bacterio-phages by adding PEG to the protein and virus solutions before chromatography. Mildly hydrophobic, PEG is inert to most hydrophilic surfaces.

In order to understand SXC, consider an unpurified mixture of virus particles and contaminating proteins and DNA. If PEG is added to such solution, a thermodynamic destabilization takes place. Because the PEG is sterically excluded from the surface of the biomolecules, a PEG-deficient zone appears on their surface (the molecules get preferentially hydrated). The thickness of the PEG-deficient zone is proportional to the hydrodynamic radius of the PEG (dependent on its molecular mass). The bigger molecules (viruses) in the system will be more affected than the smaller ones (proteins). Additional variables accentuate these effects: increasing PEG concentration and size, increasing virus/protein concentration.

This system will shift to a new equilibrium by decreasing the contact area between the PEG-deficient zone and the bulk solvent, thereby promoting molecular association of the most affected molecules (viruses). Since PEG is also sterically excluded from
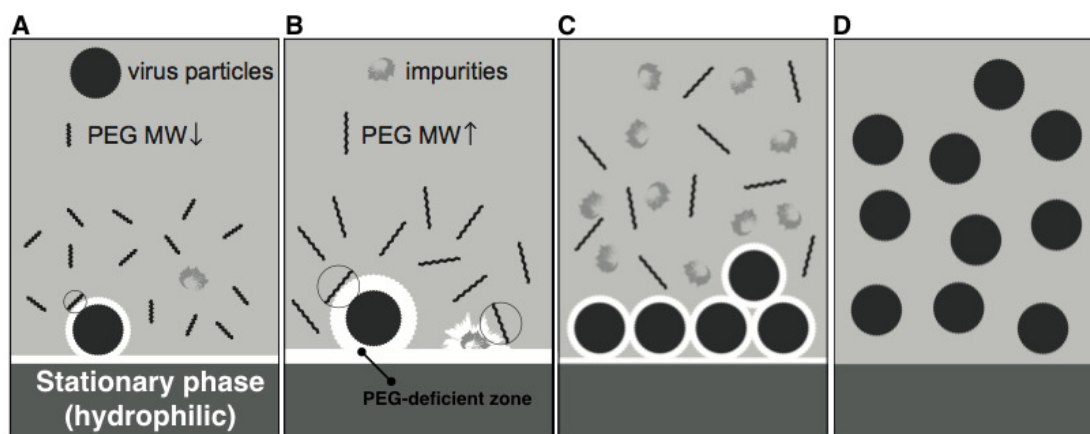
Figure 1.8. Mechanism of SXC. (A) Polyethylene glycol (PEG) is sterically excluded from the surface of macromolecules and the hydrophilic stationary phase, creating a PEG-deficient zone (white area) where the PEG concentration is lower compared to the bulk solvent. The size of the PEG-deficient zone is proportional to its hydrodynamic size (given by its mass). (B) At higher PEG concentrations, smaller molecules such as impurities are excluded too from the bulk solvent too from the bulk solvent. (C) The addition of PEG creates a thermodynamically unfavorable condition that is alleviated my minimizing the PEG-deficient contact area with the bulk solvent by the most affected molecules (virus particles) associating with each other and also at the stationary phase. There is no direct chemical interaction between and the unaffected smaller molecules (impurities) are washed away. (D) The purified virus particles are recovered by reducing the PEG concentration in the mobile phase and thus disrupting their interaction.

hydrophilic surfaces, if such a mixture is fed onto a hydrophilic stationary phase, the association between viruses and the hydrophilic surface will also be favored [117]. Smaller contaminants that are not affected by the presence of the PEG will not bind and get washed away. Finally, by removing the PEG from solution, this interaction is stopped and thus the purified virus particles can be recovered.

When used with convective stationary phases (i.e., monoliths and membranes), SXC seems to be a powerful technique for the purification of virus particles yielding high recoveries [118].

The increased viscosity due to the PEG is not a mass transfer issue with convective media. Moreover, monoliths and membranes have higher capacity in mass per surface because a solute mass increases by volume rather than by area. Beads in this sense are disadvantageous because diffusive restrictions with larger solutes hinders them from achieving surface saturation. Lastly, the absence of eddies in convective media reduces turbulent shear, which causes anti-parallel forces that can damage mechanically labile biomolecules. The advantages of convective media over diffusive media (i.e., porous beads) for the purification of large biomolecules like viruses are discussed extensively elsewhere [2, 119, 120].

In 2017, Marichal-Gallardo et al. reported the use of regenerated cellulose [121] membranes as an alternative stationary phase to hydroxylated monoliths for the purification of cell-based influenza A virus [122]. Subsequent reports [118, 123] detailed the successful chromatographic capture and purification of other viruses (e.g., YFV, AAV) and EVs that will be described in more detail in this work.

CHAPTER 2

Materials & Methods

For all experiments, ultrapure water from a Milli-Q® Advantage A10 water purification system (Merck; Darmstadt, Germany) was used. All chemicals had a purity of ≥99% unless stated otherwise. All solution concentrations expressed as percentage (%) are mass/volume (m/v), unless otherwise stated.

2.1 Analytical methods

2.1.1 Quantitation of total protein and host cell DNA

Total protein was measured using a Bradford BioRad assay (# 5000006; BioRad Laboratories; Hercules, USA). The calibration curve was made with bovine serum albumin (BSA) (# A3912; Sigma-Aldrich Chemie GmbH; Munich, Germany) in the range of 5–40 $\mu g\,mL^{-1}$ and had a limit of detection (LOD) of 0.4 $\mu g\,mL^{-1}$. Alternatively, a Quant-iT™ Protein Assay Kit (# Q33120; Life Technologies GmbH; Darmstadt, Germany) in the range of 250–5000 ng was used according to the manufacturer's instructions and had a LOD of 945.4 ng.

The concentration of dsDNA was estimated with a Quant-iT™ PicoGreen® assay (# P7581; Life Technologies GmbH; Darmstadt, Germany). The standard curve was made with lambda DNA (# D1501; Promega; Madison, USA) for the range of 4–250 $ng\,mL^{-1}$ (intermediate range) and had a LOD of 1.6 $ng\,mL^{-1}$. This assay is referred as "PicoGreen" hereafter. Alternatively, a Quant-iT™ DNA Assay Kit (# Q33210; Life Technologies GmbH; Darmstadt, Germany) in the range of 0–100 ng was used according to the manufacturer's instructions and had a LOD of 7.1 ng. This assay is referred as "PicoGreen Kit" hereafter.

The concentration of ssDNA was determined with a Threshold$^{®}$ Total DNA Assay Kit (# R9009; MDS Analytical Technologies; Sunnyvale, USA) using a workstation from the same manufacturer. The assay range was 6.2 to 4000 $pg\,mL^{-1}$ (low range) with a relative standard deviation (RSD) of $\leq 10\%$ according to the manufacturer.

2.1.2 Particle size distribution

Differential centrifugal sedimentation (DCS). Differential centrifugal sedimentation (DCS) analysis was performed as reported by Pieler et al. [124]. A CPS DC24000 UHR disc centrifuge (CPS Instruments Inc.; Los Angeles, USA) at 24 000 revolutions per minute (rpm) with 4–16% (m/v) sucrose gradient in 50 mM Tris, 150 mM NaCl, pH 7.4 buffer was used. The gradient consisted of nine 1.6 mL steps with different sucrose concentration each, i.e. 16%, 14.5%, 13%, 11.5%, 10%, 8.5%, 7%, 5.5%, and 4% sucrose (m/v), with a total volume of 14.4 mL. The gradient quality was evaluated by injecting a 239 nm particle standard (0.3–0.5% solid content, polyvinyl chloride, CPS Instruments Inc.; Los Angeles, USA) directly after gradient injection. Then, it was equilibrated for 10 min, followed by another 239 nm particle standard injection for measurement calibration. Finally, 100 µL of sample (1:1) were injected for the size distribution measurements of chromatography elution fractions. Additional density parameters for solutions and particles (ρ and ρ_p, respectively) introduced into the software were 1.072 $g\,cm^{-3}$ for the gradient buffer, 1.385 $g\,cm^{-3}$ for the calibration particles, 1.180 $g\,cm^{-3}$ for influenza A virus, 1.250 $g\,cm^{-3}$ for YFV [125], and 1.230 $g\,cm^{-3}$ for MVA virus. According to Pieler et al. [124], the particle size distributions are displayed as normalized weight average in percentage against apparent hydrodynamic diameter (d_h) in nm.

Dynamic light scattering (DLS). Samples were analyzed by dynamic light scattering (DLS) at room temperature with a Malvern Zetasizer Nano ZS90 (Malvern, Worcestershire, UK) equipped with a He-Ne laser (633 nm) using a 90° light scattering detector angle in disposable 100 µL cuvettes. Data analysis was done with the Malvern Zetasizer Software (version 7.12) using multiple narrow modes as data processing option. The refractive index and viscosity of the dispersant were assumed as 1.33 and 0.954 cP, respectively. All samples were measured undiluted and with 1:5 and 1:10 dilutions in phosphate buffered saline (PBS). These measurements were performed by Keven Lothert at the Technische Hochschule Mittelhessen in Giessen, Germany.

Nanoparticle tracking analysis (NTA). NTA was performed as reported by Steppert et al. [126] using a NanoSight instrument (Malvern Instruments Ltd., Worcestershire, UK). These analyses were done by Matthias Prömmel at IDT Biologika GmbH in Dessau, Germany.

2.1.3 Transmission electron microscopy

Transmission electron microscopy (TEM) of virus particles was done by negative staining. A solution containing virions was applied to glow-discharged carbon coated 400 mesh copper grids, and stained with 1% uranyl acetate. Alternatively, the solution was vitrified on cryo-electron microscopy sample preparation buffer. Virions were adsorbed to a continuous carbon film, attached to a Quantifoil (3.5/1) (Quantifoil, Jena, Germany) grid and freeze-plunged in a Leica EM GP (Leica, Wetzlar, Germany) employing the blotting sensor at 75% humidity and $-24\,°C$. Images were taken in a Philips CM120 electron microscope (Philips Inc.) using a TemCam F416 CMOS camera (TVIPS, Gauting, Germany). TEM experiments were performed by either Dietmar Riedel at the Max-Planck-Institute for Biophysical Chemistry in Göttingen, Germany or Martin Obr at the Heidelberg University Hospital in Heidelberg, Germany.

2.1.4 Size-exclusion chromatography

SEC for analytical and preparative experiments was made with a packed-bead Superdex 200 Increase 10/300 GL (# 17517501; GE Healthcare; Uppsala, Sweden) column in the same chromatography system used for SXC (Section 2.2.6). The sample injection volumes ranged 100–500 µL and the flow rate ($\dot{Q}$) was 0.75 mL min^{-1}.

2.1.5 Influenza virus quantitation

Influenza virus quantitation by hemagglutination activity (aHA) assay. The virus content was estimated by titration of viral HA as previously described by Kalbfuss et al. [127]. The aHA values are reported as hemagglutination units (HAU) $(0.1\ \mathrm{mL})^{-1}$. The RSD of duplicate measurements was $\leq13.3\%$.

Influenza virus antigen quantitation by single radial immunodiffusion (SRID) assay. Total HA protein content was quantified by a SRID assay as previously reported by Wood et al. [128]. Samples were dialyzed as mentioned above and lyophilized using 1% sucrose as cryo-protectant. Resuspension was made by adjusting the HA content of the samples to the HA content of a reference produced in-house as described by Opitz et al. [129]. The assay setups consisted of a 7×7 diffusion matrix made out of a 1% agarose gel with 64 µg$_{\mathrm{anti\ A/PR\ antigen}}$ mL^{-1} (# 03/242; NIBSC; Hertfordshire, UK). Measurements are reported in µg$_{\mathrm{HA}}$ mL^{-1}. The RSD of duplicate measurements was $\leq17.3\%$.

Infectious titer by TCID$_{50}$. For the quantification of infectious influenza virus particles, a TCID$_{50}$ assay was used as described by Genzel et al. [130]. Cell free, sterile supernatant was stored until measurement at $-80\,°C$. Confluent MDCK cells (# 84121903; European Collection of Animal Cell Cultures (ECACC); Public Health, Salisbury, UK) cultivated in 96 well plates were infected with a serial dilution of virus samples and incubated for 24 h ($37\,°C$, 5 % CO_2). MDCK cells were then fixed with an ice cold acetone solution (80%),

stained with an anti-influenza A/PR/8/34 H1N1 HA serum (# 03/242; NIBSC; Ridge, UK) and an Alexa Fluor donkey anti-sheep IgG antibody (# A11015; Thermo Fisher Scientific; Waltham, USA) as a secondary fluorescence label. Fluorescence positive and negative wells were counted using a fluorescence microscope (Axio Observer.A1, Zeiss, Oberkochen, Germany) and infectious titer was calculated from eight replicates. Results are reported as $TCID_{50}$ mL^{-1}.

2.1.6   Yellow fever virus quantitation

Infectious titer by plaque assay. Infectious virus titer was determined by a modified plaque assay from Bae et al. [131]: porcine kidney stable epithelial (PS) cells — kindly provided by M. Niedrig, Robert-Koch Institute, Germany — were seeded in 24-well plates at 4×10^5 cells $well^{-1}$ together with unknown samples and incubated at $37\,°C$ for 4 h. Afterwards, each well was overlaid with 1.6% carboxyl-methyl-cellulose in Z-Medium (composition in Section 2.2.2) and incubated at $37\,°C$ for 4 days. Subsequently, the cell monolayer was fixed with 3.7% (v/v) formaldehyde in PBS for 15 min and stained with napthalene black (1 g naphthol blue black, 13.6 g sodium acetate, and 60 mL glacial acetic acid completed to 1 L with water) for 30 min. Plaques were counted and titers expressed as plaque forming units (PFU) mL^{-1} in accordance to de Madrid & Porterfield [132].

2.1.7   Adeno-associated virus quantitation

Biological activity of AAV. Susceptible cells (e.g., HEK-293T or SF539) were feed with AAV particles (in different dilutions in a total volume of 80 µL per well in 96-well plates) and transduction rates and mean fluorescence intensity of the reporter transgene-encoding AAV vector were determined by microscopy. The cells were incubated for 36–48 h at $37\,°C$ and 5% (v/v) CO_2 in a humidified atmosphere. Positive cells were determined by flow cytometry as reported by Herrmann et al. [133].

Cleavage and polyadenylation specificity factor subunit 6 (CPSF6) knockdown was evaluated by transduction of U87 cells as reported by Bejarano et al. [134] with wild-type AAV-6 and DJP2 encoding the non-silencing (NS) short hairpin RNA (shRNA) with a cyan fluorescent protein (CFP) reporter or triple-shRNA cassettes (shCPSF6a&b). The two vectors (wtAAV6 and DJP2) encode the NS shRNA with either a CFP reporter or triple-shRNA cassettes (shCPSF6a&b) in order to knockdown CPSF6. Additionally, transduction of monocyte-derived macrophages (MDM) from two different human donors was performed [134]. Transduction experiments were made by Kathleen Börner and David Bejarano at the Heidelberg University Hospital in Heidelberg, Germany.

AAV particle count by PCR. Viral genome quantification was done by quantitative real-time PCR (qRT-PCR) as reported previously by Börner et al. [135] using a thermo cycler ABI7500 (Applied Biosystems) and Power SYBR® Green PCR Master Mix (Applied

Biosystems). All reactions were made in triplicates in a final volume of 25 µL. Alternatively, Droplet Digital™ PCR (ddPCR) was made as described by Hermann et al. [133] using a QX200 ddPCR system (BioRad Laboratories; Hercules, USA. Titers are reported as viral genomes (vg) mL^{-1}.

2.2 Experimental methods

2.2.1 Influenza virus production

Production of influenza virus was made in suspension MDCK (MDCK$_{sus}$) cells using several systems. The process diagrams can be found in the Appendix A.

Production in a 5 L stirred tank reactor (STR). The production of influenza virus A/Puerto Rico/8/34 H1N1 (Robert Koch-Institute; Germany) was made as reported by Marichal-Gallardo et al. [122] using a 5 L STR with MDCK$_{sus}$ cells grown in chemically-defined SMIF8 medium. The process diagram is shown in Figure A.1.

Production of several influenza virus strains in shaker flasks. The production of influenza virus strains A/Puerto Rico/8/34 H1N1, A/Switzerland/9715293/2013 H3N2 (National Institute for Biological Standards and Control (NISBC); Hertfordshire, UK), and B/Phuket/3073/2013 (Yamagata) (NISBC; Hertfordshire, UK) were produced as reported by Fortuna et al. [136] in shaker flasks of 600 mL with MDCK$_{sus}$ cells grown in chemically-defined SMIF8 medium. The process diagram is shown in Figure A.2.

Production in a 1 L fed-batch/perfusion alternating tangential flow (ATF) system. Influenza virus A/Puerto Rico/8/34 H1N1 was also produced in a fed-batch/perfusion ATF system as reported by Vázquez-Ramírez et al. [137]. Avian AGE1.CR.pIX suspension cells were grown using chemically defined CD-U3 medium. The virus particles were harvested from the 0.65 µm ATF module.

Production in a 1 L STR with Xeno™ chemically-defined medium. The following is a description of the optimized suggested process detailed in Figure A.4. The virus production was performed by Thomas Bissinger and Yixiao Wu (from East China University of Science and Technology, Shanghai, China) at the Max-Planck-Institute for Dynamics of Complex Technical Systems. *Cell culture and virus production.* A MDCK$_{sus}$ cell line was previously generated by adapting adherent MDCK (MDCK$_{adh}$) cells (NBL-2, ATCC® CCL-34™) to grow in single-cell suspension in serum-free medium [138]. This suspension cell line was adapted over four passages to a newly developed chemically-defined medium referred here as "Xeno-CD" (BioEngine Sci-Tech; Shanghai, China). All cell culture experiments described in this work were made with the MDCK$_{sus}$ cell line adapted and grown in the Xeno-CD medium. Influenza virus A/Puerto Rico/8/34 H1N1 was propagated in MDCK$_{adh}$ cells (# 84121903; ECACC) and adapted for five passages to the MDCK$_{sus}$ cell line described above using a multiplicity of infection (MOI) of 10^{-5}. This adapted

virus, called "seed virus" hereafter, was used to perform all infections and had a $TCID_{50}$ titer of 1.8×10^9 virions mL^{-1}.

For small scale experiments, MDCK cells were cultivated in either 125 or 250 mL shake flasks (# 431143; # 431144; polycarbonate Erlenmeyer Flask, Corning®) with either 30 or 60 mL working volume at $37\,°C$, 5% CO_2 atmosphere, and shaking frequency of 100 rpm (Multitron Cell, Infors HT; 25 mm shaking throw). Cells were passaged every three days with a seeding density of 0.5×10^6 cells mL^{-1}.

$MDCK_{sus}$ were cultivated in 1 L DASGIP STR with a working volume of 300–600 mL (# 76DS0700ODSS; Eppendorf). The bioreactors were controlled by a DASGIP Parallel Bioreactor System (# 76DG04CC, Eppendorf) using the DASware control software (# 76DGCS; Eppendorf). A macrosparger with an air-oxygen mixture was used for aeration. pH was controlled by CO_2 flow to the sparger and by addition of a 1 M NaOH solution. A single 30 pitched 3-blade stirrer (O.D. mm) at 80 rpm was used for agitation.

The infection of the cell culture with influenza virus was carried out as follows: The cells were diluted to 5×10^6 cells mL^{-1} with fresh Xeno-DM medium, followed by the addition of trypsin (# 27250-018; Gibco; 5000 U mL^{-1} stock) to a final concentration of 30 U mL^{-1}. Finally, the seed virus was diluted with PBS and added to the cell suspension at a MOI of 10^{-3}. After infection, samples named hereafter as "virus broth" were taken at several time points expressed as hours post infection (hpi). *Virus harvest and sample conditioning.* The virus broth was harvested by centrifugation at 800 relative centrifugal force (rcf) for 10 min at $4\,°C$ in order to remove cells and cell debris. The supernatant was clarified by a 0.45 µm filtration. This "clarified virus harvest" was chemically inactivated with β-propiolactone (# 33672.01; Serva Electrophoresis; Heidelberg, Germany) added to a final concentration of 6 mM and incubated at $37\,°C$ for 24 h with or without an enzymatic nucleic acid digestion prior to inactivation.

The enzymatic DNA digestion was carried out with an unspecific nuclease by supplementing the sample with magnesium chloride (# M8266-1KG; Sigma-Aldrich Chemie GmbH; Munich, Germany) to a final concentration of 2 mM, 10 units mL^{-1} Denarase® (named "Denarase" hereafter, #2DN100KU99; Sartorius Stedim Biotech; Göttingen, Germany). The sample was incubated under mixing for 24 h at $37\,°C$.

Following inactivation, the material was further 0.2 µm clarified and stored at $-80\,°C$ until further use.

2.2.2 Yellow fever virus production

Cell culture and virus production. YFV production was made by Luiz F. Almeida (from Federal University of Rio de Janeiro, Brazil) at the Max-Planck-Institute for Dynamics of Complex Technical Systems. Two different YFV substrains from the parent 17D strain were used: 17D-204, used in several of the commercial YF vaccines, obtained from the

Robert-Koch Institute (Berlin, Germany), and 17DD from a commercial vaccine produced by Bio-Manguinhos of the Oswaldo Cruz Foundation (FIOCRUZ; Rio de Janeiro, Brazil). Both viral substrains were propagated in a mammalian-based platform as follows, with at least three biological replicates per experiment unless otherwise noted.

Vero cells from the WHO certified cell bank were obtained from the ECACC (# 88020401) and originally grown in "Z-medium", comprised of Glasgow Minimum Essential Medium (GMEM) (# 22100093; Gibco, USA) containing 10% (v/v) fetal bovine serum (# F7524; Sigma-Aldrich Co. LLC.; St. Louis, USA), 2% lab-FMV peptone (# MC033; Lab-M Ltd.; Heywood, UK,), 2 mM L-glutamine, and 2 mM pyruvate. Cells were subsequently adapted to serum-free conditions by culture in OPTI-MEM Glutamax (# 51985034; Thermo Fischer Scientific; Massachusetts, USA) and a working cell bank was produced.

For virus production, cells were grown in either T-flasks (# 7356-50EA, Greiner Bio One International GmbH; Frickenhaussen, Germany) or roller bottles (# 5668-0170, Greiner Bio One International GmbH; Frickenhaussen, Germany) at $37\,°C$ and 5% (v/v) CO_2.

Infection was carried out on the 5th day post-inoculation with viral seed banks of either the 17D-204 ($7.15\log_{10}\pm0.26\,\mathrm{PFU\,mL^{-1}}$) or the 17DD ($7.70\log_{10}\pm0.14\,\mathrm{PFU\,mL^{-1}}$) substrains: the supernatant was discarded and cells were infected with a MOI of 2×10^{-3} $\mathrm{PFU\,cell^{-1}}$. After 1 h of virus adsorption at $34\,°C$, fresh medium was added and cells incubated under 5% (v/v) CO_2 atmosphere. The cultivation was stopped latest at 96 hpi and the liquid phase was named "virus broth" hereafter.

Virus harvest and sample conditioning. The virus broth was harvested by centrifugation at 10 000 rcf for 20 min at room temperature; this sample is named "virus harvest" hereafter. Virus harvests were optionally chemically inactivated: inactivated samples were spiked with 37% (v/v) formaldehyde (#252549-1L; Sigma-Aldrich Chemie GmbH; Munich, Germany) to a final concentration of 0.5% and incubated for at least 12 h at $4\,°C$ without mixing.

Depending on its volume, the virus harvest was clarified either with 0.2 μm surfactant-free cellulose acetate syringe filters (# 16534K; Sartorius Stedim Biotech; Göttingen, Germany) or 0.2 μm regenerated cellulose filters (# 10410314; GE Healthcare; Uppsala, Sweden) fitted to a reusable bottle top device (# 528199-325; VWR; Radnor, USA). This sample is named "clarified virus harvest" hereafter.

Clarified virus harvests were optionally treated with nuclease for DNA digestion by supplementing with magnesium chloride (# M8266-1KG; Sigma-Aldrich Chemie GmbH; Munich, Germany) to a final concentration of 2 mM, 10 $\mathrm{Units\,mL^{-1}}$ Denarase and incubated under mixing for ≥1 h at room temperature. Next, the sample was either stored at $4\,°C$ for ≤4 h before chromatography or spiked with sucrose (# 84100; Sigma-Aldrich Chemie GmbH; Munich, Germany) to a final concentration of 8% and frozen at $-80\,°C$ for longer term storage.

Stability of infectious YFV. In order to investigate how some experimental parameters might influence the infectivity of clarified virus harvests, a central composite face experimental design was planned using the software MODDE version 11 (Umetrics; Malmö, Sweden). The following factors were tested: number of freeze-thaw cycles (0–4), stabilizer (sucrose) concentration (0–8.5%), incubation time (0–8 h), and incubation temperature (4 and $22\,°C$). The infectious virus titer quantified by plaque assay was the only measured response, expressed as a percentage normalized against a positive control consisting of a clarified virus harvest spiked with 8% sucrose and frozen immediately at $-80\,°C$. The 17DD substrain was used as the model virus for these stability experiments.

2.2.3   Adeno-associated virus production

These production of AAV vectors was done by Kathleen Börner at the Heidelberg University Hospital in Heidelberg, Germany. Small-scale AAV vector stocks named "crude lysates" were prepared by seeding in 6-well plates 3.5×10^5 HEK-293T cells per well in 4 mL Dulbecco's Modified Eagle Medium (DMEM). Cells were incubated at $4\,°C$ and 5% CO_2 for 24 h.

A "transfection mixture" with a required volume of 390 µL per well of DMEM without supplements was prepared by adding equal amounts of the adenoviral helper plasmid, the AAV helper plasmid 13 (encoding rep and cap genes), and the AAV vector construct encoding a reporter gene driven by the cytomegalovirus (CMV) promoter; 1.3 µg per plasmid were added, totaling 4 µg of DNA. Afterwards, 8 µL (per well) of TurboFect transfection reagent were added. The transfection mixture was vortexed and incubated for 15 min at room temperature. Each well was transfected with 400 µL of the transfection mixture and the cells incubated for 72 h.

Afterwards, the cells were transferred to 15 mL tubes and centrifuged at 1500 rcf for 15 min; the supernatant was removed and the cells re-suspended in 300 µL of PBS and transferred to 2 mL tubes followed by 5 cycles (5 min each) of freezing and thawing in order to lyse the cells with a $37\,°C$ water bath and liquid nitrogen. Lastly, the lysed cell solution was centrifuged at $10\,000$ rcf for 10 min to remove cell debris. The supernatant containing virus particles was frozen at $-80\,°C$ until further processing and was filtered by 0.45 µm before SXC.

2.2.4   Vaccinia virus production

MVA virus with a green-fluorescent-protein insertion cassette (from ProBioGen AG, Germany) was produced by Felipe Tapia in a two-stage semi-continuous STR cascade using avian AGE1.CR.pIX cells grown in chemically-defined CD-U3 medium (cultivation process detailed in: https://doi.org/10.1371/journal.pone.0182553.g001) [139]. The virus harvest was 0.8 µm filtered and stored at $-80\,°C$ until further processing.

2.2.5 Production of extracellular vesicles

The starting material for the purification of EVs were supernatants from suspension MDCK, BHK, and HEK-293T cells from regular passaging procedures. The cell cultures were sequentially centrifuged at 500 rcf and 1000 rcf for 15 min each, and filtered by 0.45 µm and 0.2 µm, except for BHK cells which were centrifuged with an additional third 8000 rcf step and only filtered by 0.45 µm. The clarified supernatants were stored at $-20\,°C$ until processing. The centrifuged BHK cells supernatants were provided by Matthias Prömmel at IDT Biologika GmbH in Dessau, Germany.

2.2.6 SXC

The chromatography experiments were performed with an ÄKTA Pure 25 (GE Healthcare; Uppsala, Sweden) liquid chromatography system. UV absorbance was monitored at 280 nm and virus particles were monitored with a NICOMP^{TM} 380 (Particle Sizing Systems; Santa Barbara, USA) submicron particle analyzer at 632.8 nm. All chromatography experiments were performed at room temperature. Alternatively, some experiments were performed with an ÄKTA start system or manually with a syringe.

Membrane-based SXC was performed as reported by Marichal et al. [122]. All virus samples were either mixed with a 32% PEG-6000 (#81260-5KG; Sigma-Aldrich Chemie GmbH; Munich, Germany) stock solution prior to chromatography or with a PEG stock in-line (either 16% or 20% PEG-6000 (#81260-5KG; Sigma-Aldrich Chemie GmbH; Munich, Germany)). The SXC columns consisted of a stack of 1.0 µm regenerated cellulose membranes (# 10410014; GE Healthcare; Uppsala, Sweden) (15–20 layers; 75–100 cm^2 total surface, S_{col}) fitted into commercial 25 mm (d) stainless steel casings as described before [122] (Figure 2.1). Smaller devices of 13 mm were also used as described before [122] and are mentioned where appropriate. Additionally, 1.2 µm cellulose acetate membranes (# 10403012; GE Healthcare; Uppsala, Sweden) were used with the same devices described above. The maximum flow-rates used with the 2.5 mm filter housing was 15 mL min^{-1} and with the 13 mm housing was 10 mL min^{-1}.

SXC was also performed with commercial 0.34 mL CIM^{TM} OH (# 210.8140; BIA Separations; Villach, Austria) monoliths (named "OH monoliths" hereafter) as described before [122] and with 3D-printed cellulose monoliths kindly provided by Tim Huber and Conan Fee from the University of Canterbury in Christchurch, New Zealand. These monoliths (1 cm×10 cm, width×height) were mounted inside a Tricorn 10/150 column (# 28406416; GE Healthcare; Uppsala, Sweden) and were manufactured as reported by Huber et al. [140] with pore sizes of either 400 µm or 500 µm. The maximum flow-rate used with the 3D-printed monoliths was 15 mL min^{-1}. Additionally, membrane holders with a capacity of 200–1000 cm^2 were manufactured in 316 stainless steel with the kind
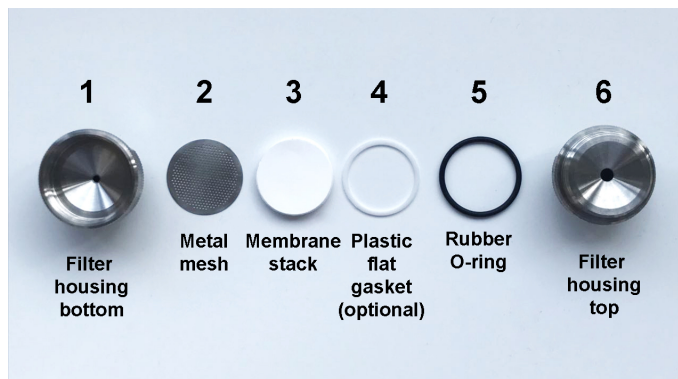
Figure 2.1. Assembly of purification column (2.5 cm in diameter) used for SXC.

assistance of Dr. Janitzio Marichal-Hidalgo (Coatzacoalcos, Mexico) and the staff of the mechanical workshop at the Max-Planck-Institute Magdeburg.

The SXC purifications were carried out in bind-elute mode. Briefly, (A) Equilibration: the column was washed with 10 column volumes (CV) of water followed by 10 CV of "SXC equilibration buffer" (50 mM Tris-HCl, 150 mM sodium chloride, 8% PEG-6000, pH 7.4). (B) Sample injection: the sample was then loaded onto the column followed by a wash step with equilibration buffer until baseline UV absorbance was achieved. (C) Elution: virus particles were recovered by washing with up to 25 CV of Tris buffer (50 mM Tris-HCl, 150 mM sodium chloride, pH 7.4). Alternatively, also PBS was used a buffer system at the PEG concentrations and mentioned were appropriate. Elution pools were spiked with sucrose at a final concentration of 2% before freezing at $-80\,°$C.

Alternatively to the purification of virus particles and EVs, several commercial purified proteins from Simga-Aldrich Chemie GmbH (BSA, IgM, IgM, and mucin from porcine stomach) were loaded at 8% PEG-6000 to a 100 cm^2 device as described above (with Tris as buffer system in all steps). Instead of a step elution, a decreasing PEG concentration gradient was made to 50 mM Tris-HCl, 150 mM sodium chloride, pH 7.4 (%B) in the following steps: 60%B, 5 CV; 75%B, 10 CV; 75%B, 5 CV; 85%B, 10 CV; 85%B, 2.5 CV; 100%B, 10 CV).

For mass balances and estimations of recovery, yield, and productivity of the SXC step, the equations described below were used.

The total mass of component A was calculated as:

$$q_A = \sum_{i=1}^{F} [A]_i \cdot V_i \tag{2.1}$$

where $[A]_i$ is the concentration of component A in fraction i, V_i the volume of fraction i, and F the total number of fractions.

The percentile recovery of component A was estimated as:

$$\zeta_A = \left(q_A^{\text{out}}/q_A^{\text{in}}\right) \cdot 100 \tag{2.2}$$

where q_A^{in} is the total mass of component A in the SXC feed and q_A^{out} the total mass of component A recovered in all chromatography fractions (i.e., flow-through, wash, elutions).

Based on Equation 2.1, the mass of component A recovered in the chromatography eluate (product fraction) was defined as:

$$q_A^{\text{elut}} = \sum_{i=1}^{E} [A]_i \cdot V_i \tag{2.3}$$

where E the total number of elution fractions. Likewise, the mass of target product $Prod$ in the product fraction was defined as:

$$q_{Prod}^{\text{elut}} = \sum_{i=1}^{E} [Prod]_i \cdot V_i \tag{2.4}$$

where $[Prod]_i$ is the concentration of the target product.

Therefore, the percentile yield (or product recovery in the elution fraction) was calculated as:

$$\xi_{Prod} = \left(q_{Prod}^{\text{elut}}/q_{Prod}^{\text{in}}\right) \cdot 100 \tag{2.5}$$

The productivity of the SXC step in terms of the purified target product was calculated as:

$$\varphi = \frac{q_{Prod}^{elut}}{t_{SXC} \cdot S_{col}} \tag{2.6}$$

where t_{sxc} the total chromatography time, and S_{col} the surface area of the column (sum of the membranes' stack surface).

The purity ratio (χ) of component A (in this case either DNA or total protein) to the target product was defined as:

$$\chi_{A,Prod} = q_A^{elut}/q_{Prod}^{elut} \tag{2.7}$$

Alternatively, χ was expressed in product doses by normalizing against the appropriate quantity of product per dose. For example, for YFV, χ was expressed as pg_{DNA} per dose or ng_{prot} per dose with:

$$\chi_{A,yfv} = 10^{-4.74} \cdot \left(q_A^{elut}/q_{Prod}^{elut}\right)$$

The value of $10^{4.74}$ refers to the total infectious titer in PFU for a commercial, live-attenuated YFV vaccine. An equivalent normalization in terms of product doses was used for expressing productivity (Equation 2.6).

The percentile reduction value (RV) of DNA and protein contamination in the product fraction was calculated as:

$$\text{RV} = \left(q_A^{elut}/q_A^{in} \right) \cdot 100 \tag{2.8}$$

The reduction of DNA and protein contamination in the product fraction was also expressed as a logarithmic reduction value (LRV):

$$\text{LRV} = \log_{10} \left(\frac{q_A^{\text{in}}}{q_A^{\text{elut}}} \right) \tag{2.9}$$

Finally, the dynamic binding capacity (DBC) of the SXC step at x% breakthrough was estimated by:

$$DBC_x = \frac{[A] \cdot V_{b,x\%}^{\text{in}}}{S_{col}} \tag{2.10}$$

where $V_{b,x\%}^{\text{in}}$ is the total feed volume at x% of product breakthrough.

2.2.7 Pseudo-affinity chromatography with a sulfated cellulose membrane adsorber

The SXC elutions were further purified by pseudo-affinity chromatography using self-made sulfated cellulose membrane adsorber (SCMA) with the same stainless steel housings as described above for SXC, but using 10 layers (50 cm^2 total surface) of sulfated cellulose sheets [129, 141]. The polishing of SXC-purified influenza virions with SCMA was carried out too in bind-elute mode as previously reported by Fortuna et al. [136]. Briefly, (A) Equilibration: the column was washed with 10 CV of water followed by 10 CV of "SCMA equilibration buffer" (10 mM Tris-HCl, 4 mS cm^{-1}, pH 7.4). (B) Sample injection: the sample was then loaded onto the column followed by a wash step with equilibration buffer until baseline UV absorbance was achieved. (C) Elution: virus particles were recovered by washing with 20 CV of "SCMA elution buffer" (10 mM Tris-HCl, 1.0 M NaCl, pH 7.4). Elution pools were dialyzed with 14 kDa molecular mass cut-off (MMCO) membranes as described by Fortuna et al. [136].

2.3 Statistical methods

Student's t-tests were made for evaluating statistical significance. Unless otherwise stated, the values shown in figures and tables are arithmetic means $\pm$ standard deviation of the mean (SE), also known as the standard error.

The SE, $s\left(\bar{x}\right)$, is defined as [142]:

$$s\left(\bar{x}\right) = \frac{s}{\sqrt{n_{\mathrm{rep}}}} \tag{2.11}$$

where $\bar{x}$ is the mean, s is the standard deviation, and n_{rep} the number of replicates.

Results & Discussion

Results pertinent to particular viruses are first examined below. While some experimental observations are shared among the different viruses investigated here and discussed individually in their respective subchapters, a more general discussion on the mechanics and characteristics of SXC is found in Section 3.6.

3.1   SXC of influenza virus

There are few reports in literature that describe SXC for purifying large biomolecules, and most of these are for pure protein mixtures, with the exception of purification of bacteriophages.

The first experiments to purify influenza virus with SXC were made with OH monoliths. As a proof of concept, crude samples containing influenza A virus from $MDCK_{adh}$ cell cultures were tested. Loading approximately 17 mL at 8% PEG-6000 resulted in a recovery in elution pools of 70.7% ($16\,570.0 \pm 2002.6$ HAU, Figure 3.1) determined by aHA assay. Around 5% (1235 ± 126.7 HAU) of virus particles were found in the flow-through. The residual amounts of dsDNA and protein in the elution pools were 2.1% (1126.9 ± 45.8 ng) and 7.8% (29.5 ± 0.8 µg), respectively. The missing aHA was attributed to possible matrix fouling. The product in the eluate was below detection limit for negative controls where the crude sample was loaded at 0% PEG-6000, confirming the successful capture of influenza A virus with OH monoliths.

SXC requires a hydrophilic matrix for capturing the target product and it was speculated that cellulose membranes could be used as stationary phase instead of OH monoliths for SXC thanks to the highly hydroxylated surface of cellulose. The same sample was

loaded onto a 75 cm^2 column packed with regenerated cellulose membranes of 1.0 µm pore size (Figure 3.1, panel A).

There was no detectable aHA in the flow-through and the elution pool had around 83% aHA (18 429.4 ± 1505.1 HAU, statistically not significant compared to the OH monolith, $P = 0.257$, further discussion in Ref. [122]). Although these experiments were performed at different linear velocities (212 cm h^{-1} for the OH monolith and 122 cm h^{-1} for the regenerated cellulose membranes), no differences in performance were expected for this particular parameter since the mass transfer in both matrices is convective and thus independent from fluid velocity. Nonetheless, the lack of influence from the flow rate was confirmed by additional experiments using the membranes at linear velocities exceeding 260 cm h^{-1} with comparable results to 122 cm h^{-1} (data not shown).

The measured product yield suggests that a concentration of 8% PEG-6000 was enough to capture influenza A virus. The amount of product in the flow-through when using the OH monoliths (5%, 1235.0±126.7 HAU) could be due to either a lower density of hydroxyl groups or a slightly more hydrophobic backbone in the OH monoliths compared to the regenerated cellulose membranes. This observation coincides with Tao et al. [143], who demonstrated that increasing the hydrophilicity of the stationary phase improved the retention of γ-globulin during SXC.

SXC of influenza virus produced in 5 L STR. Having demonstrated the successful capture of influenza A virus using cellulose membranes, additional samples were tested of influenza A virus produced with MDCK$_{sus}$ in 5 L STRs with chemically-defined SMIF8
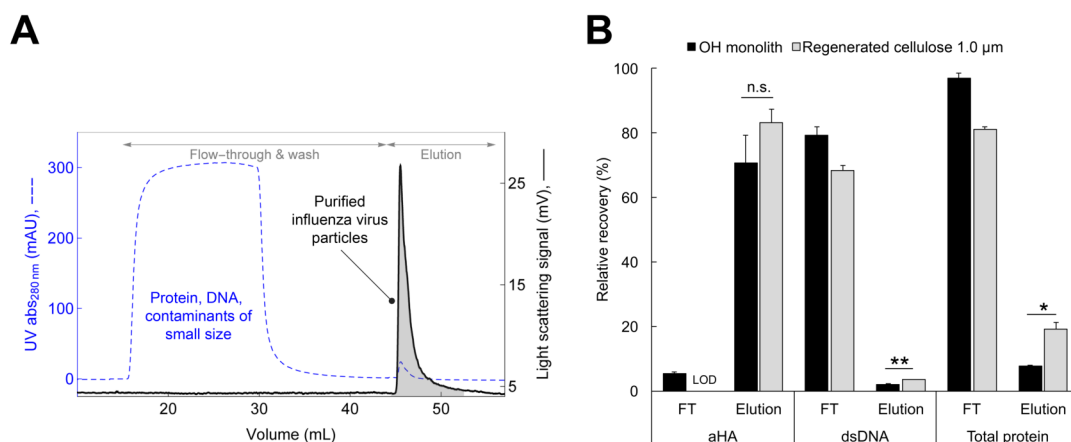
Figure 3.1. (A) SXC of influenza virus A/Puerto Rico/8/34 H1N1 produced in MDCK$_{adh}$ cells (loading at 8% #81260-5KG; Sigma-Aldrich Chemie GmbH; Munich, Germany, 75 cm^2 regenerated cellulose column). The gray shaded region is the collected product fraction. (B) Relative recovery of product (as hemagglutination activity) and impurities for SXC purifications with the regenerated cellulose membranes and OH monoliths. Data shown are means ± standard deviation of the mean of chromatography replicates (n=3). FT=flow-through; LOD=limit of detection. *$P < 0.05$; **$P < 0.01$; n.s., not significant.

medium. The SXC feed was clarified inactivated virus broth either untreated or nuclease-treated for DNA digestion. An overall process diagram is shown in Figure A.1.

Virus material from three different bioreactors was independently tested. The mass balances are shown in Table 3.1 and the recoveries in Table 3.2; a representative chromatogram and overlays of the light scattering signal from elution pools are shown in Figure 3.2. These results were reported in Ref. [122].

There was no detectable product by aHA assay in the flow-through fractions from all three bioreactors with a load of 100 mL of clarified sample. Recoveries of aHA in the elution pools were virtually complete with values of 99.2–116.8% (Table 3.2). Regarding virus yield, values of around 65% have been reported previously by Opitz et al. for immobilized metal affinity chromatography [144] and pseudo-affinity chromatography with SCMA (with 20% product loss in the flow-through) [129]. More recently, Fortuna et al. [136] reported a product yield of 57.4%±0.6 using SCMA with a production process for influenza A/Puerto Rico/8/34 H1N1 virus that resembles more the one used in this work — suspension cells in serum-free medium — compared to Opitz et al. [129]. Additional reported recoveries are 57% aHA yield using a Cellufine™ sulfate resin as well as an aHA yield of 63% and 75% using IEC with two different cation exchange membranes [129]. Moreover, Kröber et al. [145] reported 80% aha yield using SEC in batch mode and 70% in simulated moving bed mode.

Apart from the aHA, the total amount of the HA antigen present in the SXC elution pools from the three different bioreactors was quantified by SRID. The mean HA antigen yield from the three bioreactors (Table 3.2) was 103.9% ± 3.9. Based on these results, it seems that membrane-based SXC achieves higher product recoveries for influenza A virus than other chromatography techniques.

It was possible to deplete 99.7% (2.5 LRV) of DNA without a nuclease treatment prior to chromatography. Weigel et al. [146] reported a LRV of 1.6 with only 80% aHA yield
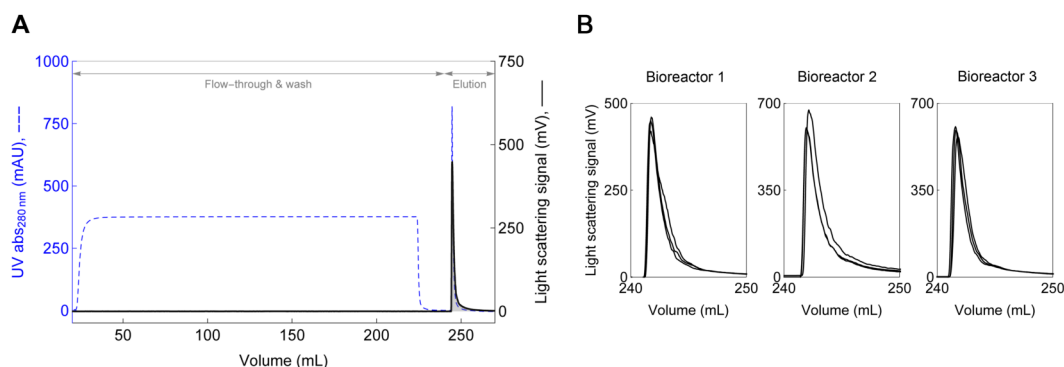
Figure 3.2. SXC (75 cm^2 regenerated cellulose column) of influenza virus A/Puerto Rico/8/34 H1N1 produced in a 5 L stirred tank reactor with MDCK$_{sus}$ cells in SMIF8 chemically-defined medium. The gray shaded region is the collected product fraction. This figure was published in Ref. [122].

Table 3.1

Mass balances of SXC of influenza virus A/Puerto Rico/8/34 H1N1 produced in a 5 L stirred tank reactor (n=3) with MDCK$_{sus}$ cells in SMIF8 chemically-defined medium. These balances refer to the process in Figure A.1. Refer to Table 3.2 for percentile recoveries and logarithmic reduction value of impurities. Data shown are means ± standard deviation of the mean of chromatography replicates (n=3).

				Virus product		Impurities		
	Nuclease-treated[f]	Sample	Volume (mL)	aHA[a] HAU $(0.1\,\mathrm{mL})^{-1}$	HA[b] $(\mathrm{\mu g\,mL}^{-1})$	dsDNA[c] $(\mathrm{ng\,mL}^{-1})$	ssDNA[d] $(\mathrm{ng\,mL}^{-1})$	Protein[e] $(\mathrm{\mu g\,mL}^{-1})$
Bioreactor 1	No	Feed	200.0	140.8	n.d.	2155.4	n.d.	22.4
		Flow-through	200.0	<LOD	n.d.	1839.5 ± 25.7	n.d.	20.9 ± 0.5
		Eluate	15.0	2097.9 ± 86.7	n.d.	88.3 ± 5.3	61.6[g]	22.7 ± 0.9
Bioreactor 1	Yes	Feed	200.0	161.5	0.5	12.5	n.d.	16.8
		Flow-through	200.0	<LOD	n.d.	8.9 ± 0.3	n.d.	15.0 ± 0.2
		Eluate	10.0	3202.8 ± 69.1	10.7[g]	27.0 ± 0.9	4.4[g]	28.9 ± 0.5
Bioreactor 2	Yes	Feed	200.0	180.1	0.6	31.6	n.d.	21.3
		Flow-through	200.0	<LOD	n.d.	11.0 ± 0.3	n.d.	20.2 ± 0.0
		Eluate	10.0	3804.1 ± 293.1	12.3[g]	94.0 ± 5.4	19.3[g]	52.4 ± 1.9
Bioreactor 3	Yes	Feed	200.0	231.3	0.9	6.8	n.d.	21.7
		Flow-through	200.0	<LOD	n.d.	<LOQ	n.d.	20.2 ± 0.0
		Eluate	10.0	5405.4 ± 405.4	16.7[g]	31.9 ± 0.5	4.8[g]	41.7 ± 0.8

HA=hemagglutinin; HAU=hemagglutination units; LOD=limit of detection; LOQ=limit of quantitation

n.d., not determined

[a] by hemagglutination activity (aHA) assay

[b] by single radial immunodiffusion (SRID) assay

[c] by PicoGreen assay

[d] by Threshold assay

[e] total protein by Bradford assay

[f] nuclease treatment before SXC

[g] eluate pool of 3 chromatography replicates

Table 3.2
Percentile recoveries and logarithmic reduction value of impurities for SXC of influenza virus A/Puerto Rico/8/34 H1N1 produced in a 5 L stirred tank reactor (n=3) with MDCK$_{sus}$ cells in SMIF8 chemically-defined medium. Data shown are means ± standard deviation of the mean of chromatography replicates (n=3).

| | | Virus product | | Impurities | | | | | |
| | | | | DNA[a] | | | Protein[b] | | |
	Nuclease[c]	aHA[d](%)	HA[e](%)	(%)	LRV[f]	LRV[g]	(%)		LRV[f]
Bioreactor 1	No	111.7 ± 4.6	n.d.	0.3 ± 0.0	2.5	-	7.6	± 0.3	1.1
Bioreactor 1	Yes	99.2 ± 2.1	114.4	10.8 ± 0.4	1.0	3.1	8.6	± 0.1	1.1
Bioreactor 2	Yes	105.6 ± 8.1	102.3	14.9 ± 0.9	0.8	2.8	12.3	± 0.4	0.9
Bioreactor 3	Yes	116.8 ± 8.8	98.1	23.5 ± 0.4	0.6	3.2	9.6	± 0.2	1.0

HA=hemagglutinin; LRV=logarithmic reduction value, see Equation 2.9; n.d., not determined

[a] dsDNA by PicoGreen assay
[b] total protein by Bradford assay
[c] nuclease treatment prior to chromatography
[d] by hemagglutination activity (aHA) assay
[e] by single radial immunodiffusion (SRID) assay
[f] of SXC step
[g] of nuclease treatment + SXC step

for the same strain used here. Seemingly, SXC is able to deplete large quantities of DNA, an observation first made by Leet et al. [117] while purifying bacteriophage M13K07 with OH monoliths; the authors report 93% DNA depletion in the purified product compared to the unpurified *E. coli* harvest.

A lower DNA clearance (76.5–89.2%) was observed when the bioreactor harvests were treated with nuclease before SXC. For all three reactors, the relative residual DNA in the elution pools greatly exceeded the one mentioned above (0.3%): 10.8%, 14.9%, and 23.5% (Table 3.2) , respectively. Although these relatives amounts are higher, the total DNA amount in the elution fraction was lower (270, 940, and 319 ng) than the value with the undigested sample from bioreactor 1 (1324.5 ng). There was no correlation between the DNA concentrations of the three bioreactors before digestion (4311, 6225, and 5074 $ng\,mL^{-1}$) and the residual amount after SXC. Judging by the small variation in the chromatograms (Figure 3.2) and the error within bioreactors (Table 3.1), the difference in performance seems to be due to batch-to-batch biological variation between the bioreactors.

It is clear from these observations that the DNA is not totally digested by the nuclease and is co-purified with the virus particles. EVs and cellular chromatin might account for the presence of undigested DNA in the SXC feed. EVs are released from most prokaryotic and eukaryotic cells types that transmit information and carry complex cargo, including a wide variety of nucleic acids and proteins [73, 77, 147–150]. Nucleic acid inside EVs would be protected by nuclease digestion. Additionally, due to the size of the EVs (ectosomes, 100–1000 nm in diameter; exosomes, 40–100 nm in diameter), they might get captured and co-purified (especially exosomes) with the virus particles while performing SXC. The presence of exosomes in the product fraction was confirmed by TEM and is discussed further below.

The second possibility is the presence of residual cellular chromatin, which is known to be resistant to nuclease digestion [151]. Chromatin is a complex assortment made of DNA, nucleosome arrays, single nucleosomes, histones, and non-histone proteins. Chromatin is a persistent contaminant in biopharmaceuticals and its characterization and clearance present significant challenges that have been reported elsewhere [152–155]. The presence of histones in the product fraction was observed also by stimulated emission depletion microscopy (data not shown). Eluates dialyzed with pore sizes higher than 100 kDa still contain the same DNA concentrations, evidencing that the residual DNA is either attached to the virus particles or related to the exosomal impurities, although a co-localization of DNA with virus particles was not observed by stimulated emission depletion (STED) microscopy for these particular samples [122]. Nonetheless, the LRV of DNA were at least 2.5 for SXC with undigested feed and 2.8–3.2 for SXC with digested feed (Table 3.2).

What's more, there is a discrepancy between the measured DNA concentrations of the Threshold and PicoGreen assays. Lower DNA concentration were always measured
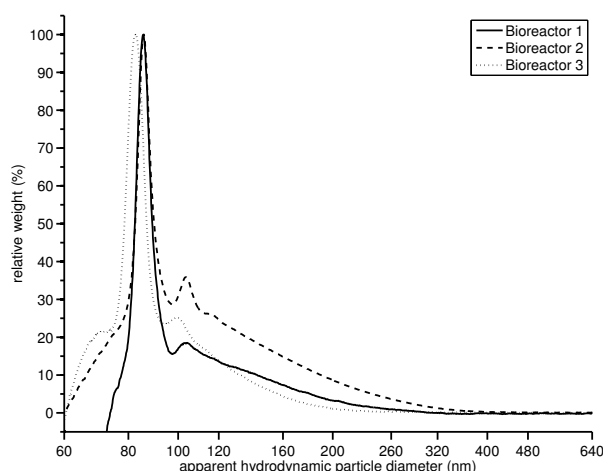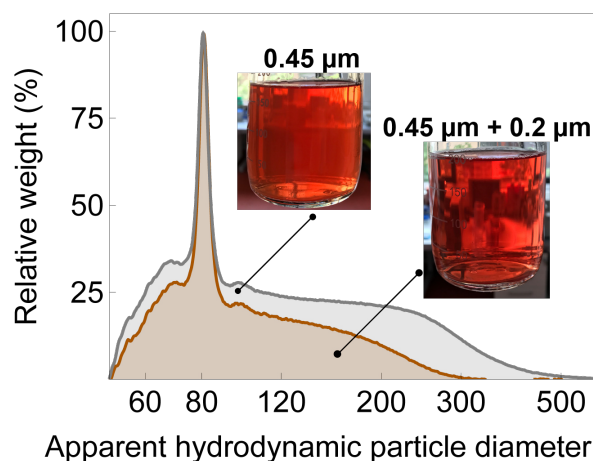
Figure 3.3. Particle size distribution by differential centrifugal sedimentation of SXC-purified influenza virus A/Puerto Rico/8/34 H1N1 produced in a 5 L stirred tank reactor with MDCK$_{sus}$ cells in SMIF8 chemically-defined medium. Each curve is the average of three chromatography replicates per bioreactor. The influenza virus monomer has an apparent hydrodynamic particle diameter of 82–86 nm and dimers of 100–105 nm; low levels of larger aggregates are also observed. This figure was published in Ref. [122].

with the Threshold (4.4–19.3 ng mL^{-1}, Table 3.1) compared to the PicoGreen (27.0–94.0 ng mL^{-1}, Table 3.1). Weigel et al. [156] reported previously Threshold values about 4–9 times lower (in this work 5–7 times lower) than those with the PicoGreen. The Threshold assay is based on an immuno-enzymatic reaction and measures ssDNA larger than 100 bp [156–158]. In contrast, the PicoGreen assay shows fluorescence after the selective binding of a dye to dsDNA, and can measure fragments as small as 20 bp [159, 160].

The residual total protein in the eluates ranged 289–524 µg (Table 3.1). This equates to a total protein recovery of 7.6–12.3% in the product. In contrast, Weigel et al. reported 28% ± 7 using a CaptoCore 700 resin [156] and 28% ± 2 using a SCMA [146]; Opitz et al. achieved 14.7% using too a SCMA, and Kalbfuss 35% using SEC.

The particle size distribution by DCS of the pooled product fractions show a distinct monomeric peak with a particle diameter of 82–86 nm and small levels of dimers and larger aggregates (Figure 3.3). This particle size is consistent with reported values for influenza viruses (80–120 nm) [161].

SXC can be used for separating macromolecues by size: Lee et al. resolved IgM aggregates from monomers using OH monoliths [117] and Wang et al. fractionated BSA from γ-globulin using cryogels [162]. Although monoliths provide more resolution than membranes, the possibility of fractionating influenza virus aggregates from monomers by membrane-based SXC seems feasible and will be discussed in Section 3.6.

TEM pictures of the elution pools show vesicular impurities co-purified with the virus particles (Figure 3.4), which have an approximate size of 100 nm. The discrepancy compared to the size measured by DCS is most likely due to the many sample processing

differences between the methods, noting that with DCS an *apparent* hydrodynamic size is measured.

Although SXC is not an adsorptive process [117] (further discussion in Section 3.6), some experiments were made to estimate capacity of the columns used. It was found that by loading approximately 250 mL of a clarified virus harvest (from bioreactor 1; Table 3.1), 5% of aHA was found in the flow-through. Based on the total amount of the recovered HA antigen by SRID, the dynamic binding capacity at 5% breakthrough ($DBC_{5\%}$) calculated with Equation 2.10 was 3.4 $\mu g_{HA}cm^{-2}$.

SXC of influenza virus produced in a perfusion/ATF system. Virus purification from other production systems besides the 5 L STR was tested, for example, from a hybrid fed-batch/perfusion strategy with an ATF system. Avian AGE1.CR.pIX cells were grown to high densities in a chemically defined medium and infected with influenza virus A/Puerto Rico/8/34 H1N1 as described by Vázquez-Ramírez et al. [137]. Unlike the 5 L STR used in the experiments above, virus broth was continuously harvested through a hollow-fiber module of 0.65 µm pore size. Afterwards, this sample (5 mL) was diluted to a final concentration of 8% PEG-6000 and purified by SXC. The product yield by aHA was $56.2\% \pm 0.2$ ($80\,968.7 \pm 346.4$ HAU), while the depletion of DNA and total protein in the flow-through were $86.9\% \pm 2.2$ (387.5 ± 13.0 µg) and $80.0\% \pm 2.9$ (737.9 ± 38.2 µg), respectively. The lower recovery compared to the 5L STR and the lack of aHA signal in the flow-through suggested product loss due to fouling of the cellulose membranes. Since
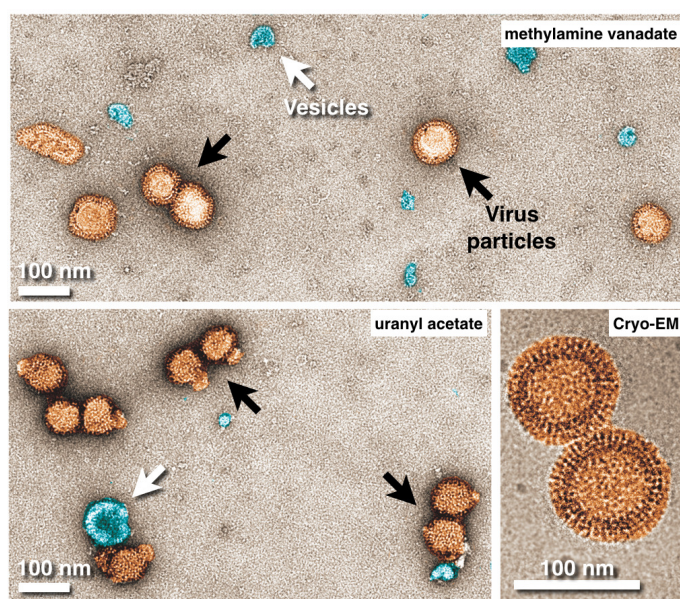
Figure 3.4. Transmission electron micrographs with different contrast agents from SXC-purified influenza virus A/Puerto Rico/8/34 H1N1 produced in a 5 L stirred tank reactor with MDCK$_{sus}$ cells in SMIF8 chemically-defined medium. The virus particles (orange) are homogeneous in shape and size with an approximate size of 100 nm. Vesicular impurities (blue) can also be observed. Pictures taken by Dietmar Riedel from the Max-Planck-Institute for Biophysical Chemistry in Göttingen, Germany.
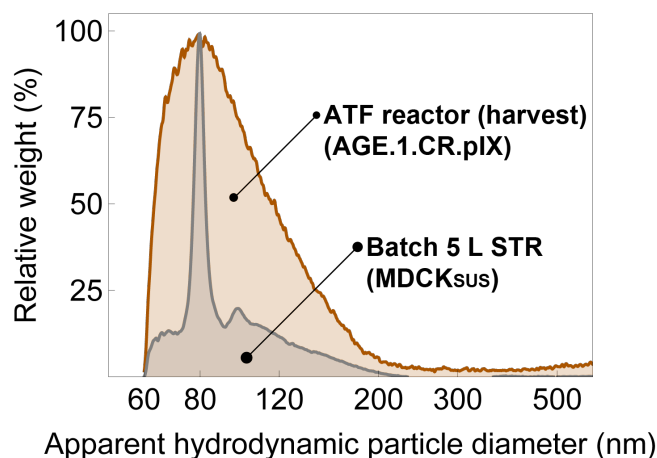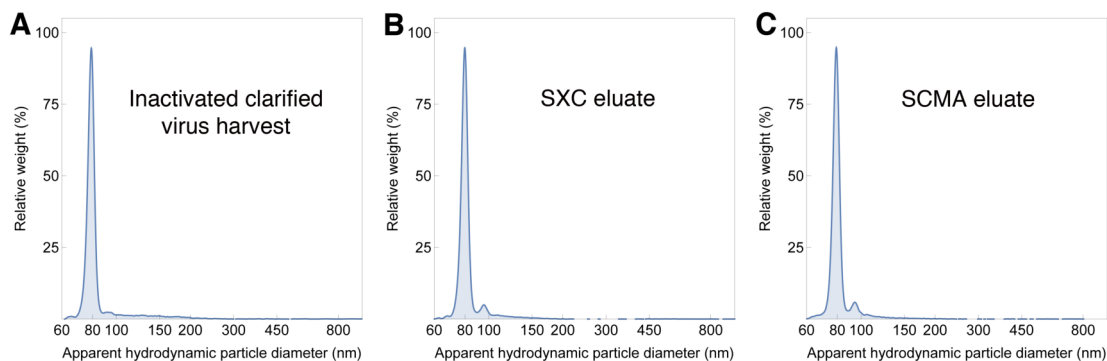
Figure 3.5. Particle size distributions by differential centrifugal sedimentation of influenza virus A/Puerto Rico/8/34 H1N1 produced in a 5 L stirred tank reactor (STR) with MDCK$_{sus}$ cells in SMIF8 chemically-defined medium (blue) and in a fed-batch/perfusion alternating tangential flow process with AGE1.CR.pIX suspension cells in CD-U3 chemically-defined medium (red). Notice the broader size distribution and the absence of a distinctive influenza virus monomer signal from the perfusion process.

this behavior was not observed before, either virus aggregation or remaining cell debris were suspected causes for the lower yields. DCS analysis of the unconditioned SXC feed (before the addition of PEG) confirmed a broad size distribution (Figure 3.7) without a defined monomer peak.

SXC of several influenza virus strains produced in shaker flasks. After successful SXC purification of the influenza virus A/Puerto Rico/8/34 H1N1 strain, a broader range of influenza viruses were tested.

The possibility of purifying different strains using the same process conditions has appeal also from a public health perspective: with antigenic drift, annual updates are required for the vaccine. The variations between strains might require that USP and DSP be adapted. For example, structural variations between viruses have to be carefully considered with purification methods such as IEC, where even slight changes in the virus can alter the chromatographic fingerprint. This reduces predictability and slows process development since the conditions have to be adapted to new influenza A virus strains. SXC is strongly based on the virus particle size, which is most likely not affected by mutations causing antigen drift, making it a relatively robust unit operation.

Aside from the A/Puerto Rico/8/34 H1N1 strain, the following strains were produced in shaker flasks and processed as described in Materials and Methods: A/Switzerland/9715293/2013 H3N2, B/Phuket/3073/2013 (Yamagata). An older sample of influenza B/Brisbane/63/2014 (Victoria) was tested only for the SXC step.

In parallel, influenza A virus purification was established by Ana Raquel Fortuna by using pseudo-affinity with SCMA as a capture step [136]. It was decided to combine SXC and SCMA in a single process that would allow a purification platform for influenza

viruses with two orthogonal chromatography steps. SXC was placed as the capture step as shown previously here. Since the SCMA requires low conductivity ($< 5\,\text{mS}\,\text{cm}^{-1}$) for sample loading, and theoretically with SXC the product can be eluted in any suitable buffer system [122], the binding buffer for the SCMA was used as the elution buffer for SXC. This was done to avoid sample processing steps between the unit operations and for connecting the process in a more seamless way. The process diagram is shown in Figure A.2.

The first SXC experiments with the A/Puerto Rico/8/34 H1N1 strain produced in shaker flasks gave a product yield of $55.4\% \pm 10.7$ regarding aHA, much lower than what was obtained with the sample produced in a 5 L STR (99.2–116.8%; Table 3.2). Since the aHA in the flow-through was nil, membrane fouling was suspected for the lower recovery.

The sample was clarified with 0.45 µm prior to SXC (Figure A.2); the sample was further filtered with 0.2 µm and both 0.45 µm and 0.2 µm specimens were analyzed for aHA and particle size distribution with DCS.

Although the 0.45 µm and 0.2 µm-filtered sample had lower turbidity, it did not show a significantly lower aHA (1117.0 HAU $(0.1\ \text{mL})^{-1}$) compared to the 0.45 µm-filtered sample (1131.1 HAU $(0.1\ \text{mL})^{-1}$). As can be observed from the particle size distribution of both samples (Figure 3.6), a particle size distribution population of around 250–450 µm is eliminated in the 0.45 µm and 0.2 µm filtered-sample without changing the profile of the distinctive monomer peak. This suggests the presence of a higher content of cell debris from the production in shaker flasks compared to the 5 L STR process (0.45 µm-filtered).

SXC experiments were repeated at 8% PEG-6000 with the 0.45 µm and 0.2 µm filtered sample. This time, an aHA yield of 100.1% (295 121.0 HAU) was observed, consistent with previous results for the 5 L STR. Also lower PEG-6000 concentrations (4% and 6%) were tested for loading but only 8% PEG-6000 showed full virus yield (Figure 3.7). The

Figure 3.6. Particle size distributions by differential centrifugal sedimentation of influenza virus A/Puerto Rico/8/34 H1N1 (produced in shaker flasks with MDCK$_{\text{sus}}$ cells in SMIF8 chemically-defined medium) clarified with either 0.45 µm or a sequence of 0.45 µm and 0.2 µm filters.

optimal PEG loading concentration for the A/Puerto Rico/8/34 H1N1 strain was also used for the A/Switzerland/9715293/2013 H3N2, the B/Phuket/3073/2013 (Yamagata), and the B/Brisbane/63/2014 (Victoria) strains. Surprisingly, virtually full virus yield at 8% PEG-6000 was observed for all tested strains (Figure 3.7), showing that any differences between the virus strains had little influence on SXC at the tested conditions.

Once the optimal conditions for the capture with SXC were determined, further polishing of the samples with the SCMA was evaluated. As mentioned earlier, the SXC process was slightly changed in order to streamline the workflow to include a subsequent SCMA step: instead of eluting the virus particles with 50 mM Tris-HCl, 150 mM sodium chloride, pH 7.4 ($\approx$18 mS cm^{-1}) as done before, the elution was done with 10 mM Tris-HCl, pH 7.4 (4.5 mS cm^{-1}), which is the binding buffer for the SCMA. This change required an additional wash step before elution with 8% PEG-6000 10 mM Tris-HCl, pH 7.4 (4.5 mS cm^{-1}) in order to reduce the conductivity of the mobile phase while keeping the virus particles still attached at the membrane surface.

The aHA recoveries for the A/Puerto Rico/8/34 H1N1 strain with low conductivity elution were as before, showing full product yield (112.2%, 148 397.0 HAU). When testing the A/Switzerland/9715293/2013 H3N2 strain, however, a lower yield of $\approx$ 25% with the low conductivity elution buffer was observed. A follow up experiment was performed with a subsequent elution step at around 18 mS cm^{-1}. The remaining virus particles eluted during the second elution as expected (Figure 3.8) and both pools accounted to around 97% of aHA yield. A similar effect was observed with the B/Phuket/3073/2013
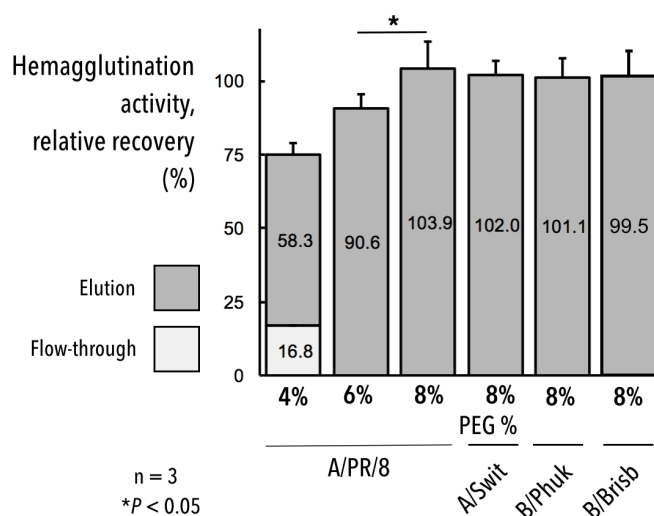
Figure 3.7. Recovery of several SXC-purified influenza virus strains produced with MDCK$_{sus}$ cells in shaker flasks (n=3). Different loading polyethylene glycol (PEG) concentrations were tested for the A/Puerto Rico/8/34 H1N1 strain. The optimal loading value of 8% PEG-6000 was used for the all the other strains (A/Switzerland/9715293/2013 H3N2, B/Phuket/3073/2013 (Yamagata), and B/Brisbane/63/2014 (Victoria)) yielding similar recoveries. Data shown are means $\pm$ standard deviation of the mean of chromatography replicates (n=3).
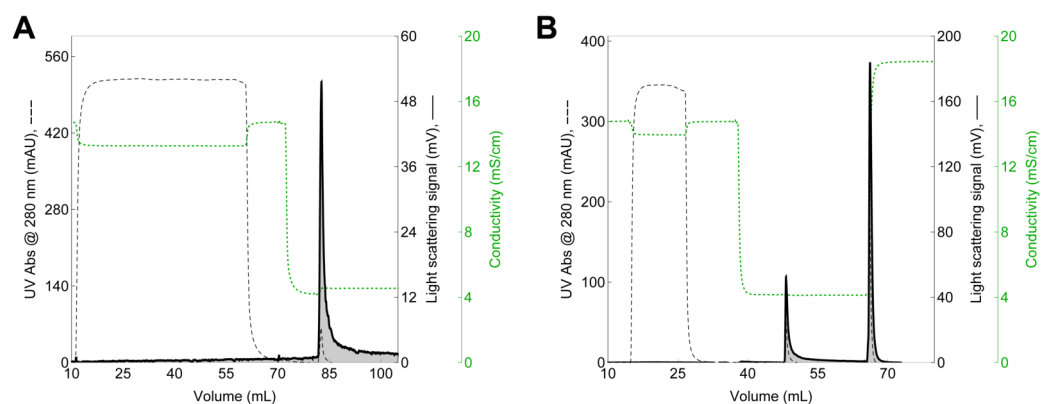
Figure 3.8. SXC of influenza virus A/Switzerland/9715293/2013 H3N2 eluted with one step at low conductivity (4.5 mS cm^{-1}, panel A) or with two steps at low and medium conductivity (18 mS cm^{-1}, panel B). Notice the higher virus recovery at the higher conductivity in panel B.

(Yamagata) strain with 70.2% aHA yield when eluting at low conductivity (data not shown).

It seems that differences between virus strains accounted for this behavior, most probably the pI of the A/Puerto Rico, A/Switzerland, and B/Phuket strains (further discussed in Ref. [122]). Based on the lower yield at low conductivity, it was decided to use the higher conductivity in the elution step to guarantee the highest yield so far for all strains. This was not an issue after all since the buffer system for the SXC and the SCMA was the same (Tris buffer) and it would only require a mild dilution of the SXC eluate for injection onto the SCMA.

Overall, full aHA yield was achieved with SXC (Figure 3.7) and a mean yield of around 77% for the SCMA step for the A/Switzerland/9715293/2013 H3N2 and B/-Phuket/3073/2013 (Yamagata) strains (data not shown). The SXC+SCMA setup for this particular process is illustrated in Figure A.3.

Table 3.3

DNA concentrations after different combinations of influenza virus inactivation and nuclease treatment steps (process diagram in Figure A.4).

hpi	DNA (ng mL^{-1})[a]	
	inact→nuc[b]	nuc→inact[c]
18	57.6 ± 2.3	29.5 ± 2.3
21	75.0 ± 2.5	33.9 ± 2.3
24	90.2 ± 2.5	40.3 ± 2.3
27	118.3 ± 2.5	46.7 ± 2.3
30	172.1 ± 2.5	65.3 ± 2.5
36	292.9 ± 2.5	92.0 ± 2.5

hpi=hours post infection

[a] dsDNA by PicoGreen assay
[b] virus inactivation before nuclease treatment
[c] virus inactivation after nuclease treatment

Figure 3.9. Particle size distributions by differential centrifugal sedimentation of influenza virus A/Puerto Rico/8/34 H1N1 (produced in a 1 L stirred tank reactor (n=3) with MDCK$_{sus}$ cells in Xeno™ chemically-defined medium, panel A) after SXC (panel B) and subsequent polishing with a sulfated cellulose membrane adsorber (panel C).

SXC of influenza virus produced in a 1 L STR with Xeno™ chemically defined medium. One last production system for influenza virus A/Puerto Rico/8/34 H1N1 was tested. After clarification of the virus broth with 0.45 µm, it was evaluated if the nuclease treatment was more efficient either before or after virus inactivation with β-propiolactone. Several time points after infection were evaluated (18, 21, 24, 27, 30, and 36 h). The DNA levels were lower when the nuclease treatment was made before the inactivation (Table 3.3) compared to after the inactivation and the optimal harvest point was at 21–24 hpi [163]). The samples from these time points were pooled and had a concentration of the HA antigen of 4.3 µg mL^{-1}.

This might be due to the chemical modification of DNA or its cross-linking by β-propiolactone that makes DNA unrecognizable by the nuclease [164, 165] if the digestion step is performed after the chemical inactivation as in the other processes described before. After the nuclease digestion, the sample was filtered with 0.2 µm and purified by SXC followed by a polishing step with a SCMA (Figure 3.10).

The mass balances for these experiments are detailed in Table 3.4. For the SXC step, there was full product yield for both aHA and SRID assays. The elution pool contained around 232 µg of the HA antigen and 192 ng of residual DNA, giving this setup the highest ratio of antigen over DNA amount. The following pseudo-affinity step with a SCMA was expected to deplete impurities further, but the difference was barely noticeable: as shown in Figure 3.10, the flow-through signal in the SCMA polishing step is practically nil. The concentrations of antigen and impurities in the SCMA elution pool were very similar compared to the SXC pool, demonstrating that contamination levels could not be further improved in a significant way.

Product yield by aHA after the SCMA step was around 84% (Table 3.4), consistent with previously obtained results, however, antigen yield by SRID was 56.0% (105.2 µg$_{HA}$; Table 3.4). It was concluded that the polishing step with the SCMA was not worth it for
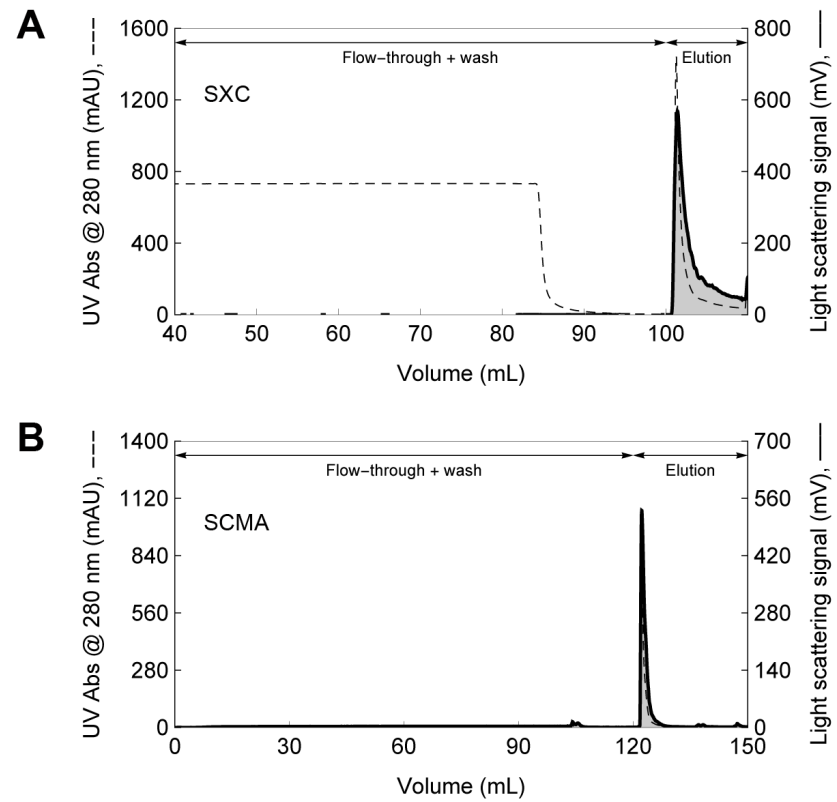
Figure 3.10. SXC (panel A) and subsequent polishing with a sulfated cellulose membrane adsorber (SCMA) (panel B) of influenza virus A/Puerto Rico/8/34 H1N1 produced in a 1 L stirred tank reactor (n=3) with MDCK$_{sus}$ cells in Xeno™ chemically-defined medium. Refer to Table 3.4 for mass balances and percentile recoveries.

Table 3.4

Mass balances and percentile recoveries of SXC and subsequent polishing with a sulfated cellulose membrane adsorber (SCMA) of influenza virus A/Puerto Rico/8/34 H1N1 produced a 1 L stirred tank reactor (n=3) with MDCK$_{sus}$ cells in Xeno™ chemically-defined medium. Data shown are means ± standard deviation of the mean of chromatography replicates (n=1).

| | | | Virus product | | | | Impurities | | | |
| | | | aHA[a] | | HA[b] | | Protein[c] | | DNA[d] | |
Step	Sample	Volume (mL)	HAU $(0.1\ \mathrm{mL})^{-1}$	%	$(\mathrm{\mu g\,mL^{-1}})$	%	$(\mathrm{\mu g\,mL^{-1}})$	%	$(\mathrm{ng\,mL^{-1}})$	%
SXC	Feed	73.6	1070.8 ± 71.6	100.0	2.8	100.0	22.7 ± 0.1	100.0	12.7 ± 0.7	100.0
	Elution	25.0	3633.5 ± 209.9	115.2 ± 10.2	9.3	110.4	39.1 ± 0.1	58.4 ± 0.4	7.7 ± 0.7	20.6 ± 6.2
SCMA	Feed	104.6	568.5 ± 104.6	100.0	1.8	100.0	7.8 ± 0.0	100.0	<LOD	
	Elution	8.9	5584.4 ± 115.4	83.6 ± 15.5	11.8	56.0	45.3 ± 0.3	49.3 ± 0.4	7.9 ± 0.7	43.6 ± 5.5

HAU=hemagglutination units; LOD=limit of detection;

[a] by hemagglutination activity (aHA) assay

[b] by single radial immunodiffusion (SRID) assay

[c] total protein by Bradford assay

[d] dsDNA by PicoGreen assay
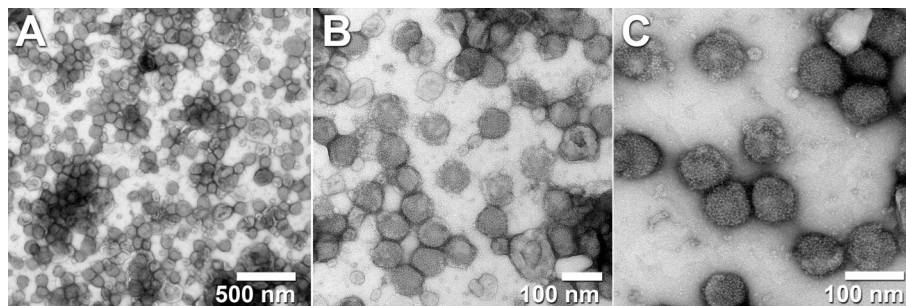
Figure 3.11. Transmission electron micrographs of influenza virus A/Puerto Rico/8/34 H1N1 (produced in a 1 L stirred tank reactor with MDCK$_{sus}$ cells in Xeno™ chemically-defined medium) purified with SXC and pseudo-affinity chromatography with a sulfated cellulose membrane adsorber. All images are from the same sample at different magnifications. Pictures taken by Dietmar Riedel from the Max-Planck-Institute for Biophysical Chemistry in Göttingen, Germany.

this particular process because the SCMA step failed to substantially deplete impurities after SXC at the expense of losing 15–45% of the product.

The residual DNA (estimated from Table 3.4) was 12.5 ng$_{dsDNA}$ dose^{-1} (monovalent, 15 µg$_{HA}$). However, this value was estimated by the PicoGreen assay, which gives a measurement 5–10 times higher than the Threshold assay as discussed elsewhere [122].

As a comparison, the 5 L STR process (Figure A.1) gave residual DNA amounts of 37.9, 114.6, and 28.7 ng$_{dsDNA}$ dose^{-1} and 6.2, 23.5, and 4.3 ng$_{ssDNA}$ dose^{-1} after SXC of each independent bioreactor triplicate (values calculated from Table 3.1). Considering that in this case the ssDNA values are on average 6 times lower to the dsDNA values, the 12.5 ng$_{dsDNA}$ dose^{-1} after SXC from the 1 L STR process (Figure 3.10) would be equivalent to 2.1 ng$_{ssDNA}$ dose^{-1}. After the SCMA polishing, the residual DNA was 10.0 ng$_{dsDNA}$ dose^{-1} (and 1.6 ng$_{ssDNA}$ dose^{-1} with the same assumption).

The amounts of total protein per dose after the SXC and SCMA steps (Figure 3.10) were 63.1 and 57.6 µg$_{prot}$ dose^{-1}, respectively, both below the regulatory requirements (Table 1.3). For the 5 L STR process (Figure A.1) the values ranged 37.5–63.9 µg$_{prot}$ dose^{-1} (values calculated from Table 3.1).

The productivity of the 1 L STR process with Xeno™ chemically-defined medium was the highest of all influenza production systems tested in this work with a value of 69 459 µg$_{HA}$ m^{-2} h^{-1} (4680 doses m^{-2} h^{-1}).

The particle size distribution (Figure 3.9) of the starting material before purification and after the SXC and SCMA purification steps shows a monodisperse virus peak and was the cleanest size distribution fingerprint measured from all the influenza virus processes discussed above. This was mainly attributed to the cell line and media used and to the optimization performed during USP by monitoring impurities and product (by both aHA and SRID assays) and optimizing the harvest time based on both).

It is evident from the examples above that differences in the upstream process (e.g., batch vs perfusion, harvesting time) greatly influence the outcome after DSP.

3.2 SXC of yellow fever virus

It was assumed at first that YFV would require more concentration of PEG-6000 due to its smaller size of around 40 nm compared to the 80–120 nm influenza viruses which were successfully captured at 8% PEG-6000. The first attempts for purifying YFV by SXC were made by loading at 10% PEG-6000. These experiments yielded infectious recoveries of 59% (1.05×10^8 PFU mL^{-1}) that were first attributed to the chromatography step.

YFV is known to be labile: all YF vaccines are lyophilized and the WHO provides guidelines so that certain stability standards are met for YF vaccines. YF vaccine manufacturers state that the vaccine must be held on ice after reconstitution and discarded after 1 h. For practical purposes in the field, however, the WHO recommends a longer interval of 6 h if the reconstituted vaccine is kept on ice [8].

These facts imply that the handling of YFV samples in the laboratory could be problematic due to the known lability of the virus particles. For example, Tânia Pato [166] observed infectivity losses of YFV during its purification with IEC (discussed further below). Thus, it was decided to assess the short-term infectious stability of YFV particles in a series of experiments where the following variables were tested: number of freeze-thaw cycles, concentration of stabilizer (sucrose), temperature, and incubation time. The 17DD substrain was used for these experiments.

First, the number of freeze-thaw cycles and sucrose concentration were tested in a single experimental set (Figure 3.12). The number of freeze-thaw cycles had little influence on virus infectivity and that the sucrose concentration was the dominant factor: when samples were not spiked with sucrose, there was approximately a 20% decrease in infectivity relative to the control sample, equivalent to a loss of up to 1.5 log$_{10}$ PFU mL^{-1}. This correlates with reported losses of 1.5–2.5 log$_{10}$ PFU per dose after thawing for YF vaccines lyophilized without stabilizers [167]. It was equally observed that the infectivity loss happened from the very first freezing cycle, staying relatively unchanged until cycle four (Figure 3.12), indicating an end-point of infectivity loss under the tested conditions.

Sucrose concentrations ≥4% seemed to be effective in avoiding infectivity losses. Sugars act as a water substitute by stabilizing proteins and membranes via hydrogen bonding to the polar residues of biomolecules. An additional protection mechanism regarding crystallization plays an important role as well: concentrated sugar solutions prevent the formation of large ice crystals in the interspace between virions during freezing by lowering the nucleation temperature of water [168]. The use of stabilizers for *Flavivirus* preparations has also been reported. For example, Mundle et al. [169] mixed pseudoinfectious *Flavivirus* particles 1:1 with 20% sorbitol in Minimum Essential Medium before freezing at −80 °C.

Additional experiments were made by narrowing the sucrose concentration range to 4–8% at different incubation times (0–8 h) and incubation temperatures (4 and 22 °C).
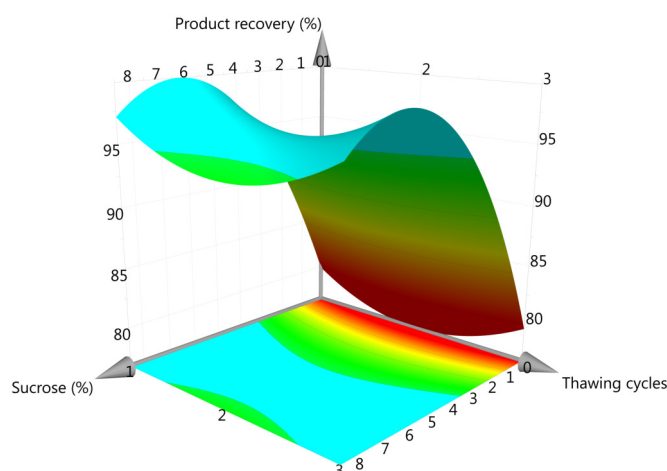
Figure 3.12. Response density plot for the stability of yellow fever virus (substrain 17DD) quantified as plaque forming units (PFU) mL^{-1}. The variables studied were the number of freeze-thaw cycles and the sucrose concentration. Infectious virus titer is expressed here as percentile recovery of PFU.

At 22 °C and time $\geq$4.5 h, a reduction of 5% (0.37 log$_{10}$ PFU mL^{-1}) in titer was observed with $\leq$6% sucrose, whereas for 8% sucrose the reduction was <2% (0.14 log$_{10}$ PFU mL^{-1}). Both lower titers were regarded as barely significant considering the highest SE observed in the plaque assay ($\pm$0.2 log$_{10}$ PFU mL^{-1}). No change in infectious titer was observed at 4 °C for 4–8% sucrose and 4–22 °C (data not shown).

A final set of experiments was made testing 0–4% sucrose in the same time and temperature ranges. As expected, the highest loss in titer (8%; 0.57 log$_{10}$ PFU mL^{-1}) was observed at the longest incubation time (8 h) for the highest temperature (22 °C) without sucrose. Based on these results, it was decided to spike all virus harvests with 8% sucrose before freezing. Likewise, virus harvests without sucrose were handled $\leq$1 h at 18–22 °C or otherwise kept at 4 °C for up to 4 h.

It is pertinent to stress that the virus samples in these stability experiments were in cell culture medium, suggesting that the components in the medium [170] that may act as stabilizers — polyols, ions, amino acids, and sugars — were not enough to protect the virus from damage. These findings imply that when unaccounted for, sample handling (e.g., freezing cultivation samples without adding a cryo-protectant) can have a negative impact that, at best, leads to under-estimation of virus titers during handling of virus harvests or downstream processing.

As a capture step for YFV, a first objective was to maximize the yield of infectious particles and so the loading of clarified virus harvests (without nuclease treatment) was tested at PEG-6000 concentrations of 6%, 8%, and 10% (flow rate: 5 mL min^{-1}). After purification, infectious virus recoveries of 40–100% were observed (Figure 3.13).

The difference in product yield between the substrains 17DD and 17D-204 was not

statistically significant for all PEG concentrations ($P = 0.17$, $P = 0.23$, $P = 0.49$, respectively). Only at 10% PEG-6000, almost full yield of infectious virus particles was achieved for both substrains with flow-through losses of $\leq 0.5\%$. Hence, we decided to use a loading concentration of 10% PEG-6000 for future chromatography experiments.

The target species' retention in SXC is influenced strongly by its size (38 nm for YFV): larger species bind at lower PEG concentrations [117]. Findings here correlated with previous reports where 8% PEG-6000 was enough to achieve complete yield of influenza viruses (Section 3.1), which are in the range of 80–120 nm.

After screening the PEG concentrations for sample loading, the membrane capacity (total particle load per membrane surface), flow rate, and digestion of the host cell DNA with an unspecific nuclease prior to SXC were characterized. More specifically, the goal with these tests was to confirm full virus yield at higher virus loads using 10% PEG-6000, and to verify the purity of the recovered product with respect to official requirements in terms of total protein and host cell DNA amount per dose (250 µg and 10 ng, respectively). For these experiments (see mass balances with relative recoveries in Table 3.5 and a representative chromatogram in Figure 3.14.A), the clarified virus harvest was digested with Denarase for 1 h at room temperature; for SXC, the virus particle load was increased approximately ten times (300–350 mL of clarified virus harvest) and the flow rate doubled to 10 mL min^{-1}.

The dsDNA concentrations in the clarified virus harvests before nuclease treatment were 4761.5 ng mL^{-1} (substrain 17DD) and 4415.8 ng mL^{-1} (substrain 17D-204); after the nuclease treatment, around 98% of dsDNA was depleted: 102.3 ng mL^{-1} (substrain 17DD) and 87.5 ng mL^{-1} (subtstrain 17D-204).
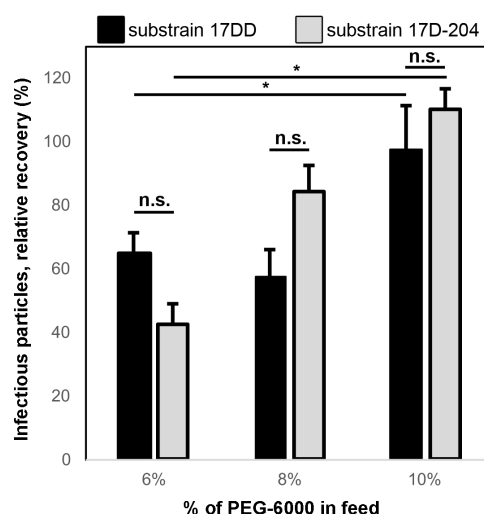
Figure 3.13. Screening for loading concentration of PEG-6000 during SXC of yellow fever virus particles (substrains 17DD and 17D-204) produced with adherent Vero cells in serum-free medium. Infectious virus titer is expressed as percentile yield. Data shown are means $\pm$ standard deviation of the mean of chromatography replicates (n=3). *$P < 0.05$; n.s., not significant.
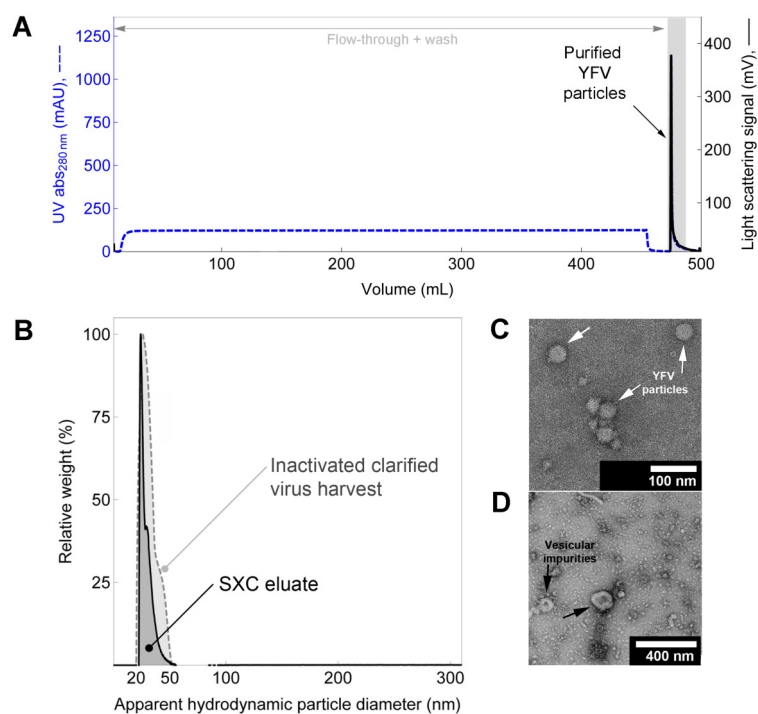
Figure 3.14. Representative SXC (panel A) of yellow fever virus (YFV) particles (strain 17D) produced in adherent Vero cells in serum-free medium. Particle size distributions by differential centrifugal sedimentation of starting material and SXC-purified YFV particles (panel B); the curves show a monodisperse peak of 25–55 nm with no species larger than 60 nm, indicating neither underlying nor SXC-induced aggregation. Transmission electron micrographs of purified YFV particles (white arrows, panel C) and co-eluted vesicular impurities (black arrows, panel D).

Table 3.5 shows the mass balances for the SXC experiments of these nuclease-treated samples. The depletion of host cell DNA and total protein in the elution pools was 62–73% and 92%, respectively. Most infectious virus particles were recovered in the first 5 mL (eluate 1) and virtually complete yield of infectious particles was recovered in 10 mL of eluate (eluate 1 and 2); this elution volume is partially an outcome from the geometric design of the columns used and in agreement for previous results with influenza virus.

The product recovery in the eluate was $101.1\% \pm 10.9$ and $108.9\% \pm 26.8$ the 17DD and the 17D-204 substrains, respectively (Table 3.5). As a comparison, Tânia Pato [166] achieved a yield of 58–93% of infectious virus particles (quantified by plaque assay) using IEC with a commercial Q membrane adsorber of 75 cm^2 (further discussion on Section 3.6).

Particle size distribution by DCS of the clarified virus harvest and elution fraction (Figure 3.14.B) showed a monodisperse peak of 25–55 nm; the absence of additional peaks indicates neither previously present nor SXC-induced aggregation. Offline DLS of elution fractions showed peaks of 40–50 nm with additional species in the range 200–600 nm (data not shown); the signal in the hundred nanometer range is attributed to the presence of EVs that cannot be detected by differential centrifugal sedimentation due to their lower density (1.096 g cm^{-3} [171]) compared to that of YFV (1.250 g cm^{-3}); we confirmed the

co-elution of these impurities by TEM (Figure 3.14.D).

The elution fractions from the experiments detailed in Table 3.5 had 565.0–704.4 pg_{dsDNA} $dose^{-1}$ depending on the substrain (considering a value of $\geq 4.74 \log_{10} PFU$ $dose^{-1}$ for currently commercially live-attenuated YF vaccines [8]). The oncogenicity and infectivity of host cell DNA are considered potential risks for vaccines: the 1997 WHO Expert Committee on Biological Standards reported that levels up to 10 ng DNA and ≤ 200 bp per dose of injected product from continuous cell lines — such as Vero cells — are acceptable. This limit of 10 ng per dose does not apply to products derived from microorganisms, diploid cell strains or primary animal cells or to oral vaccines made with continuous cell lines [172]. The same elution fractions (Table 3.5) had 105.3–137.5 ng_{prot} $dose^{-1}$, below the 250 μg total protein limit for live-attenuated YF vaccines [8].

In an attempt to purify a higher amount of YFV by further increasing the loaded volume from 300–350 mL to around 1000 mL of clarified virus harvest (Table 3.6), it was noticed that both the total protein and dsDNA per dose were lower (5–11 times and 23–29 times, respectively) compared to those in the experiments in Table 3.5.

The difference might be due to a possible displacement effect of protein and DNA by YFV particles during chromatography as a consequence of the virion's higher hydrodynamic radius, which correlates with their retention at the membrane surface. Further discussion on the DNA binding mechanism during SXC is found in Section 3.6.

Recent reports [33, 166] describe the purification of cell culture-based YFV with IEC as a capture step. The authors applied clarified virus harvests (substrain 17DD) onto 75 cm^2 quaternary ammonium (Q) anion-exchange membrane adsorbers at the same flow rate used in this work (10 mL min^{-1}; 122 cm h^{-1}); product recoveries were 59–86% (by plaque assay) and as much as $93.2\% \pm 30.2$ (by enzyme-linked immunosorbent assay (ELISA)) depending on the chromatography conditions.

When using IEC, the sample needs to be titrated to a specific pH to guarantee binding of the virus particles; for instance, Pato et al. [33] loaded YFV at pH 8.4 onto Q membrane adsorbers, although the authors had determined before that the stability of YFV was optimal at pH 7.2–7.4 and decreased towards higher pH values. With the work here using SXC, it was possible to keep the YFV sample at pH 7.4 without compromising neither binding during purification nor virus stability.

The experiments in Table 3.6 show DNA levels of 19–31 pg_{dsDNA} $dose^{-1}$, comfortably below the regulatory limit of 10 ng. Total protein levels were 9–27 ng_{prot} $dose^{-1}$, below the maximum 250 μg per dose limit.

As a comparison, Pato et al. [173] reported recoveries for YFV of 52.7% with 1.17 ng_{DNA} $dose^{-1}$ with a purification process consisting of an anion exchange capture step (75 cm^2 membrane adsorber) and a polishing step with Capto™ Core 700.

Table 3.7 shows selected column capacities for purification of *Flavivirus* or YFV. The capacities obtained with SXC media used in this work were in the same order of

magnitude or slightly higher to those reported in the literature. It seems that for IEC regardless of the medium used for purification (monolith or membrane), the maximum capacities for *Flavivirus* are in a similar range [33, 166, 169] (refer to specific capacity values in Table 3.7).

Since SXC is not an adsorptive process, the reported capacity of 6.02×10^7 PFU cm^{-2} was the one achieved with the maximum viral particle yield we evaluated in this work (Table 3.6). The capacity of the membrane-based SXC process is most likely higher as recoveries were high and follow-up studies should be performed to better determine the capacity.

It is pertinent to note that these values can be further improved since virtually full yield of virus particles was observed, indicating that an even larger virus challenge per membrane area is possible.

Depending on the virus titer of eluates of the corresponding substrain, the maximum number of purified doses obtained were $\geq 31\,000$ for 17DD and $\geq 109\,000$ for 17D-204 with a concentration factor of about 100-fold (Table 3.6). Productivities were as high as 2.78×10^{11} PFU PFU $m^{-2}\,h^{-1}$ (5.06×10^6 doses $m^{-2}\,h^{-1}$). For comparison purposes, the commercial egg-based YF vaccine process has a yield of 100–300 doses per egg [8]. The inability to quickly replace vaccine stockpiles is a critical factor in YF vaccine availability and supply shortage [32]. With the process established, around $100\,000$ doses could be purified from roughly 1 L of virus broth, an amount of doses that would require 300–1000 eggs.

With the achieved productivity, it would be possible to purify ≥ 90 million YFV doses per hour with an 18 m^2 column; membrane devices with this binding surface are already commercially available. However, these devices are usually made from cellulose membranes that are functionalized for other kinds of chromatography techniques, e.g., IEC or hydrophobic interaction chromatography. A simple replacement for non-functionalized cellulose membranes would allow SXC to be carried out at large scale.

Table 3.5

Mass balances and percentile recoveries of SXC of yellow fever virus produced with adherent Vero cells in serum-free medium. Data shown are means ± standard deviation of the mean of chromatography replicates (n=1 per substrain).

Substrain	Sample	Volume (mL)	Infectious titer in virus product $\log_{10}(x)$	(PFU mL^{-1}) (x)	%	Impurities Protein[a] (μg mL^{-1})	%	DNA[b] (ng mL^{-1})	%
17DD	Feed	443.2	6.28 ± 0.06	$1.90 \times 10^6 \pm 2.00 \times 10^5$	100.0	49.4 ± 0.2	100.0	61.7 ± 5.2	100.0
	Flow-through	463.2	4.92 ± 0.02	$8.27 \times 10^4 \pm 2.51 \times 10^3$	4.5 ± 0.5	44.7 ± 0.1	94.6 ± 0.5	<LOD	<LOD
	Eluate$_1$[c]	5.0	8.20 ± 0.03	$1.58 \times 10^8 \pm 7.52 \times 10^6$	93.5 ± 10.8	163.4 ± 1.6	7.5 ± 0.0	1093.4 ± 35.8	37.6 ± 2.0
	Eluate$_2$	5.0	7.10 ± 0.08	$1.28 \times 10^7 \pm 1.75 \times 10^6$	7.6 ± 1.3				
	Σ				105.6 ± 10.9		102.1 ± 0.5		37.6 ± 2.0
17D-204	Feed	437.3	6.18 ± 0.03	$1.53 \times 10^6 \pm 7.52 \times 10^4$	100.0	53.6 ± 7.2	100.0	63.1 ± 3.7	100.0
	Flow-through	457.3	4.76 ± 0.08	$5.76 \times 10^4 \pm 7.52 \times 10^3$	4.0 ± 0.6	47.0 ± 5.2	91.7 ± 16.0	<LOQ	<LOQ
	Eluate$_1$[c]	5.0	8.12 ± 0.16	$1.35 \times 10^8 \pm 3.51 \times 10^7$	101.4 ± 26.7	182.0 ± 1.5	7.8 ± 1.0	747.6 ± 33.0	27.1 ± 1.7
	Eluate$_2$	5.0	6.98 ± 0.19	$1.00 \times 10^7 \pm 3.01 \times 10^6$	7.5 ± 2.3				
	Σ				112.9 ± 26.8		99.5 ± 16.0		27.1 ± 1.7

PFU=plaque forming units; LOD=limit of detection; LOQ=limit of quantitation; n.d., not determined

[a] total protein by Bradford assay
[b] dsDNA by PicoGreen assay
[c] stated values represent a pool of eluate$_1$ + eluate$_2$ for protein & DNA measurements

Table 3.6

Calculated yellow fever vaccine doses from optimized and scaled-up SXC experiments. Doses are calculated considering ≥ 4.74 $\log_{10}$ plaque forming units (PFU) per dose for a live attenuated commercial vaccine. Data shown are means $\pm$ standard deviation of the mean of chromatography replicates (n=1 per substrain).

Substrain	Volume (mL)		Concentration factor (fold)	Infectious titer in purified product			Protein per dose (ng)[c]	DNA per dose (pg)[d]
	starting[a]	final[b]		PFU	Recovery (%)	no. of doses		
17DD[e]	1009.4	10.0	100.9	$1.75 \times 10^9 \pm 1.75 \times 10^8$	92.0 ± 13.8	$31\,845 \pm 3185$	27.0 ± 2.7	31.1 ± 3.1
17D-204[f]	896.1	10.0	89.6	$6.02 \times 10^9 \pm 1.27 \times 10^8$	107.4 ± 6.1	$109\,546 \pm 2311$	9.2 ± 0.2	19.4 ± 0.4
Σ					99.7 ± 7.5			

[a] nuclease-treated clarified virus harvest before conditioning with PEG
[b] SXC elution pools
[c] total protein by Bradford assay; max. 250 µg total protein per dose
[d] dsDNA by PicoGreen assay; max. 10 ng DNA per dose
[e] total infectious titer: $1.90 \times 10^9 \pm 2.51 \times 10^8$ PFU
[f] total infectious titer: $5.60 \times 10^9 \pm 3.29 \times 10^8$ PFU

Table 3.7

Capacities of various convective media used for purification of cell culture-based *Flavivirus* or yellow fever virus (YFV) particles.

Virus	Strain	Purification mode	Stationary phase						Ref.
			Kind	Support[a]	Ligand	Pore size	Volume/surface	Specific capacity	
Flavivirus	–	IEX	Monolith	poly(glycidyl methacrylate-*co*-ethylene dimethacrylate)	Quaternary ammonium	1.3 µm	1.0 mL	4.5×10^9 FFU mL^{-1}	[169]
YFV	17D	IEX	Membrane	stabilized reinforced cellulose	Quaternary ammonium	3–5 µm	75 cm^2	2.26 µg$_{Eprotein}$ cm$^{-1,\,b}$ 5.39×10^7 PFU cm$^{-2,\,c}$	[33, 166]
YFV	17D	SXC	Membrane	regenerated cellulose	None	1.0 µm	100 cm^2	$\geq 6.02 \times 10^7$ PFU cm^{-2}	this work

IEX=ion exchange chromatography; FFU=focusing forming units; PFU=plaque forming units; SXC=steric exclusion chromatography;

[a] as stated by the manufacturer
[b] reported as dynamic binding capacity at 10% breakthrough (DBC$_{10\%}$)
[c] calculated from ratios of reported PFU and µg of the E protein antigen in elution pools

3.3 SXC of adeno-associated virus

The purification of AAV presents different challenges compared to other viruses discussed before. AAV is one of the smallest viruses known to infect humans and its small size of around 20–25 nm could potentially challenge SXC purification. Secondly, AAV is not exported to the cell medium and because it is not lytic, it has to be extracted from the cells. This means that additional downstream steps are needed for harvesting the virus, most typically freeze-thawing cycles in small scale and cell lysis with detergents at industrial scale. Finally, the amount of impurities in AAV harvests can be higher because of the presence of intracellular impurities from the cell lysis.

The first SXC experiments were made with wild-type serotypes AAV-1, AAV-2, AAV-6, and AAV-8 using 11 cm^2 columns (13 mm filter holder). These experiments were performed with "small scale lysates" (1 mL generated from a pool of three wells from 6-well plates). It was decided to load at 12% PEG-6000 based on AAV's size and previous results with YFV. *In vitro* expression of the transgene reporter was used to assess the biological activity of AAV. As observed in Figure 3.15, there was no detectable expression of the fluorescent transgene reporter in the flow-through fractions, suggesting no product losses during loading. The elution fractions had a significantly higher transduction ratio compared to the feeds (PEG-conditioned unpurified samples). The residual total protein and DNA are listed in Table 3.8.

A typical chromatogram is shown in Figure 3.16 with a picture of SF539 cells successfully expressing the fluorescent reporter after infection with purified AAV-2 particles.

Further experiments from "medium scale lysates" (5 mL generated from a pool of six 15-cm dishes) were made. These test unfortunately failed as the sample turned turbid
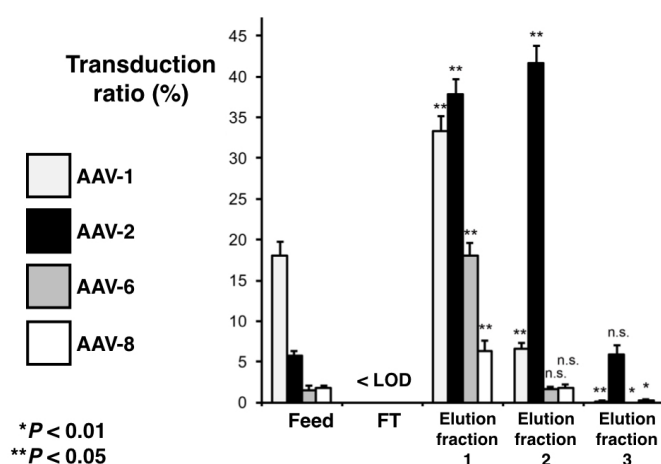
Figure 3.15. Reporter expression in transduced cells with different wild-type adeno-associated virus (AAV) serotypes purified with SXC (n=1). The elution fractions are compared against the feed. Data shown are means ± standard deviation of the mean of analytical replicates (n=9). FT=flow-through LOD=limit of detection.

immediately upon addition of the PEG, suggesting product aggregation. This issue could not be resolved by adding less PEG. Regarding precipitation dependent of the number of particles, Polson et al. remark that: "[...] when a suspension which had a small number of monomeric particles per unit volume is precipitated, the aggregates formed are composed of small numbers of virions" [174]. Thus, this was attributed to a higher concentration of AAV particles compared to the small scale lysates. It was decided to continue working with small scale lysates and the outlook on medium scale lysates is addressed further below.

The PEG concentration was reduced to 10% and experiments repeated for the wild-types AAV-2, AAV-6 and additional recombinant/chimeric particles denoted as AAV-DJP2, AAV-1P5, and AAV-9A2. Transgene reporter expression levels for selected virus particles are shown in Figure 3.17.

As observed, the lack of gene expression in the flow-through fractions is a general trend. Note that the unpurified crude lysates ("start") show lower expression and transduction signals compared to the PEG-conditioned sample before SXC. This was attributed to reduced potency by product dilution (the load was 10 times less concentrated compared
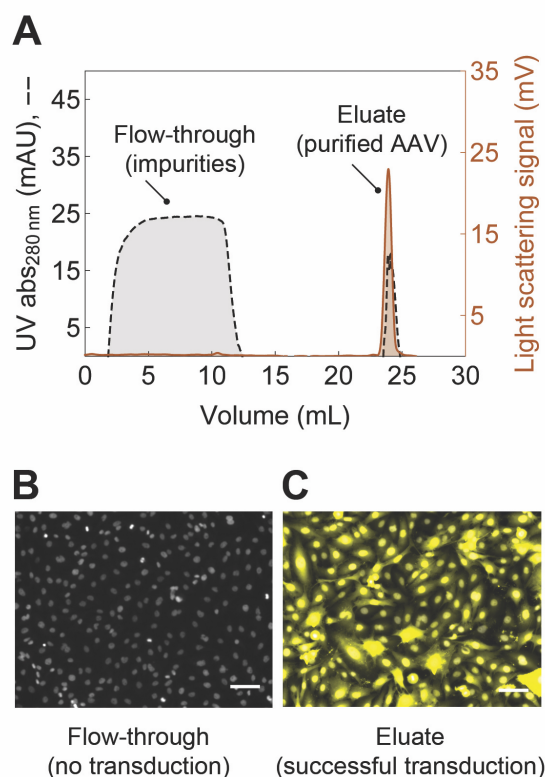
Figure 3.16. SXC of adeno-associated virus (AAV) particles produced in HEK cells. Representative chromatogram from a purification of AAV-2 (panel A). The panels below show the reporter expression in transduced SF539 cells with flow-through fractions (panel B, no detectable expression) and elution fractions (panel C, successful expression of the yellow fluorescent protein reporter). The scale bar represents 100 µm. Transduction assays performed by Kathleen Börner at the Heidelberg University Hospital in Heidelberg, Germany.

to the crude lysates). A PEG concentration of 10% was selected for AAV, although these results suggest that it could be lowered slightly more.

Besides gene expression, gene knockdown was also evaluated (CPSF6): U87 cells were transduced with different AAV vectors (wild-type AAV-6 and AAV-DJP2) encoding a NS shRNA with a CFP reporter or triple-shRNA cassettes (shCPSF6a&b, Figure 3.19). Additionally, MDM from two different human donors were transduced with SXC-purified AAV particles and the results showed a significant reduction in CPSF6 gene expression (Figure 3.19.D) compared to non-transduced cells.

The total amount of virus particles quantified by PCR in elution pools ranged between 1.27×10^{10} and 1.70×10^{11} vg depending on the serotype/variant used, with average recoveries of 101.0%±25.6. Although at times it was estimated that flow-through fractions contained 5.00×10^8 to 7.80×10^8 vg mL^{-1}, chromatograms and transduction assays indicate that genome titers in the flow-through are not related to functional AAV particles, as shown previously (Figure 3.17). The product recoveries stated above represent a measured productivity of approximately 1.02×10^{14} vg m^{-2} h^{-1}. Nevertheless, because of the lack of product signal in the flow-through, it is believed the capacity of the 100 cm^2 device is at least 3–5 times higher. This should be addressed in future work by challenging the column with higher amounts of product.

Figure 3.18 shows TEM pictures of crude lysates and SXC-purified AAV particles. The purified virus particles are homogeneous in shape and size with an approximate diameter of 25 nm. Although there are more full capsids than empty ones, it can't be speculated it was possible to enrich the full capsids with SXC.

IEC has been used to separate full capsids from empty shells and depends strongly

Table 3.8

Percentile recoveries for residual impurities from SXC experiments with several wild-type adeno-associated virus (AAV) serotypes.

Serotype	Sample	Protein (%)[a]	DNA (%)[b]
AAV-1	Feed	100.0	100.0
	Flow-through	97.3	75.6
	Elution	12.8	<LOD
AAV-2	Feed	100.0	100.0
	Flow-through	93.9	<LOD
	Elution	13.6	<LOD
AAV-6	Feed	100.0	100.0
	Flow-through	97.7	77.7
	Elution	12.7	<LOD
AAV-8	Feed	100.0	100.0
	Flow-through	95.6	81.7
	Elution	9.9	<LOD

LOD=limit of detection

[a] total protein by Quant-iT Kit assay
[b] dsDNA by PicoGreen Kit assay
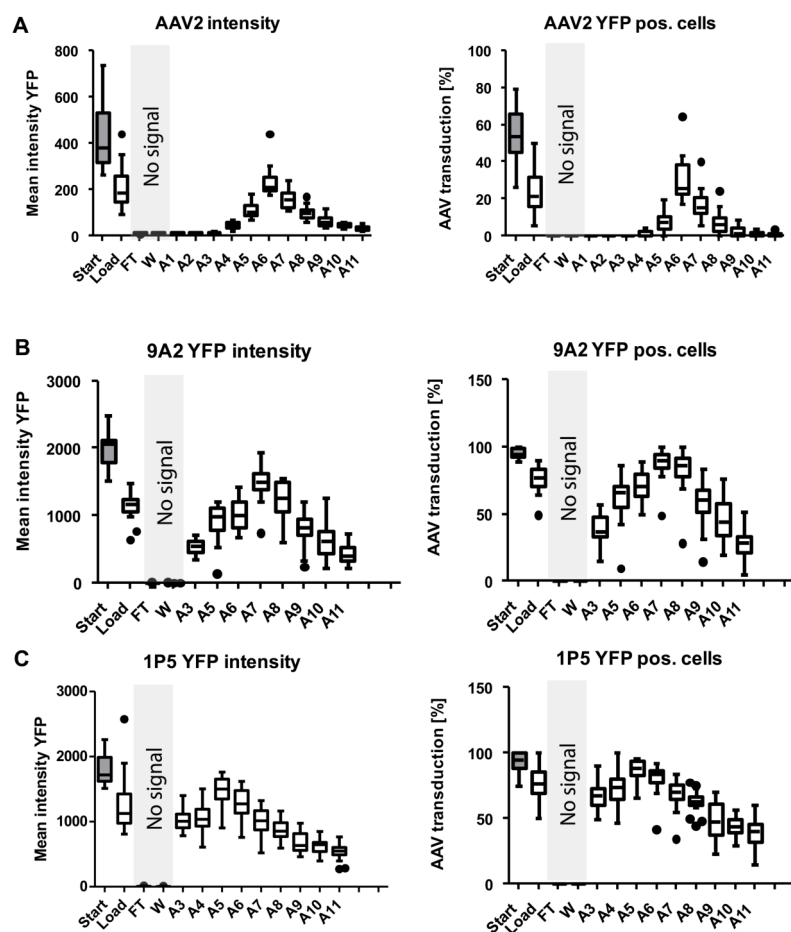
Figure 3.17. Transgene reporter expression levels and reporter-positive cells transduced with selected adeno-associated virus (AAV) serotypes and display mutants purified by SXC (n=1). Transduction experiments performed by Kathleen Börner at the Heidelberg University Hospital in Heidelberg, Germany. Start=unpurified crude lysates; Load=PEG-conditioned sample before SXC; FT=flow-through; W=wash; AXX=elution fractions.
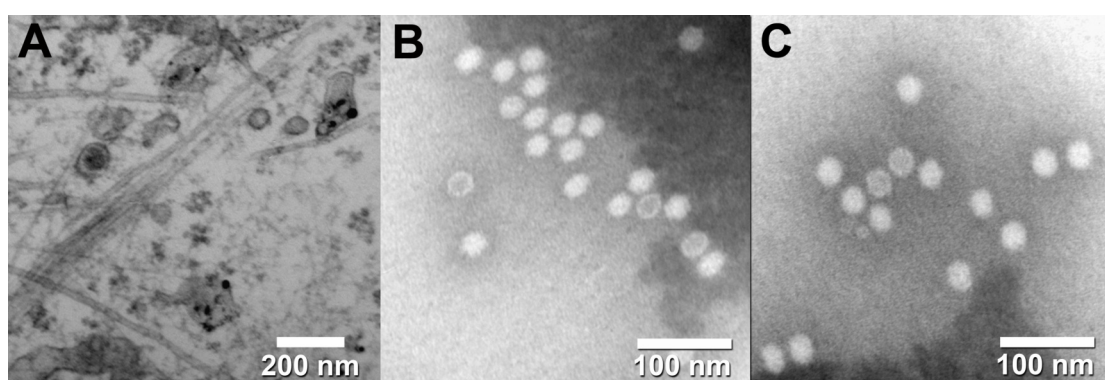
Figure 3.18. Transmission electron micrographs of adeno-associated virus (AAV) clarified crude lysates before purification (panel A) and after SXC purification (panels B and C). Impurities such as subcellular structures and aggregates can be observed in the unpurified sample. The purified AAV particles are homogeneous in shape and size with an approximate diameter of 25 nm. The genome-containing particles (white arrow) appear completely white in the negative staining, as opposed to empty capsids (dark arrow), which appear as a white rim with a dark core. Pictures taken by Martin Obr at the Heidelberg University Hospital in Heidelberg, Germany.
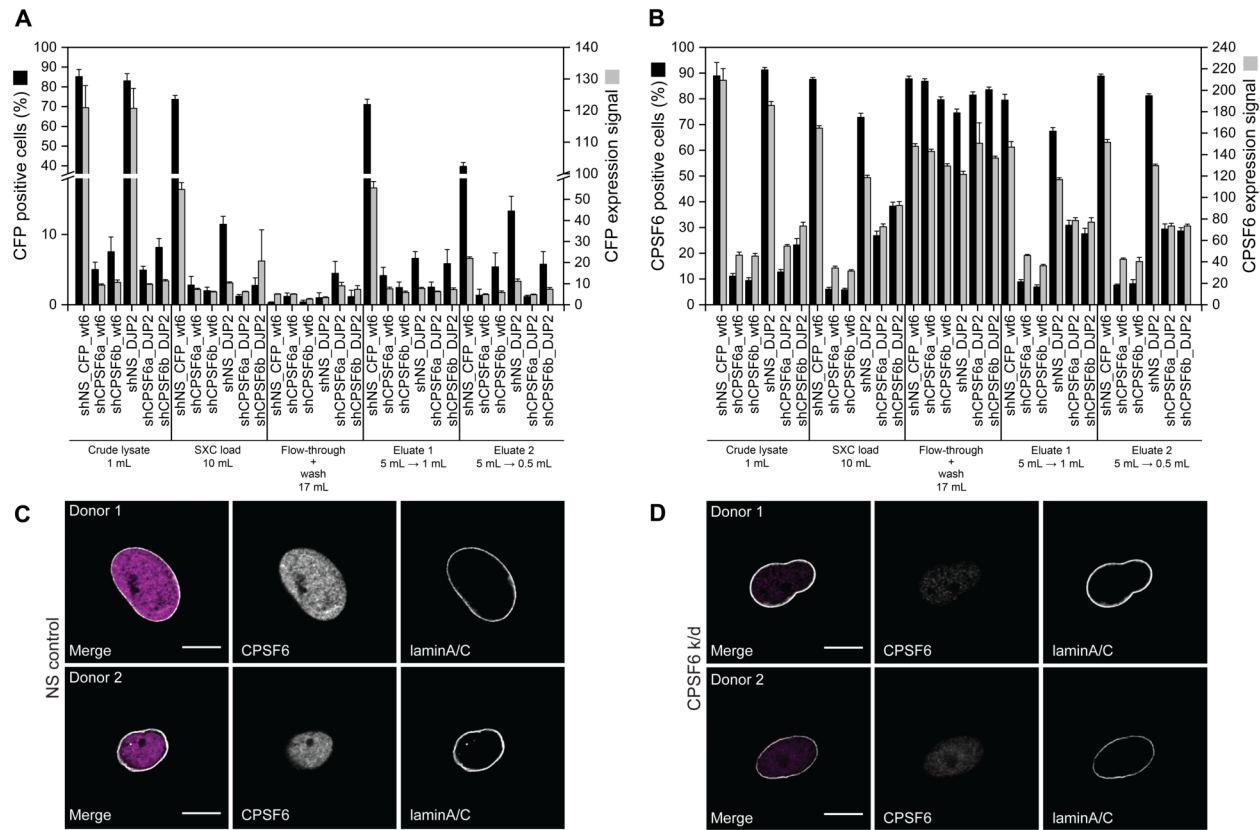
Figure 3.19. Cleavage and polyadenylation specificity factor subunit 6 (CPSF6) knockdown by transduction with adeno-associated virus (AAV) vectors (wild-type AAV-6 and DJP2) at several stages of their purification with SXC. U87 cells were transduced with different AAV vectors (wtAAV6 and DJP2) encoding the non-silencing (NS) short hairpin RNA (shRNA) with a cyan fluorescent protein (CFP) reporter or triple-shRNA cassettes (shCPSF6a&b). The two vectors (wtAAV6 and DJP2) encode the non-silencing shRNA (NS) with either a CFP reporter or triple-shRNA cassettes (shCPSF6a&b) in order to knockdown CPSF6. (a) CFP positive cells and the CPSF6 expression levels. (b) Transduction of MDM from two different donors with SXC-purified AAV particles (Eluate 1 from panels A and B) carrying either a non-targeted shRNA (panel C) or three shRNAs targeting CPSF6 (panel D). Transduction experiments performed by Kathleen Börner and David Bejarano at the Heidelberg University Hospital in Heidelberg, Germany.

on pH and conductivity. At times, these factors, which also play a role in SXC, influence separation performance as heavily as the hydrodynamic size of the target product [94, 107, 117, 122]. These facts point to the possibility of separating full capsids from empty using SXC, an intriguing and exciting scope for future work.

Although AAV has to be harvested by cell lysis, virus particles may be found in the supernatants due to cell death. The purification of AAV present in the cell culture medium is attractive because it involves less DSP steps and potentially a reduced amount of impurities compared to cell lysates. Purification from supernatants was tested for AAV-6 and AAV-1P5. Before SXC, the cell supernatants were clarified with a series of 0.45 µm and 0.2 µm filters and mixed in-line with a 20% PEG-6000 stock. The elution fractions were collected, dialyzed (100 kDa) and lyophilized before doing transduction assays. In the case of AAV-6, there was no measurable gene expression in cells transduced with non-purified clarified samples, most probably due to a very low virus concentration. Purified fractions, however, showed a transfection ratio of 18.4% for the eluate (concentrated 10×) and 82.6% for the reconstituted lyophilized eluate (concentrated ≈400×). For AAV-1P5, the clarified samples before SXC had a transfection ratio of 60%, the eluate around 95% and the reconstituted lyophilized eluate >98% (data not shown).

A direct comparison between these two examples above is complex since the gene expression varies greatly between serotypes and variants. For instance, Piras et al. [175] reported that the proportion of viral particles in the media increased from 76% at day 3 to 94% at day 7 for AAV-8 packaged with Factor VIII. The proportional shift, however,
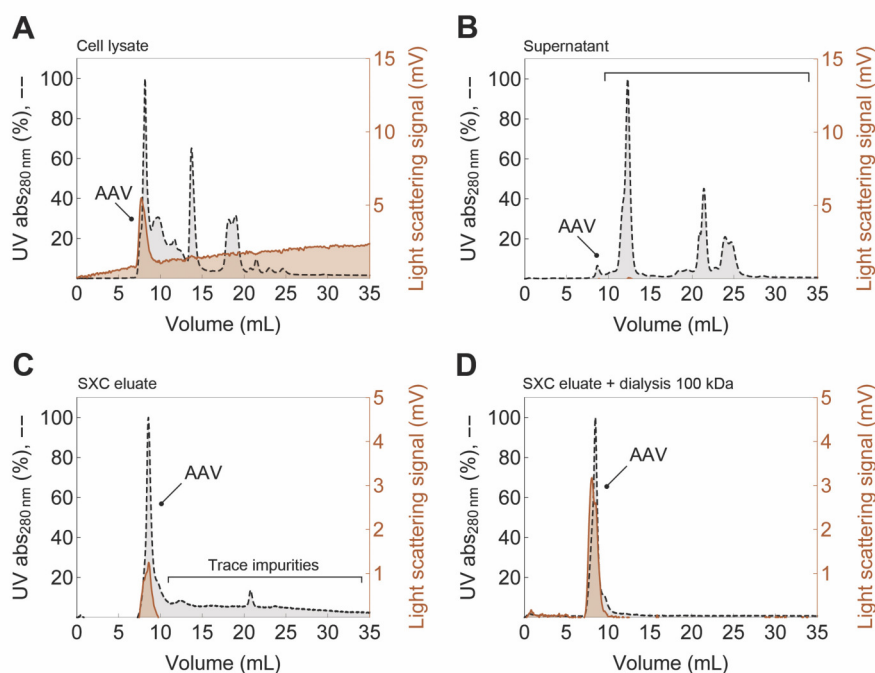
Figure 3.20. Size exclusion chromatography fingerprints of adeno-associated virus samples. (A and B) Unpurified starting material. (C) SXC eluate. (D) SXC eluate after dialysis.

was dependent on the packaged vector, but *in vivo* function was equivalent in both the early cell lysate and the late supernatant harvests.

Density gradient ultracentrifugation is not a viable option for purifying AAV from supernatants due to the reduced volume the centrifuges can handle and the long processing times, besides the manual handling. Processing vast volumes, however, would not be an issue for SXC.

Although the total protein load might be higher from late-cultivation supernatant harvests, the impurity profile from cell lysates is still more complex: in SEC, virus particles elute in the void volume due to their inability to diffuse into the beads' pores (Figure 3.20.A).

The void-eluted virus peak from crude lysates was not resolved from the rest of the impurities in SEC, making size separation complex even with this efficient chromatography method for biomolecules in the 20–300 nm range. On the other hand, the void-eluted virus peak from supernatants was resolved, amid AAV being present at much lower concentration (Figure 3.20.B). SXC-purified AAV particles show a low UV signal impurity trace (Figure 3.20.C) that is successfully cleared by 100 kDa or 300 kDa dialysis (Figure 3.20.D).

3.4   SXC of Modified Vaccinia Ankara virus

MVA virus was produced in a two-stage STR cascade [139] and purified using 8% PEG-6000 and 1.0 µm regenerated cellulose membranes. Preliminary results showed an infectious titer yield of 123.3% by $TCID_{50}$ (Table 3.9). The product yield of more than 120% is attributed to the analytical error of the assay, which is typically not well suited for this kind of balance. A PCR or an ELISA would compliment the $TCID_{50}$ results. MVA was the biggest virus (220–450 nm long and 140–260 nm wide) purified with SXC in this work. There were concerns at the beginning that the size of the virus might cause blockage of the 1.0 µm pore size membranes used.

Particle association promoted by the presence of PEG was measured over time by

Table 3.9

Infectious titer recovery from SXC experiments of Modified Vaccinia Ankara virus.

Sample	Volume (mL)	Infectious titer[a]	
		$(TCID_{50}\ mL^{-1})$	Recovery (%)
Feed	20.0	3.0×10^8	100.0
Flow-through	35.0	<LOD	
Eluate$_1$	10.0	5.6×10^8	93.3
Eluate$_2$	10.0	1.8×10^8	30.0

LOD=limit of detection; vp=virus particles

[a] by tissue culture 50% infective dose ($TCID_{50}$) assay
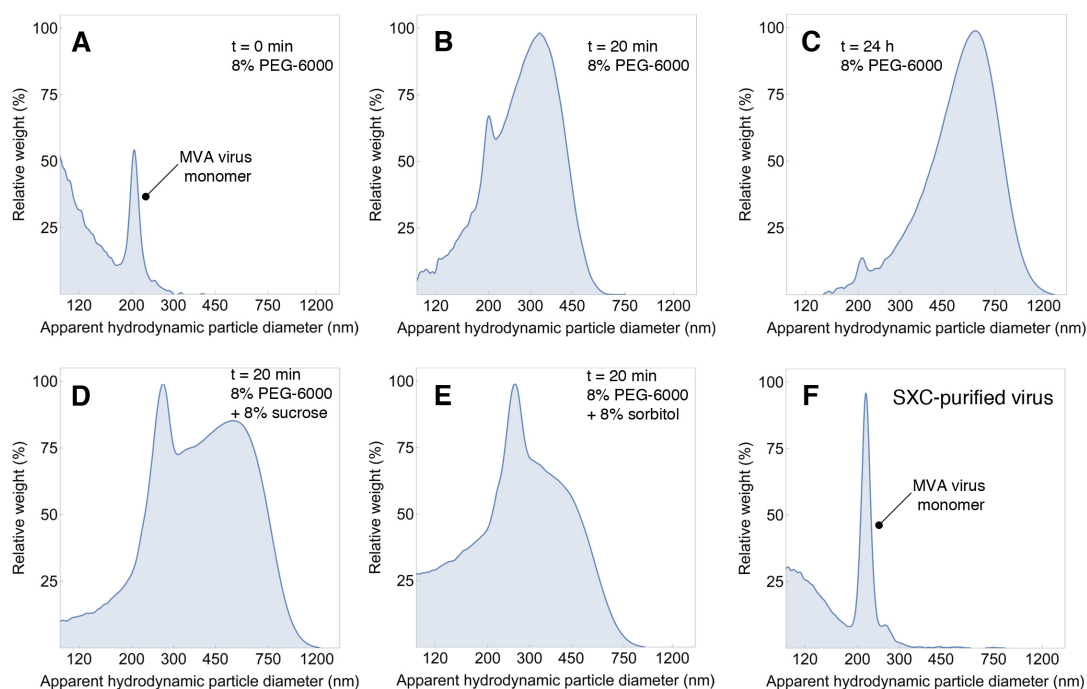
Figure 3.21. Particle size distributions by differential centrifugal sedimentation of Modified Vaccinia Ankara (MVA) virus incubated at different time points with 8% PEG-6000. (A to E) Unpurified MVA virus. (F) SXC-purified MVA virus.

DCS (Figure 3.21). Before the addition of PEG, a clear MVA virus monomer is observed at around 220 nm. As soon as 20 min after the addition of the polymer, aggregates of 300-400 nm appear; this pattern is even more pronounced after 24 h where aggregates of approximately 700 nm become visible with the virus monomer peak barely perceivable. It seems that with the short loading times used, this behavior didn't cause any issues but should be considered when feeding larger samples volumes. Alternative options could be mixing the PEG in-line or the use of membranes with pore sizes larger than 1.0 µm, which would be desirable for the purification of other large viruses, such as measles virus.

Incubation of the PEG-conditioned sample in the presence of stabilizers (either sucrose or sorbitol) showed different particle size distribution profiles; although a main peak slightly bigger than the virus monomer peak was observed, it seemed that the stabilizers prevented the formation of larger aggregates. Using sorbitol reduced the formation of aggregates compared to sucrose. Regardless, the SXC-purified virus displayed no signs of aggregations with a monomer peak at around 220 nm (Figure 3.21.F). A combination of larger membrane pore sizes and the use of stabilizers in the PEG-conditioned sample could be used to mitigate the risk of fouling for complex mixtures and large viruses. Finally, given the virus size, more studies are required to assess its capture at PEG-6000 concentrations lower than 8% or different PEG sizes.

3.5 SXC of extracellular vesicles

In the following, preliminary results for the SXC purification of EVs are shown.

Based on the results obtained for SXC of influenza virus, TEM analysis of SXC-purified influenza virus showed contamination of vesicular structures very similar in size to the virus particles (Figure 3.4). Based on these results, it was speculated that EVs could be purified by SXC from cell supernatants.

To assess the applicability of using SXC for purifying EVs, supernatants from different cell lines were used (MDCK, BHK, and HEK cells) and the EVs quantified by NTA.

Loading PEG-6000 concentrations of 8, 10 and 12% were tested initially for MDCK and BHK cells supernatants clarified by a combination of centrifugation and microfiltration steps (20 mL loaded). The yield of EVs increased with higher PEG concentration: at 12% PEG-6000, 86.9% and 35.7% of loaded particles were recovered from MDCK and BHK supernatants, respectively, with particle concentrations in the main eluate (5 mL) in the range 2.30×10^9–1.09×10^9 particles/mL for MDCK cells and 5.18×10^{10}–7.95×10^{10} particles/mL for BHK cells. The total amount of particles in the flow-through was 12.0–26.6% for MDCK cells and 26.8–46% for BHK cells; although the particle recovery in the eluate increased slightly with higher PEG concentrations, there was no benefit in terms of minimizing the particles in the flow-through. It was decided to use 10% PEG-6000 as loading concentration to minimize the capture of contaminating
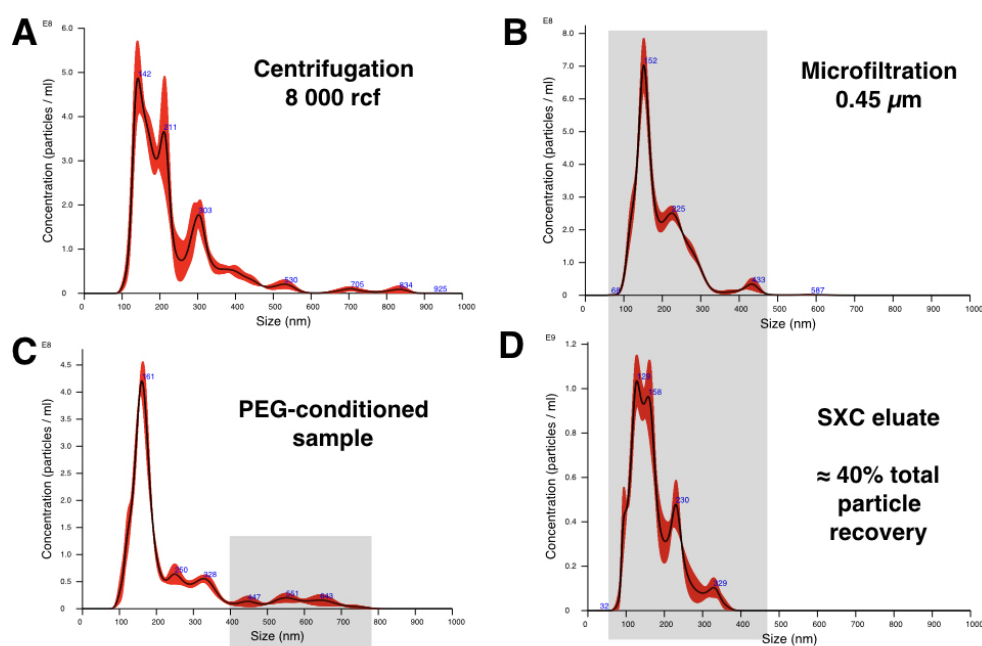
Figure 3.22. Nanoparticle tracking analysis (NTA) of BHK cells supernatants through sequential clarification steps (panels A, B, and C) and after SXC (panel D). NTA was performed by Matthias Prömmel at IDT Biologika GmbH in Dessau, Germany.

proteins since at this PEG concentration, particle yield was higher (47.6% for MDCK cells and 30.3% for BHK cells) than what is typically achieved with ultracentrifugation (5–25%, [176–178]).

NTA revealed that the PEG-conditioned sample contained a population of particles in the range of 400–700 nm that was not detected in the previous 0.45 µm clarification step (Figure 3.22 for BHK samples).

This is yet another confirmation of the particle aggregation induced by SXC and a possible reason for decreased particle recovery due to matrix fouling (bigger vesicles might start blocking the membrane pores). Fouling and particle loss might be more noticeable with EVs since they are less rigid than virus particles because they lack a solid protein shell. Additionally, PEG is known to induce vesicle fusion [179, 180].

The purified fractions showed a similar particle size distribution to the 0.45 µm filtered sample before SXC with mean particle diameters of 160—230 nm for MDCK cells and 157—189 nm for BHK cells. This population size is the one with most interest in the EVs field for both diagnostics and drug delivery [88, 176, 177, 181–183].

There was also interest for analytical characterization [184] of EVs from HEK-293-F cells. Cells grown using a chemically-defined "FreeStyle 293 Expression Medium", however, showed very low protein and EVs content in the clarified supernatant, indicating a need for concentration. The SEC fingerprint from the clarified supernatant showed no detectable signal of EVs (Figure 3.23). To this end, around 900 mL of clarified supernatant were purified with SXC loading at 10% PEG-6000 with a 100 cm^2 column with an in-line mixing approach.

SEC analysis of the elution pools showed both protein and EVs signals eluting in the void volume of the column demonstrating successful concentration of the EVs and very low levels of trace impurities. A subsequent dialysis step of the elution fraction with a 300 kDa pore size showed no notable impurities in SEC analysis and overlaying protein and EVs signals (Figure 3.23).

These results above show promise for using SXC in the preparative purification of
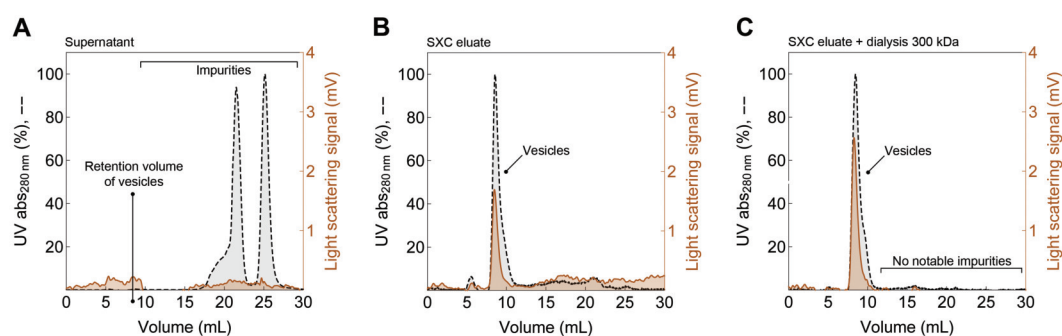
Figure 3.23. Size exclusion chromatography fingerprints of extracellular vesicles from HEK cell supernatants. (A) Unpurified starting material. (B) SXC eluate. (C) SXC eluate after dialysis.

EVs. With traditionally used methods such as ultracentrifugation, the purification of nearly 1 L of cell supernatant would take several days with notable manual work and using SEC would be virtually impossible for a small laboratory (a column of nearly 47 L would be required). Even using a large SEC column (e.g., HiLoad Superdex 200 prep grade, 320 mL) for a small laboratory, it would require more than 75 chromatography runs lasting several hours each to purify EVs from 1 L of supernatant, not to mention dilution of the purified sample.

Of course, methods other than SXC offer different advantages and their use is not mutually exclusive as has been discussed for virus particles. SXC might be used to concentrate huge volumes of supernatants quickly with relatively high yield and the concentrated purified sample can be further purified by other methods for specific analysis, e.g., affinity chromatography for the enrichment of particular EVs populations.

3.6   Mechanism and characteristics of SXC

Protein precipitation induced by PEG has been explained by excluded volume effects, which are the principle behind SXC [106, 108]: as the concentration of PEG increases, the chemical potential of the protein increases as well, eventually exceeding that of its solid phase, at which precipitation occurs [109]. This observation, however, is based on a three component system in solution without a stationary phase. The addition of a hydrophilic matrix gives a notable advantage: since the PEG is also sterically excluded from the stationary phase, the shift to a new equilibrium makes use of the matrix by minimizing the PEG-excluded zone, and thus the product binds at the surface. The consequence of this is a faster product capture and purification without the need of low temperatures and incubation as commonly used in PEG precipitation.

PEG-6000 was chosen for the experiments here based on literature reports where common molecular masses of PEG for precipitation of viruses and VLPs are mostly in the range of 4000–8000 Da [26, 111–116, 185]. Additionally, PEG-6000 was used for monolith-based SXC studies [117, 143, 162]. As discussed by Lee et al. [117], the dominant factor for separation in SXC is the hydrodynamic size of the target species. Additional factors that also have an influence on product yield such as isoelectric point of the product, hydrophilicity, and pH are examined elsewhere [107, 186, 187]. For example, Lee et al. extensively discussed the influence of conductivity and pH for SXC of IgM. The target species binds more strongly as the pH approaches the pI of the product, following the same trend known for precipitation with PEG. Additionally, salts weaken the retention proportionally to their concentration and Hofmeister series ranking. Weaker binding in this regard is due to smaller PEG-deficient zones caused by the salts. Accordingly, this effect can be reversed by increasing the PEG concentration.

This applies, however, to idealized systems with pure proteins but are more complicated with heterogeneous species such as the virus particles used in this work. Besides from the much higher degree of complexity of viruses, they are physically and biologically stable on a relatively narrow range of conductivity and pH, not to mention the analyses that are required for their quantitation. A similar trend was observed, however, when the yield of influenza virus was lower at lower conductivity during elution (Figure 3.8), agreeing with Lee's conclusions that lower salt concentration would increase the influence of PEG and thus result in stronger retention to the stationary phase.

The selectivity of the product retention can be tweaked by the choice of the polymer molecular mass and its concentration, which increases or decreases the size of the polymer-deficient zone around the macromolecule. A general trend arises from this behavior: higher molecular mass PEG are more efficient at facilitating binding at lower concentrations compared to lower molecular mass PEG. As a result, plots of product retention against

PEG concentration are steeper for higher mass PEG, giving lower mass PEG a broader concentration range to work with (Figure 3.24).

However, using both extremes of PEG mass is disadvantageous: higher molecular mass PEG increase drastically the solution viscosity (e.g., 20 000 Da) and might give experimental difficulties during chromatography or related operations, such as pumping, mixing, and filtration. On the other hand, some lower mass PEG are available as liquid only as solid wax-like substances (<1000 Da), rather than small flakes (>1000 Da) and need to be melted for buffer preparation. All these reasons account for the most common PEG masses used to be 4000–8000 Da.

As discussed by Lee et al. [117], high-capacity binding of DNA during SXC is unfavorable due to the DNA's mutual charge repulsion limiting the packing density of DNA on the stationary phase. Besides the short length of the digested DNA (ideally, 2–5 bp [122]) which should prevent its biding during SXC, YFV is negatively charged at pH 7.4 (pI=4.2–5.2) [188], creating also a charge repulsion between virus and DNA. This behavior was observed by Levanova and Poranen [189] who studied the binding of dsDNA on OH monoliths: the authors observed that at least 400 mM of NaCl was required to achieve retention of dsDNA (500 bp, 1800 bp, and 48 502 bp) as is negligible (0.5–5%) without any salt up to 20% PEG-6000. This coincide with results that show that total DNA (from 100–46 500 bp) precipitation can be achieved with 15% PEG-6000 and 550 mM NaCl [190].

Based on the results of Levanova and Poranen discussed above, it seems any bound
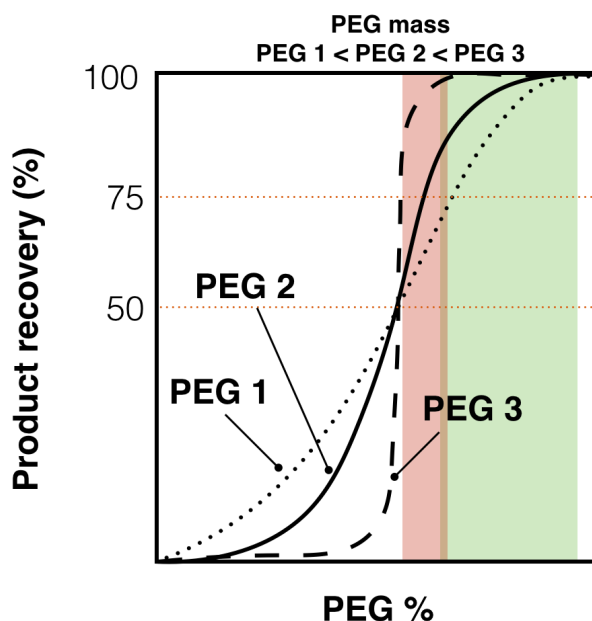
Figure 3.24. The working range for steric exclusion chromatography (SXC) depends on the mass and concentration of polyethylene glycol (PEG) used. Lower mass PEG display a broader range.

dsDNA at the conditions usually used in this work (8–10% PEG-6000, 150 mM NaCl) would be negligible, even more so if the DNA was previously digested. It is advantageous then, to place the DNA digestion step before SXC not only to clear residual DNA, but the nuclease (54 kDa) too. Although the residual nuclease in purified fractions was not quantified in any experiment here, SXC with BSA (66 kDa) loaded at 8% PEG-6000 (Figure 3.25) showed a residual amount in the eluate of only 0.1% — that would be easily cleared in any following dialysis/ultrafiltration step afterwards.

The elution behavior of several biomolecules (BSA, IgG, IgM, influenza virus, and mucin from porcine stomach) was studied here with by decreasing the PEG-6000 concentration in a gradient elution with a 100 cm^2 device. It was observed that the elution time increased proportionally to the hydrodynamic size of the target product, as theory predicts (Figure 3.25). Correspondingly, the amount of product recovered relative to the feed was proportional to its size. For example, merely 0.12% of BSA and 7% of IgG were found in the elution pools. The fractionation of different-sized molecules was feasible despite the low bed height of around 2 mm and the discontinuous matrix made of stacked membranes. It can be argued that columns with larger bed heights might improve the separation between different molecules and/or aggregates. For example, Lee et al. resolved IgM monomers and aggregates using OH monoliths [117] and Wang et al. separated BSA from γ-globulin using cryogels [162].

Since molecular crowding is related to precipitation, the question arises if the product capture during SXC (with offline mixing of the PEG and the unpurified sample) is mere a filtration effect by consequence of molecular association and the subsequent recovery
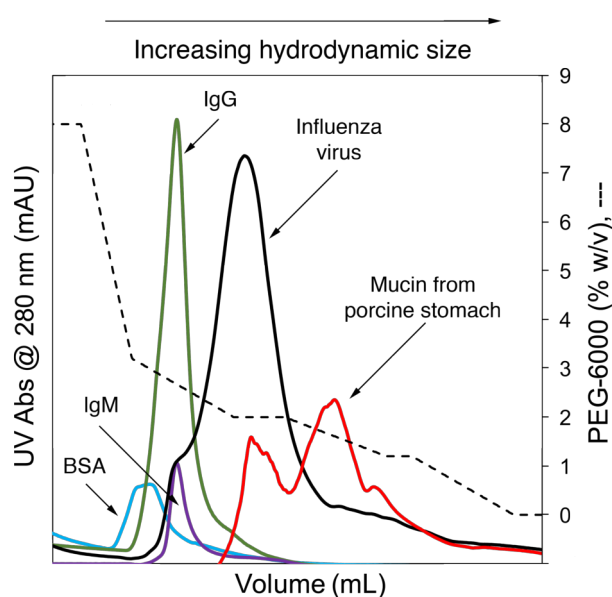
Figure 3.25. SXC overlay of several biomolecules eluted independently with a decreasing PEG-6000 gradient on a 100 cm^2 column packed with regenerated cellulose membranes of 1.0 μm pore size.

of the product by sieving the monomeric species through the matrix once the polymer is removed. This was tested by loading a column with influenza A virus coupled with a fluorescent IgG antibody against the HA protein. Instead of eluting the product, the device was disassembled and each membrane in the stack analyzed individually for fluorescence and virus quantification by aHA assay (Figure 3.26).

The disassembled column contained around 200 µL of liquid in the dead space on top of the membrane stack. This volume had nil aHA, so a mere filtration effect is unlikely. Product quantitation from the individual layers showed that the top two layers had approximately 83% of the loaded virus and the third layer around 16%. As expected, the fluorescence intensity decreased in the deeper layers and the surface under the sealing gasket becomes more available as the liquid flow expands radially inside the device (Figure 3.26.B).

These observations show that the virus particles bind at the internal surface of the membranes rather than being large aggregates/oligomers getting filtered on a cake-like basis [191] upstream of the stack. Wang et al. visualized protein precipitates on the surface of cryogel monoliths using scanning electron microscopy (SEM) [162]; the precipitates were dissolved after reducing the PEG concentration. Nonetheless, it is evident that fouling from cell debris (page 48) or the formation of large aggregates (as observed with MVA virus, Figure 3.21) can lead eventually to filtration effects or operational difficulties. For instance, Lee et al. tried to purify IgM using porous particles, but the required PEG concentration caused the protein to precipitate in the tubing of the chromatography system, probably clogging the column bed and increased the pressure above acceptable levels [117]. Moreover, viscosity reduces diffusive transport — the mass transport mechanisms in packed beds — and increases shear in the interparticle space [2]. When the authors used OH monoliths of 1.2–1.5 µm pore size they did not encounter these problems.

In this work, the pressure drops were in the range of 0.3–0.6 MPa during sample loading using columns of 75–100 cm^2, except for the column capacity determination for influenza virus, were values up to 2.0 MPa were monitored (maximum pressure limit was set to 2.2 MPa) and sample loading had to be stopped. Even so, different stationary phases will display different permeabilities: Wang et al. [162] used a pressure limit of 0.7 MPa for cyrogel monoliths with 10–100 µm pore size, which seems a rather low pressure limit compared to the devices used here.

Regarding product recoveries, it was observed here multiple times that the values obtained were above 100% (Tables 3.2, 3.4, 3.5 3.6, and 3.9). This was mainly attributed to the analytical error of the assays, which in most cases were cell-based (aHA assay, plaque assay, TCID$_{50}$ assay) and also to sample preparation and manipulation (e.g., dialysis, concentration, lyophilization). The exception was the mean yield of AAV (101.0% ± 25.6, 65) based on PCR, although according to guidelines for validation of qRT-PCR methods, a RSD as high 25% is acceptable [192].
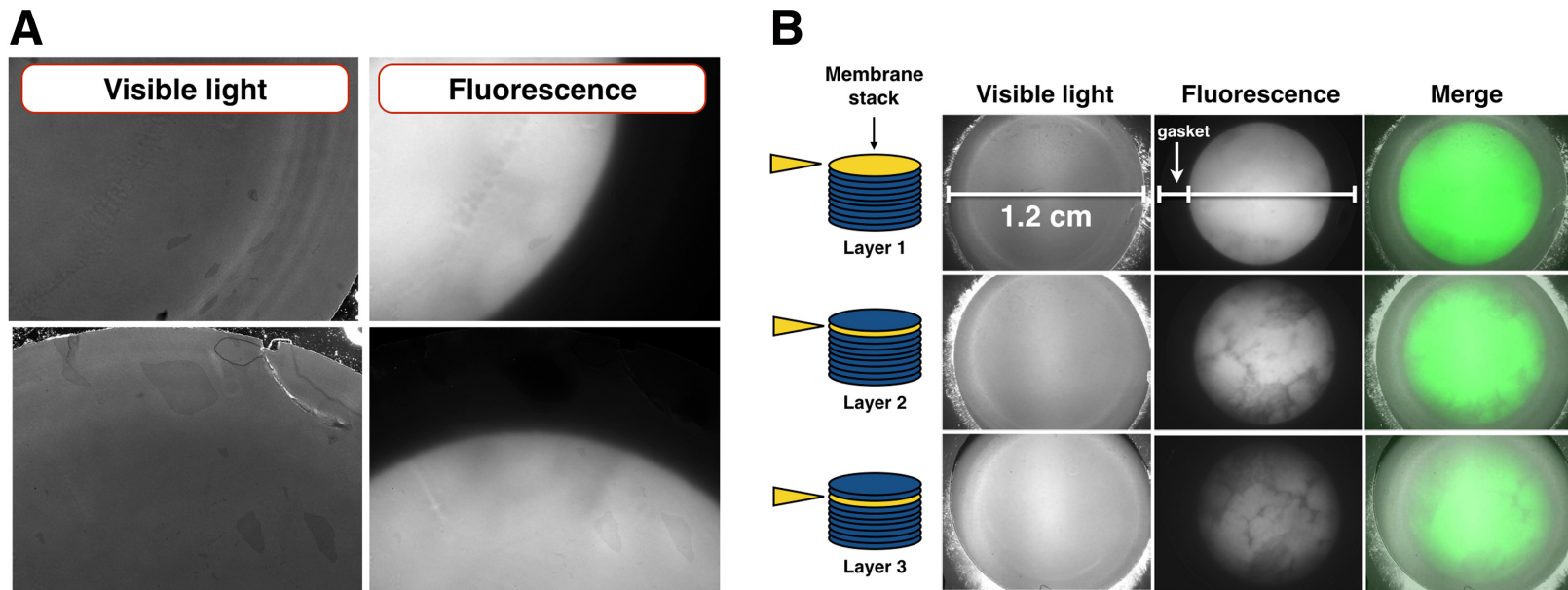
Figure 3.26. Analysis of individual membrane layers from a 13 mm column (packed with regenerated cellulose membranes, 11 cm^2) during SXC of influenza virus A/Puerto Rico/8/34 H1N1. The virus particles were coupled with an anti-hemagglutinin IgG before SXC. The fluorescent area is the virus-binding surface. Notice the absence of visible aggregates (panel A) and the fading of fluorescence intensity in the deeper layers (panel B). The pictured membranes have a diameter of 1.2 cm. These images were taken by Lilli Gallo at the Max-Plank-Institute for Dynamics of Complex Technical Systems in Magdeburg, Germany.
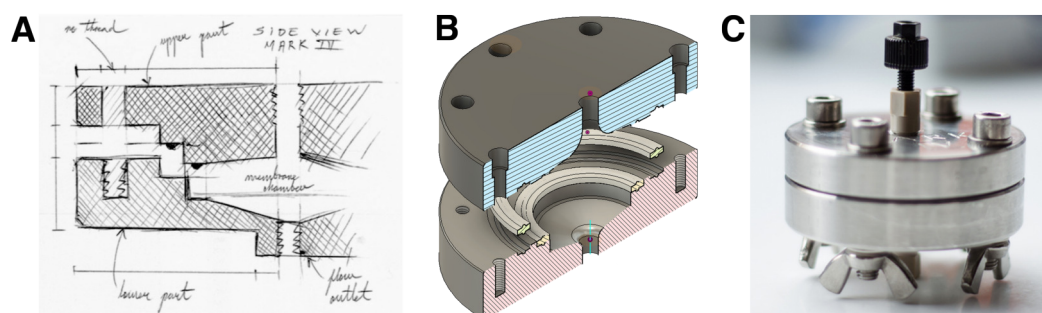
Figure 3.27. SXC self-made prototypes. (A) Drawing, (B) computer-aided design, and (C) picture of a 200 cm^2 device manufactured by Dr. Janitzio Marichal-Hidalgo (Coatzacoalcos, Mexico) and the staff at the mechanical workshop of the Max-Plank-Institute for Dynamics of Complex Technical Systems in Magdeburg, Germany.

In general, protein clearance after SXC was around 88–92% for influenza A virus (calculated from Table 3.1, process in Figure A.1), except for the process in Figure A.4 with 60.9% (calculated from Table 3.4). For YFV it was 92.2–97.9% (calculated from Table 3.5 and Table 3.6, process in Figure A.5). For AAV, the protein clearance was 86.4–90.1% calculated from Table 3.8, process in Figure A.6).

The DNA clearance in SXC eluates for influenza A virus was 76.5–89.2% with a nuclease digestion before SXC as 99.7% without nuclease digestion (both calculated from Table 3.1, process in Figure A.1). For the influenza A virus process in Figure A.4 the DNA clearance was 79.4% (calculated from Table 3.4). For YFV the clearance was 62.4–72.9% (calculated from Table 3.5) and for AAV the DNA amounts in the eluates were below LOD but the DNA in flow-through fractions ranged 75.6–81.7% (Table 3.8).

Scale-up with SXC is done linearly by simply increasing the membrane surface. Most experiments in this work were done with devices of 100 cm^2 made with commercially available filter housings. In an effort to generate bigger devices, membrane holders with a capacity of 200–1000 cm^2 were manufactured in 316 stainless steel (one example in Figure 3.27); ideally, bigger column designs would be done with spiral-wound geometries (radial flow [193]) and a disposable housing.

SXC with supermacroporous 3D-printed cellulose monoliths [194, 195] was also evaluated with two different designs for the solid phase: a "Schoen gyroid" with a pore size of 500 µm (Figure 3.28) and a "Schwarz diamond" with a pore size of 400 µm. Both 3D-printed monoliths were compared in terms of product yield against a column packed with regenerated cellulose membranes of 1.0 µm pore size and another with cellulose acetate membranes of 1.2 µm pore size (Figure 3.29). Unlike the usual high yield achieved with regenerated cellulose, the cellulose acetate column had a yield of 37.9% ± 9.7 based on aHA for influenza virus A/Puerto Rico/8/34 H1N1. It was speculated before that the lower yield of OH monoliths (70.7%, page 38) compared to regenerated cellulose could

be due to the hydrophobicity of the methacrylate backbone. Since both cellulose materials have a similar pore size, a reduced yield due to the lower hydrophilicity of cellulose acetate is likely; the latter is partially acetylated cellulose (Figure 3.30) with an acetyl content ranging from 29.0% to 44.8% — corresponding to mono-, di-, and triacetate [196]. Cellulose triacetate, for instance, is water-insoluble and hydrophobic [197].

The 500 µm and 400 µm 3D-printed cellulose monoliths had similar aHA recoveries of 35.6%±0.7 and 38.9%±3.7, respectively. It can be argued that the lower yield compared to the 1.0 µm regenerated cellulose membranes is due to the large pore size of the monoliths, which show extremely low Reynold's numbers [2] that indicate flow is almost exclusively
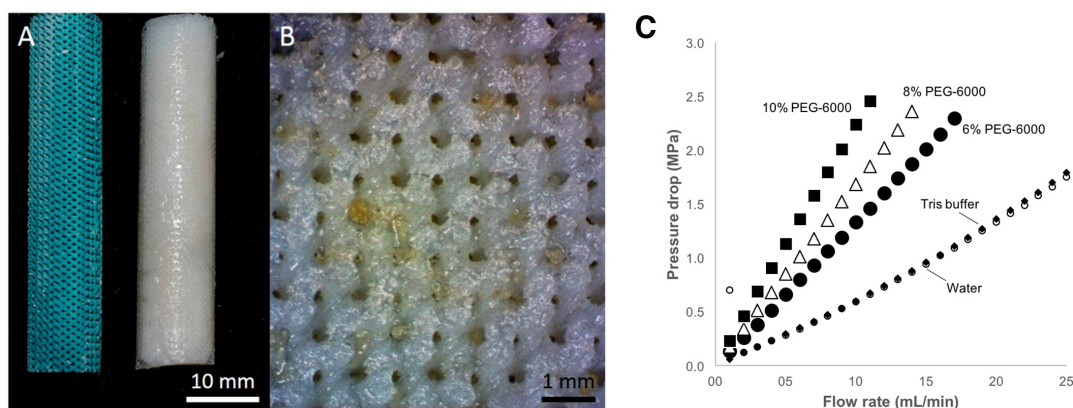
Figure 3.28. Structure of a 3D-printed Schoen gyroid cellulose monolith with pore sizes of 500 µm (left image with panels A and B from Ref. [140]). The monolith (not the actual one in the picture) was provided by Tim Huber at the University of Canterbury in Christchurch, New Zealand. Panel C shows pressure profiles from the provided 3D-printed monolith with different mobile phases relevant for SXC.
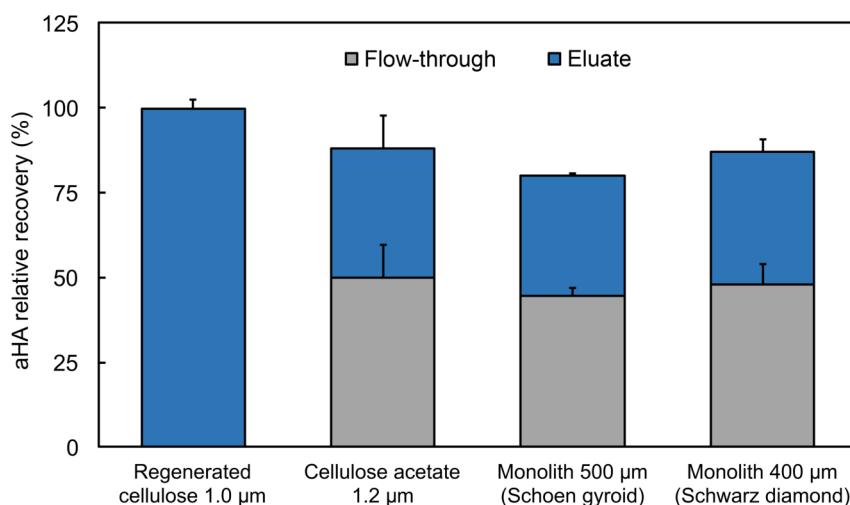
Figure 3.29. Product recovery by hemagglutination activity (aHA) assay from SXC of influenza virus A/Puerto Rico/8/34 H1N1 with two kinds of cellulose membranes and two 3D-printed cellulose monoliths.
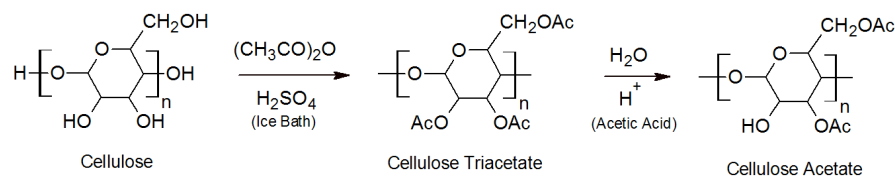
Figure 3.30. Chemical synthesis of cellulose acetate from cellulose (Ref [198]).

laminar and devoid of vortexes. Together with laminar flow, the broad, smooth, and continuous channels of the 3D-printed monoliths guarantee that many virus particles are never close to the surface for binding; testing pore sizes at least one order of magnitude smaller (10–50 μm) would be interesting to increase product yields.

With pore sizes of 0.5 mm that are easily visible with the naked eye, there can be no filtration effects using the 3D-printed monoliths: steric exclusion alone mediates sufficient force to achieve stable retention even at high flow rates.

PEG is known to retard diffusive transport in SEC columns [199] and enhance retention in ion exchange [200, 201], affinity [202], and hydroxyapatite chromatography [203]. Although SXC partially resembles hydrophobic interaction chromatography (HIC) in the sense that a modifier has to be added to the mobile phase to achieve retention, unlike the previously mentioned chromatography modes, there is no benefit of using PEG in HIC: PEG is weakly hydrophobic and competes for binding between the stationary phase and the product [117]. Take the following case: addition of 5% PEG-4000 increases recovery from 76% to 91% in IEC of hemoglobin. In contrast, recovery of hemoglobin in flow-through HIC increases from 20% to 85% when using the same polymer concentration [201]. Even though SXC cannot be used in bind-elute mode with hydrophobic matrices, increased product recovery in flow-through mode with the addition of PEG might be of interest for particular purposes, e.g., removal of lipids, which is of particular interest here considering the co-purification of EVs discussed earlier.

The lack of a direct interaction between PEG and proteins plays a notable role in SXC (Section 1.3). This characteristic has been observed experimentally with circular dichroism spectra of proteins at high PEG concentrations being similar to those of native proteins in diluted solutions [107, 109, 186]. As an example, Atha et al. [109] observed that concentrations up to as 30% of PEG did not induce a significant effect on the melting temperature of ribonuclease (neither PEG-4000 nor PEG-400). Ethanol, on the other hand, lowered the midpoint of the transition by $8\,°C$.

As explained in Section 1.3, the thermodynamically unfavorable situation caused by the presence of the PEG is relieved by reducing the surface area contact between the virus particles and the PEG by shifting folding-unfolding equilibrium and by molecular association [204].

In the first equilibrium, the unfolded state of the viral proteins has a larger surface

area than the folded state and excludes PEG more strongly, so the preferentially excluded PEG shifts the equilibrium toward the folded state, stabilizing proteins structures. This behavior is especially relevant in the purification of labile biopharmaceuticals. Most probably this stabilizing effect was observed here during the SXC of YFV (in the case of PEG) and during its incubation with sucrose, as opposed to the heavy losses reported by Pato et al. [33] without any stabilizer (page 55).

In the second kind of equilibrium, the PEG enhances intermolecular association. More over, the relatively large surface of the stationary phase makes it the dominant component of the system, so the product molecules tend to associate with the chromatography matrix rather than with each other [117], leading to the practical application of thermodynamic binding as SXC.

CHAPTER **4**

Conclusions & Outlook

This work evaluated the purification of several virus strains with SXC mainly done with devices packed with a stack of regenerated cellulose membranes with a typical surface of 75–100 cm^2.

Around 14 different cell culture-based virus strains and serotypes with a wide variety of sizes (20–250 nm) were used as target products. Additionally, several stationary phases were tested, including hydroxylated monoliths (1–2 µm pore size), cellulose membranes (1–1.2 µm pore size), and 3D-printed cellulose monoliths (400–500 µm pore size). Devices packed with regenerated cellulose membranes of 1.0 µm pore size were the most efficient in terms of product yield as were concentrations of 8–10% PEG-6000 for sample loading.

Regenerated cellulose membranes are a viable alternative to the previously reported OH monoliths used in SXC. Four different strains of influenza virus (two A and two B strains) produced in MDCK cells grown in batch systems showed product recoveries >98% with membranes of 1.0 µm pore size (loading at 8% PEG-6000). It was observed, however, that certain quality attributes of the unpurified material had great influence on product recovery, e.g., residual cell debris and/or aggregated product, although these would undoubtedly be challenges with other chromatography methods as well. For example, influenza virus samples from ATF perfusion processes showed lower yields of 56% aHA.

Determining binding capacities was challenging since there is no direct chemical bond, so the term "DBC" seems rather artificial in this regard. Because of the precipitation mechanism of SXC, it seems that the estimation of a capacity is closer to a "membrane challenge/maximum loading capacity" as is used for normal-flow filtration operations, where typically loading is stopped with increasing back-pressure. In SXC this is highly likely because the product accretion will cause a reduction in pore size, and so pressure will increase.

It was also observed that low conductivity of the elution's mobile phase was not enough to completely recover all loaded influenza virus particles (strains A/Switzerland/9715293/2013 H3N2 and B/Phuket/3073/2013 (Yamagata)), although this did not present an experimental issue as the elution steps were performed later at usual pH and conductivity with expected higher recoveries. The influence of parameters such as pI, pH, and conductivity in SXC have been briefly discussed in the literature with idealized systems (purified proteins), but require further studies with more complex samples like the ones used in this work.

The highest measured productivity (influenza virus A/Puerto Rico/8/34 H1N1) was with a 1 L STR process using Xeno™ chemically-defined medium: $69\,459$ $\mu g_{HA}\,m^{-2}\,h^{-1}$ (4680 doses $m^{-2}\,h^{-1}$). The purified fractions had 12.5 ng_{dsDNA} dose^{-1} and 63.1 μg_{prot} dose^{-1}. Polishing with pseudo-affinity chromatography using a SCMA after SXC did not increase purity in a significant way.

In the case of YFV, the 17DD and 17D-204 substrains used for commercial vaccine manufacture were propagated in Vero cells and purified (loading at 10% PEG-6000) with full recovery in elution fractions containing around 6×10^9 PFU (equivalent to more than $100\,000$ live-attenuated vaccine doses and a productivity value of 5.06×10^6 doses $m^{-2}\,h^{-1}$). This process only required a simple clarification, a nuclease digestion, and the SXC step to achieve protein and DNA contamination levels compliant with regulatory requirements for human YF attenuated vaccines.

Unlike other methods such as IEC where the virus feed has to be stabilized with molecules such as sucrose or sorbitol to avoid infectivity losses, during SXC of YFV there was no measurable loss of infectivity. This is attributed to the stabilizing properties of PEG.

For AAV, several wild-type and recombinant strains were purified using similar chromatography conditions (loading at 10% PEG-6000). No measurable losses were observed in flow-throughs, and titers in elution pools were as high as 2×10^{14} vg L^{-1}. More importantly, the AAV particles were able to successfully induce either gene expression or gene knockdown in transduced cells. TEM analysis of the purified AAV particles shows a majority of full capsids although it cannot be claimed that SXC can enrich and/or discriminate full capsids from empty ones; the latter should be addressed in future work.

Preliminary results for SXC purification of MVA virus and EVs were promising. In the case of MVA virus, virtually full yield was observed with a total TCID$_{50}$ titer of 3.7×10^9 virions. Quantitation of total particles by ELISA or PCR should be performed in the future to complement this analysis. Notably, unlike the other virus species addressed above, visible aggregation was observed upon addition of PEG as confirmed by particle size distribution analysis. Adding sucrose or sorbitol (8% of either) to the PEG-conditioned virus seemed to lower the amount of aggregates observed compared to the PEG-conditioned

sample without stabilizers. Regardless, the SXC-purified MVA virus showed a distinct monomer peak of around 220 nm without visible aggregation.

The preparative purification of EVs came as a realization that these molecules were co-eluted contaminants in virus samples. Preliminary recoveries of around 40% for BHK and MDCK cell supernatants are promising considering recoveries of 5–25% obtained by other widely used methods such as ultracentrifugation. The concentration of EVs in elution fractions was $\leq 7.95 \times 10^{10}$ particles mL^{-1}.

The ability to load and recover the product at physiological pH and conductivity as well as the conformation stabilizing properties of PEG are relevant advantages during the purification of labile biopharmaceuticals. The high product recoveries achieved so far with SXC make it possible to allow for subsequent polishing operations for improving purity without risking unacceptably low process yields. The narrow operational range of SXC makes it possible to purify viruses with a high probability of success (e.g., testing 8% PEG-6000 as a starting point) and the low cost of the membranes allows single-use operation (which avoids expensive and time-consuming cleaning and sanitization steps). Scale-up of SXC is simple, as it requires only a linear increase in membrane surface, and the use of devices of up to 20 m^2 would enable industrial-scale virus purification.

Clearance of protein and DNA were typically >85% and >75%, respectively, depending on the virus and the experimental setup (e.g., placing a DNA digestion step before SXC). In all cases, it was advantageous to have a nuclease treatment before SXC to achieve lower amounts of residual DNA.

SXC with 3D-printed cellulose monoliths with channel diameters of 400 µm and 500 µm was inefficient in terms of product yield (around 40% aHA for influenza virus A/Puerto Rico/8/34 H1N1) compared to the 1.0 µm regenerated cellulose membranes. These monoliths, however, could prove to be an interesting alternative to expanded-bed chromatography. Testing of pore sizes larger than 1.0 µm with either membranes or 3D-printed monoliths should be done in future work. Cellulose acetate membranes of 1.2 µm pore size showed a yield of 40% aHA for the same virus, most probably due to their lower hydrophilicity compared to regenerated cellulose.

Future studies should also include high-throughput screening of different PEG sizes and concentrations, gradient separations to achieve fractionation by size, preparative purification of vesicles, and screening of stabilizers for aggregation-prone products such as MVA virus. In addition, options for separating empty from full capsids in AAV preparations should be explored.

It seems that as a capture step, SXC is comparable or better than most chromatography methods available in terms of product yield, ease of use, and scalability. Overall, the results shown here are the basis for further optimization and application of this technology and they indicate that membrane-based SXC has the potential for becoming a platform technology for both viral vaccine and gene therapy applications.

List of Figures

List of Tables

Peer-reviewed publications

Complete list of publications and citations: http://goo.gl/XN9W7y

P. Marichal-Gallardo*, K. Börner*, M.M. Pieler*, V. Sonntag-Buck, M. Obr, D. Bejarano, M.W. Wolff, H.-G. Kräusslich, U. Reichl, D. Grimm, "Single-use purification of adeno-associated viral gene transfer vectors by membrane-based steric exclusion chromatography", *submitted to Human Gene Therapy (in revision).*
Own contribution: conceptualization; methodology; experimental work; data curation; visualization; writing, reviewing, and editing manuscript.

M.D. Hein, H. Kollmus, **P. Marichal-Gallardo**, S. Püttker, D. Benndorf, Y. Genzel, K. Schughart, S.Y. Kupke, U. Reichl, "OP7, a novel influenza A virus defective interfering particle: production, purification, and animal experiments demonstrating antiviral potential", *submitted to Cell Reports.*
Own contribution: methodology; experimental work; data curation; writing, reviewing, and editing manuscript.

P. Marichal-Gallardo*, L.F. Almeida*, D. Riedel, M.W. Wolff, L.R. Castilho, Y. Genzel, U. Reichl, "Single-use purification of yellow fever viral vaccine candidates by membrane-based steric exclusion chromatography", *in preparation.*
Own contribution: conceptualization; methodology; experimental work; data curation; visualization; writing, reviewing, and editing manuscript.

T. Bissinger*, Y. Wu*, **P. Marichal-Gallardo***, D. Riedel, M.W. Wolff, X. Liu, Y. Genzel, W.-S. Tan, U. Reichl, "Integrated manufacturing of an influenza A vaccine candidate with MDCK suspension cells", *in preparation.*
Own contribution: conceptualization; methodology; experimental work; data curation; visualization; writing, reviewing, and editing manuscript.

---

*authors contributed equally.

P. Marichal-Gallardo*, A.R. Fortuna*, M.W. Wolff, U. Reichl, "A single-use membrane purification platform for influenza viral vaccines: integrating steric exclusion chromatography & sulfated cellulose pseudo-affinity chromatography", *in preparation.*
Own contribution: conceptualization; methodology; experimental work; data curation; visualization; writing, reviewing, and editing manuscript.

G. Gränicher, J. Coronel, A. Pralow, **P. Marichal-Gallardo**, M. Wolff, E. Rapp, A. Karlas, V. Sandig, Y. Genzel, U. Reichl, "Efficient influenza A virus production in high cell density using the novel porcine suspension cell line PBG.PK2.1", *Vaccine* (2019) 37(47):7019–7028.
doi: 10.1016/j.vaccine.2019.04.030
Own contribution: methodology; experimental work; data curation; reviewing, and editing manuscript.

P. Marichal-Gallardo*, M.M. Pieler*, M.W. Wolff, U. Reichl, "Steric exclusion chromatography for purification of cell culture-derived influenza A virus using regenerated cellulose membranes and polyethylene glycol", *Journal of Chromatography A* (2017) 1483:110–119.
doi: 10.1016/j.chroma.2016.12.076
Own contribution: conceptualization; methodology; experimental work; data curation; visualization; writing, reviewing, and editing manuscript.

Patents

M.W. Wolff, M.M. Pieler, U. Reichl, **P. Marichal-Gallardo**, "Method for the separation of virus compositions including depletion and purification thereof", Patent *International Application Number* WO 2017/076553 A1. International Publication Date: 11 May 2017.

Posters

M.W. Wolff, **P. Marichal-Gallardo**, K. Lothert, D. Riedel, K. Börner, A.R. Fortuna, P. Czermak, U. Reichl, "A step towards globally affordable vaccines & gene therapies: Steric exclusion chromatography as a capture platform", in *Recovery of Biological Products* (2018), Asheville, NC, USA.

P. Marichal-Gallardo, M.M. Pieler, D. Riedel, M. Wolff, U. Reichl, "Chromatographic purification of cell culture-derived influenza A virus particles using cellulose filters and polyethylene glycol", in *International Symposium on Preparative and Industrial Chromatography and Allied Techniques (SPICA)* (2016), Vienna, Austria.

---

*authors contributed equally.

Oral communications

P. Marichal-Gallardo, Y. Genzel, K. Börner, D. Grimm, M.W. Wolff, U. Reichl, "A single-use chromatographic purification platform for viral gene transfer vectors & viral vaccines", in *Advancing Manufacture of Cell and Gene Therapies VI* (2019), Coronado, CA, USA.

P. Marichal-Gallardo, Y. Genzel, K. Börner, D. Grimm, M.W. Wolff, U. Reichl, "A single-use purification platform for viral vaccines & gene therapy vectors", in *International Symposium on the Separation of Proteins, Peptides, and Polynucleotides (ISPPP)* (2018), Berlin, Germany.

P. Marichal-Gallardo, A.R. Fortuna, Y. Genzel, M.W. Wolff, U. Reichl, "Purifying viruses with a sheet of paper: Single-use steric exclusion chromatography as a capture platform for vaccine candidates", in *Vaccine Technology VII* (2018), Mont Tremblant, Canada.

P. Marichal-Gallardo, K. Lothert, T. Grein, U. Reichl, P. Czermak, M.W. Wolff, "Single-use purification of cell culture-based virus particles by steric exclusion chromatography", in *National Meeting of the American Chemical Society (ACS)* (2018), New Orleans, USA.

P. Marichal-Gallardo, M.M. Pieler, D. Riedel, M.W. Wolff, U. Reichl, "Purification of cell culture-based influenza A virus particles with a cellulose membrane adsorber and polyethylene glycol", in *International Symposium on the Separation of Proteins, Peptides, and Polynucleotides (ISPPP)* (2016), Salzburg, Austria.

P. Marichal-Gallardo, M.M. Pieler, K. Börner, M.W. Wolff, D. Grimm, U. Reichl, "Disposable membrane adsorbers for size-based chromatographic purification of virus particles & gene therapy vectors", in *ÄKTA User Day* (2016), Berlin, Germany.

P. Marichal-Gallardo, M.M. Pieler, M.W. Wolff, U. Reichl, "Purification of cell culture-based influenza virus particles using membrane filters with the aid of non-ionic polymers", in *Preparative and Process Chromatography Symposium (PREP)* (2016), Philadelphia, USA.

Bibliography

1. M. W. Wolff, U. Reichl, Downstream processing of cell culture-derived virus particles, Expert Review of Vaccines 10 (2011) 1451–1475.

2. P. Gagnon, Chromatographic purification of virus particles, in: M. C. Flickinger (Ed.), Encyclopedia of Industrial Biotechnology, John Wiley & Sons, Inc., Hoboken, 2010, pp. 415–436.

3. Gene Therapy Hits a Peculiar Roadblock: A Virus Shortage, New York Times (2017).

4. K. Stöhr, Ill prepared for a pandemic, Nature 507 (2014) S20–S21.

5. S. A. Plotkin (Ed.), History of Vaccine Development, Springer, New York, 2011.

6. S. Riedel, Edward Jenner and the history of smallpox and vaccination, Baylor University Medical Center Proceedings 18 (2005) 21–25.

7. R. B. Kennedy, J. M. Lane, D. A. Henderson, G. A. Poland, Smallpox and Vaccinia, in: S. A. Plotkin, W. A. Orenstein, P. A. Offit, K. M. Edwards (Eds.), Plotkin's Vaccines, Elsevier, Philadelphia, 2018, pp. 1001–1030.e12.

8. J. E. Staples, T. P. Monath, M. D. Gershman, A. D. T. Barrett, Yellow Fever Vaccines, in: S. A. Plotkin, W. A. Orenstein, P. A. Offit, K. M. Edwards (Eds.), Plotkin's Vaccines, Elsevier, Philadelphia, 2018, pp. 1181–1265.e20.

9. F. Horaud, Viral Vaccines and Cell Substrate: A "Historical" Debate, in: History of Vaccine Development, Springer New York, New York, 2011, pp. 151–154.

10. R. Rappuoli, G. Del Giudice (Eds.), Influenza Vaccines for the Future, Springer Basel AG, Basel, 2011.

11. J. S. Bresee, A. M. Fry, S. Sambhara, N. J. Cox, Inactivated Influenza Vaccines, in: S. A. Plotkin, W. A. Orenstein, P. A. Offit, K. M. Edwards (Eds.), Plotkin's Vaccines, Elsevier, Philadelphia, 2018, pp. 456–488.e21.

12. E. D. Kilbourne, A Race with Evolution: A History of Influenza Vaccines, in: S. A. Plotkin (Ed.), History of Vaccine Development, Springer New York, New York, 2011, pp. 137–144.

13. A. Chenoweth, A. D. Waltz, J. Stoker Jr, R. G. Gladen, Active immunization with the viruses of human and swine influenza, Am J Dis Children 52 (1936).

14. R. Dolin, Influenza, in: D. L. Kasper, A. S. Fauci (Eds.), Harrison's Infectious Disease, The McGraw-Hill Companies, Inc., New York, 2010, pp. 776–784.

15. G. Del Giudice, R. Rappuoli, Learning from the First Pandemic of the Twenty-First Century, in: R. Rappuoli, G. Del Giudice (Eds.), Influenza Vaccines for the Future, Springer Basel AG, Basel, 2011, pp. 401–423.

16. T. M. Tumpey, C. F. Basler, P. V. Aguilar, H. Zeng, A. Solórzano, D. E. Swayne, N. J. Cox, J. M. Katz, J. K. Taubenberger, P. Palese, A. García-Sastre, Characterization of the Reconstructed 1918 Spanish Influenza Pandemic Virus, Science 310 (2005) 77.

17. J. Oxford, A. Gilbert, R. Lambkin-Williams, Influenza vacciones have a short but illutrious history of dedicated science enabling the rapid global production of A/Swine (H1N1) vaccine in the current pandemic, in: R. Rappuoli, G. Del Giudice (Eds.), Influenza Vaccines for the Future, Springer Basel AG, Basel, 2011, pp. 115–147.

18. U.S. Department of Health & Human Services, 2019, Influenza (Flu), URL: `https://www.cdc.gov/flu/index.htm`.

19. P. R. Dormitzer, Cell culture-derived influenza vaccines, in: R. Rappuoli, G. Del Giudice (Eds.), Influenza Vaccines for the Future, Springer Basel AG, Basel, 2011, pp. 293–312.

20. L. Simonsen, C. Vibound, R. J. Taylor, M. A. Miller, The epidemiology of influenza and its control, in: R. Rappuoli, G. Del Giudice (Eds.), Influenza Vaccines for the Future, Springer Basel AG, Basel, 2011, pp. 27–54.

21. S. Schultz-Cherry, Is It Possible? A Different Approach to Creating a Universal Influenza Vaccine, mBio 6 (2015) e01580–15–2.

22. F. Berlanda Scorza, V. Tsvetnitsky, J. J. Donnelly, Universal influenza vaccines: Shifting to better vaccines, Vaccine 34 (2016) 2926–2933.

23. R. D. de Vries, A. F. Altenburg, G. F. Rimmelzwaan, Universal influenza vaccines: a realistic option?, Clinical Microbiology and Infection 22 (2016) S120–S124.

24. Stabilizing prospects for a universal flu vaccine, Nature Biotechnology 33 (2015) 1043–1044.

25. W. E. P. Beyer, A. M. Palache, A. D. M. E. Osterhaus, Comparison of Serology and Reactogenicity between Influenza Subunit Vaccines and Whole Virus or Split Vaccines, Clin. Drug Investig. 15 (1998) 1–12.

26. B. Kalbfuss-Zimmermann, U. Reichl, Viral Vaccines Purification, in: E. Wen, R. Ellis, N. S. Pujar (Eds.), Vaccine Development and Manufacturing, John Wiley & Sons, Inc., Hoboken, 2015, pp. 97–180.

27. Influenza vaccine (whole virion, inactivated), in: European Pharmacopoeia, 2012, pp. 795–798.

28. World Health Organization, Recommendations for the production and control of influenza vaccine (inactivated), Technical Report 927, 2005.

29. World Health Organization, WHO Technical Report Series, Technical Report 978, 2013.

30. U.S. Department of Health & Human Services, 2018, Yellow fever, URL: `https://www.cdc.gov/yellowfever/index.html`.

31. R. W. Wieten, E. F. F. Jonker, E. M. M. van Leeuwen, E. B. M. Remmerswaal, I. J. M. ten Berge, A. W. de Visser, P. J. J. van Genderen, A. Goorhuis, L. G. Visser, M. P. Grobusch, G. J. de Bree, A Single 17D Yellow Fever Vaccination Provides Lifelong Immunity; Characterization of Yellow-Fever-Specific Neutralizing Antibody and T-Cell Responses after Vaccination, PLoS ONE 11 (2016) e0149871.

32. C. L. Gardner, K. D. Ryman, Yellow Fever: A Reemerging Threat, Clinics in Laboratory Medicine 30 (2010) 237–260.

33. T. P. Pato, M. C. O. Souza, A. N. M. R. Silva, R. C. Pereira, M. V. Silva, E. Caride, L. P. Gaspar, M. S. Freire, L. R. Castilho, Development of a membrane adsorber based capture step for the purification of yellow fever virus, Vaccine 32 (2014) 2789–2793.

34. R. C. Pereira, A. N. M. R. Silva, M. C. O. Souza, M. V. Silva, Patrícia P.C.C. Neves, A. A. M. V. Silva, D. D. C. S. Matos, M. A. O. Herrera, A. M. Y. Yamamura, M. S. Freire, L. P. Gaspar, E. Caride, An inactivated yellow fever 17DD vaccine cultivated in Vero cell cultures, Vaccine 33 (2015) 4261–4268.

35. E. Hanna, C. Rémuzat, P. Auquier, M. Toumi, Gene therapies development: slow progress and promising prospect, Journal of Market Access & Health Policy 5 (2017) 1265293–10.

36. T. Clayton, Viral gene therapy vectors, in: M. C. Flickinger (Ed.), Encyclopedia of Industrial Biotechnology, John Wiley & Sons, Inc., Hoboken, 2010, pp. 4773–4788.

37. Y. Lin, A. Desai, S. L. Gerson, Lentiviruses: Vectors for Cancer Gene Therapy, in: J. A. Roth (Ed.), Gene-Based Therapies for Cancer, Springer, New York, 2010, pp. 155–179.

38. W. Walther, U. Stein (Eds.), Gene Therapy of Solid Cancers, Springer, New York, 2015.

39. The Journal of Gene Medicine, 2018, Gene Therapy Clinical Trials Worldwide, URL: `http://www.abedia.com/wiley/index.html`.

40. Novartis AG, 2019, AveXis receives FDA approval for Zolgensma, the first and only gene therapy for pediatric patients with spinal muscular atrophy (SMA), URL: `https://www.novartis.com/news/media-releases`.

41. C. H. Evans, J. Huard, Gene therapy approaches to regenerating the musculoskeletal system, Nat Rev Rheumatol 11 (2015) 234–242.

42. N. Düzgünes (Ed.), Suicide Gene Therapy, Springer, New York, 2019.

43. G. R. Jayandharan (Ed.), Gene and Cell Therapy: Biology and Applications, Springer, Singapore, 2018.

44. U.S. Food and Drug Administration, 2019, Approved Cellular and Gene Therapy Products, URL: `https://www.fda.gov/vaccines-blood-biologics/` `cellular-gene-therapy-products/` `approved-cellular-and-gene-therapy-products`.

45. C. W. Freyer, Tisagenlecleucel: The First CAR on the Highway to Remission for Acute Lymphoblastic Leukemia., J Adv Pract Oncol 9 (2018) 537–544.

46. I. Scarfo, M. J. Frigault, M. V. Maus, CAR-Based Approaches to Cutaneous T-Cell Lymphoma., Front Oncol 9 (2019) 259.

47. M. C. Milone, U. O'Doherty, Clinical use of lentiviral vectors., Leukemia 32 (2018) 1529–1541.

48. S. Patel, R. A. Burga, A. B. Powell, E. A. Chorvinsky, N. Hoq, S. E. McCormack, S. N. Van Pelt, P. J. Hanley, C. R. Y. Cruz, Beyond CAR T Cells: Other Cell-Based Immunotherapeutic Strategies Against Cancer, Front Oncol 9 (2019) 196.

49. C. V. Borlongan, Concise Review: Stem Cell Therapy for Stroke Patients: Are We There Yet?, Stem Cells Transl Med 69 (2019) 904.

50. B. Lukomska, L. Stanaszek, E. Zuba-Surma, P. Legosz, S. Sarzynska, K. Drela, Challenges and Controversies in Human Mesenchymal Stem Cell Therapy, Stem Cells International 2019 (2019) 10.

51. S. Regmi, S. Pathak, J. O. Kim, C. S. Yong, J.-H. Jeong, Mesenchymal stem cell therapy for the treatment of inflammatory diseases: Challenges, opportunities, and future perspectives, Eur J Cell Biol (2019).

52. R. Bleijs, 2019, Gene Therapy Net, URL: `http://www.genetherapynet.com`.

53. S. Daya, K. I. Berns, Gene Therapy Using Adeno-Associated Virus Vectors, Clinical Microbiology Reviews 21 (2008) 583–593.

54. SignaGen Laboratories, 2019, Introduction to AAV, URL: `http://signagen.com/Introduction-to-AAV`.

55. L. S. Carvalho, L. H. Vandenberghe, Promising and delivering gene therapies for vision loss, Vision Res 111 (2015) 124–133.

56. K. Hollinger, J. S. Chamberlain, Viral vector-mediated gene therapies, Curr Opin Neurol 28 (2015) 522–527.

57. J. L. Santiago-Ortiz, D. V. Schaffer, Adeno-associated virus (AAV) vectors in cancer gene therapy, J. Control. Release 240 (2016) 287–301.

58. N. Clément, J. C. Grieger, Manufacturing of recombinant adeno-associated viral vectors for clinical trials, Mol Ther Methods Clin Dev 3 (2016) 16002–7.

59. G. Dias Florencio, G. Precigout, C. Beley, P.-O. Buclez, L. Garcia, R. Benchaouir,

Simple downstream process based on detergent treatment improves yield and in vivo transduction efficacy of adeno-associated virus vectors, Mol Ther Methods Clin Dev 2 (2015) 15024–7.

60. W. T. Hermens, O. ter Brake, P. A. Dijkhuizen, M. A. Sonnemans, D. Grimm, J. A. Kleinschmidt, J. Verhaagen, Purification of recombinant adeno-associated virus by iodixanol gradient ultracentrifugation allows rapid and reproducible preparation of vector stocks for gene transfer in the nervous system., Hum Gene Ther 10 (1999) 1885–1891.

61. S. A. Nass, M. A. Mattingly, D. A. Woodcock, B. L. Burnham, J. A. Ardinger, S. E. Osmond, A. M. Frederick, A. Scaria, S. H. Cheng, C. R. O'Riordan, Universal Method for the Purification of Recombinant AAV Vectors of Differing Serotypes, Mol Ther Methods Clin Dev 9 (2018) 33–46.

62. M. Urabe, K.-Q. Xin, Y. Obara, T. Nakakura, H. Mizukami, A. Kume, K. Okuda, K. Ozawa, Removal of Empty Capsids from Type 1 Adeno-Associated Virus Vector Stocks by Anion-Exchange Chromatography Potentiates Transgene Expression, Mol Ther 13 (2006) 823–828.

63. G. Qu, J. Bahr-Davidson, J. Prado, A. Tai, F. Cataniag, J. McDonnell, J. Zhou, B. Hauck, J. Luna, J. M. Sommer, P. Smith, S. Zhou, P. Colosi, K. A. High, G. F. Pierce, J. F. Wright, Separation of adeno-associated virus type 2 empty particles from genome containing vectors by anion-exchange column chromatography., J Virol Methods 140 (2007) 183–192.

64. F. Fenner, D. A. Henderson, I. Arita, Z. Jezek, I. D. Ladnyi, Smallpox and its eradication, World Health Organization, Geneva, 1988.

65. J. Weger-Lucarelli, H. Chu, M. T. Aliota, C. D. Partidos, J. E. Osorio, A Novel MVA Vectored Chikungunya Virus Vaccine Elicits Protective Immunity in Mice, PLoS Negl Trop Dis 8 (2014) e2970–14.

66. C. Larocca, J. Schlom, Viral Vector-Based Therapeutic Cancer Vaccines, The Cancer Journal 17 (2011) 359–371.

67. C. Verheust, M. Goossens, K. Pauwels, D. Breyer, Biosafety aspects of modified vaccinia virus Ankara (MVA)-based vectors used for gene therapy or vaccination, Vaccine 30 (2012) 2623–2632.

68. M. P. Zaborowski, L. Balaj, X. O. Breakefield, C. P. Lai, Extracellular Vesicles: Composition, Biological Relevance, and Methods of Study, BioScience 65 (2015) 783–797.

69. D. Choi, T. H. Lee, C. Spinelli, S. Chennakrishnaiah, E. D'Asti, J. Rak, Extracellular vesicle communication pathways as regulatory targets of oncogenic transformation, Seminars in Cell and Developmental Biology 67 (2017) 11–22.

70. C. Junquera, T. Castiella, G. Muñoz, R. Fernández-Pacheco, M. J. Luesma, M. Monzón, Biogenesis of a new type of extracellular vesicles in gastrointestinal stromal tumors: ultrastructural profiles of spheresomes., Histochem. Cell Biol. 146 (2016) 557–567.

71. Z.-z. Jiang, Y.-m. Liu, X. Niu, J.-y. Yin, B. Hu, S.-c. Guo, Y. Fan, Y. Wang, N.-s. Wang, Exosomes secreted by human urine-derived stem cells could prevent kidney complications from type I diabetes in rats, Stem Cell Research & Therapy 7 (2016) 24–13.

72. V. Zappulli, K. P. Friis, Z. Fitzpatrick, C. A. Maguire, X. O. Breakefield, Extracellular vesicles and intercellular communication within the nervous system, Journal of Clinical Investigation 126 (2016) 1198–1207.

73. J. H. Teixeira, A. M. Silva, M. I. Almeida, M. A. Barbosa, S. G. Santos, Circulating extracellular vesicles: Their role in tissue repair and regeneration, Transfusion and Apheresis Science 55 (2016) 53–61.

74. G. De Palma, F. Sallustio, F. Schena, Clinical Application of Human Urinary Extracellular Vesicles in Kidney and Urologic Diseases, International Journal of molecular sciences 17 (2016) 1043–14.

75. Y. Soung, S. Ford, V. Zhang, J. Chung, Exosomes in Cancer Diagnostics, Cancers 9 (2017) 8–11.

76. P. Vader, E. A. Mol, G. Pasterkamp, R. M. Schiffelers, Extracellular vesicles for drug delivery, Advanced Drug Delivery Reviews 106 (2016) 148–156.

77. C. Quek, A. F. Hill, The role of extracellular vesicles in neurodegenerative diseases, Biochemical and Biophysical Research Communications 483 (2017) 1178–1186.

78. D. Wen, Y. Peng, D. Liu, Y. Weizmann, R. I. Mahato, Mesenchymal stem cell and derived exosome as small RNA carrier and Immunomodulator to improve islet transplantation, J. Control. Release 238 (2016) 166–175.

79. M. A. Rider, S. N. Hurwitz, D. G. Meckes, ExtraPEG: A Polyethylene Glycol-Based Method for Enrichment of Extracellular Vesicles, Sci. Rep. 6 (2016) 23978–14.

80. G. Leoni, P.-A. Neumann, N. Kamaly, M. Quiros, H. Nishio, H. R. Jones, R. Sumagin, R. S. Hilgarth, A. Alam, G. Fredman, I. Argyris, E. Rijcken, D. Kusters, C. Reutelingsperger, M. Perretti, C. A. Parkos, O. C. Farokhzad, A. S. Neish, A. Nusrat, Annexin A1–containing extracellular vesicles and polymeric nanoparticles promote epithelial wound repair, Journal of Clinical Investigation 125 (2015) 1215–1227.

81. M. Hadla, S. Palazzolo, G. Corona, I. Caligiuri, V. Canzonieri, G. Toffoli, F. Rizzolio, Exosomes increase the therapeutic index of doxorubicin in breast and ovarian cancer mouse models, Nanomedicine 11 (2016) 2431–2441.

82. S. Stremersch, S. C. De Smedt, K. Raemdonck, Therapeutic and diagnostic applications of extracellular vesicles, J. Control. Release 244 (2016) 167–183.

83. Y. T. Sato, K. Umezaki, S. Sawada, S.-a. Mukai, Y. Sasaki, N. Harada, H. Shiku, K. Akiyoshi, Engineering hybrid exosomes by membrane fusion with liposomes, Sci. Rep. 6 (2016) 21933–11.

84. D. W. Greening, R. Xu, H. Ji, B. J. Tauro, R. J. Simpson, A Protocol for

Exosome Isolation and Characterization: Evaluation of Ultracentrifugation, Density-Gradient Separation, and Immunoaffinity Capture Methods, in: D. Varshney, M. Singh (Eds.), Proteomic Profiling, Springer, New York, 2015, pp. 179–209.

85. Y. Weng, Z. Sui, Y. Shan, Y. Hu, Y. Chen, L. Zhang, Y. Zhang, Effective isolation of exosomes with polyethylene glycol from cell culture supernatant for in-depth proteome profiling, Analyst 141 (2016) 4640–4646.

86. L. Balaj, N. A. Atai, W. Chen, D. Mu, B. A. Tannous, X. O. Breakefield, J. Skog, C. A. Maguire, Heparin affinity purification of extracellular vesicles, Sci. Rep. 5 (2015) 10266–15.

87. S. Kreimer, A. M. Belov, I. Ghiran, S. K. Murthy, D. A. Frank, A. R. Ivanov, Mass-Spectrometry-Based Molecular Characterization of Extracellular Vesicles: Lipidomics and Proteomics, J. Proteome Res. 14 (2015) 2367–2384.

88. M. Monguió-Tortajada, C. Gálvez-Montón, A. Bayes-Genis, S. Roura, F. E. Borràs, Extracellular vesicle isolation methods: rising impact of size-exclusion chromatography, Cellular and Molecular Life Sciences 76 (2019) 2369–2382.

89. M. G. Moleirinho, R. J. S. Silva, M. J. T. Carrondo, P. M. Alves, C. Peixoto, Exosome-based therapeutics: Purification using semi-continuous multi-column chromatography, Separation and Purification Technology 224 (2019) 515–523.

90. R. Xu, D. W. Greening, A. Rai, H. Ji, R. J. Simpson, Highly-purified exosomes and shed microvesicles isolated from the human colon cancer cell line LIM1863 by sequential centrifugal ultrafiltration are biochemically and functionally distinct, Methods 87 (2015) 11–25.

91. D. C. Watson, D. Bayik, A. Srivatsan, C. Bergamaschi, A. Valentin, G. Niu, J. Bear, M. Monninger, M. Sun, A. Morales-Kastresana, J. C. Jones, B. K. Felber, X. Chen, I. Gursel, G. N. Pavlakis, Efficient production and enhanced tumor delivery of engineered extracellular vesicles, Biomaterials 105 (2016) 195–205.

92. D. Gustafson, S. Veitch, J. E. Fish, Extracellular Vesicles as Protagonists of Diabetic Cardiovascular Pathology, Front. Cardiovasc. Med. 4 (2017) 4–12.

93. S. N. Timasheff, Thermodynamic binding and site occupancy in the light of the Schellman exchange concept, Biophys Chem 101-102 (2002) 99–111.

94. R. J. Ellis, Macromolecular crowding: obvious but underappreciated., Trends Biochem. Sci. 26 (2001) 597–604.

95. J. A. Schellman, The thermodynamic stability of proteins., Annu Rev Biophys Biophys Chem 16 (1987) 115–137.

96. J. A. Schellman, A simple model for salvation in mixed solvents: Applications to the stabilization and destabilization of macromolecular structures, Biophys Chem 37 (1990) 121–140.

97. E. F. Casassa, H. Eisenberg, Thermodynamic Analysis of Multicomponent Solutions, Adv Protein Chem 19 (1964) 287–395.

98. G. Scatchard, Physical chemistry of protein solutions; derivation of the equations for the osmotic pressure, J Am Chem Soc 68 (1946) 2315–2319.

99. A. P. Minton, Influence of macromolecular crowding upon the stability and state of association of proteins: Predictions and observations, J Pharm Sci 94 (2005) 1668–1675.

100. T. Arakawa, S. N. Timasheff, Stabilization of protein structure by sugars, Biochemistry 21 (1982) 6536–6544.

101. T. Arakawa, S. N. Timasheff, The stabilization of proteins by osmolytes, Biophys. J. 47 (1985) 411–414.

102. S. H. M. Hedberg, S. Devi, A. Duralliu, D. R. Williams, Mechanical Behavior and Structure of Freeze-Dried Cakes, in: Lyophilization of Pharmaceuticals and Biologicals, Springer New York, New York, 2018, pp. 327–351.

103. B. S. Chang, M. Reilly, H. Chang, Lyophilized Biologics, in: D. Varshney, M. Singh (Eds.), Lyophilized Biologics and Vaccines, Springer, New York, 2015, pp. 93–120.

104. P. Matejtschuk, M. Stanley, P. Jefferson, Freeze-Drying of Biological Standards, in: L. Rey, J. C. May (Eds.), Freeze-Drying/Lyophilization of Pharmaceutical and Biological Products, CRC Press, Boca Raton, 2010, pp. 317–353.

105. J. T. Blue, J. R. Sinacola, A. Bhambhani, Process Scale-Up and Optimization of Lyophilized Vaccine Products, in: D. Varshney, M. Singh (Eds.), Lyophilized Biologics and Vaccines, Springer, New York, 2015, pp. 179–210.

106. S.-L. Sim, T. He, A. Tscheliessnig, M. Mueller, R. B. H. Tan, A. Jungbauer, Protein precipitation by polyethylene glycol: A generalized model based on hydrodynamic radius, Journal of Biotechnology 157 (2012) 315–319.

107. R. Bhat, S. N. Timasheff, Steric exclusion is the principal source of the preferential hydration of proteins in the presence of polyethylene glycols., Protein Sci. 1 (1992) 1133–1143.

108. V. Kumar, V. K. Sharma, D. S. Kalonia, Effect of polyols on polyethylene glycol (PEG)-induced precipitation of proteins: Impact on solubility, stability and conformation, Int J Pharm 366 (2009) 38–43.

109. D. H. Atha, K. C. Ingham, Mechanism of precipitation of proteins by polyethylene glycols. Analysis in terms of excluded volume., J. Biol. Chem. 256 (1981) 12108–12117.

110. J. C. Lee, L. L. Y. Lee, Interaction of calf brain tubulin with poly(ethylene glycols), Biochemistry 18 (2002) 5518–5526.

111. C. Ladd Effio, L. Wenger, O. Ötes, S. A. Oelmeier, R. Kneusel, J. Hubbuch, Downstream processing of virus-like particles: Single-stage and multi-stage aqueous two-phase extraction, J Chromatogr A 1383 (2015) 35–46.

112. L. V. Q. Fontes, G. S. Campos, P. A. Beck, C. F. L. Brandão, S. I. Sardi, Precipitation of bovine rotavirus by polyethylen glycol (PEG) and its application to produce polyclonal and monoclonal antibodies, J Virol Methods 123 (2005)

147–153.

113. C. Aizawa, S. Hasegawa, C. Chih-Yuan, I. Yoshioka, Large-scale purification of Japanese encephalitis virus from infected mouse brain for preparation of vaccine., Appl Environ Microbiol. 39 (1980) 54–57.

114. M. Trudel, P. Payment, Concentration and purification of rubella virus hemagglutinin by hollow fiber ultrafiltration and sucrose density centrifugation, Can. J. Microbiol. 26 (1980) 1334–1339.

115. A. Poison, Purification and Aggregation of Influenza Virus by Precipitation with Polyethylene Glycol, Preparative Biochemistry 4 (1974) 435–456.

116. A. J. Hagen, C. N. Oliver, R. D. Sitrin, Optimization of Poly(ethylene glycol) Precipitation of Hepatitis A Virus Used To Prepare VAQTA, a Highly Purified Inactivated Vaccine, Biotechnol. Prog. 12 (1996) 406–412.

117. J. Lee, H. T. Gan, S. M. A. Latiff, C. Chuah, W. Y. Lee, Y.-S. Yang, B. Loo, S. K. Ng, P. Gagnon, Principles and applications of steric exclusion chromatography, J Chromatogr A 1270 (2012) 162–170.

118. M. M. Pieler, A. Heyse, M. W. Wolff, U. Reichl, Specific ion effects on the particle size distributions of cell culture–derived influenza A virus particles within the Hofmeister series, Eng. Life Sci. 17 (2017) 470–478.

119. H. M. Oksanen, A. Domanska, D. H. Bamford, Monolithic ion exchange chromatographic methods for virus purification, Virology 434 (2012) 271–277.

120. A. Jungbauer, R. Hahn, Polymethacrylate monoliths for preparative and industrial separation of biomolecular assemblies, J Chromatogr A 1184 (2008) 62–79.

121. S. Wang, A. Lu, L. Zhang, Recent advances in regenerated cellulose materials, Progress in Polymer Science 53 (2016) 169–206.

122. P. Marichal-Gallardo, M. M. Pieler, M. W. Wolff, U. Reichl, Steric exclusion chromatography for purification of cell culture-derived influenza A virus using regenerated cellulose membranes and polyethylene glycol, J Chromatogr A 1483 (2017) 110–119.

123. P. Marichal-Gallardo, A. R. Fortuna, Y. Genzel, M. W. Wolff, U. Reichl, Purifying viruses with a sheet of paper: Single-use steric exclusion chromatography as a capture platform for vaccine candidates, in: A. Kamen, T. Mukhopadhyay, N. Garcon, C. Lutsch (Eds.), Vaccine Technology VII, ECI Symposium Series, 2018.

124. M. M. Pieler, A. Heyse, M. W. Wolff, U. Reichl, Specific ion effects on the particle size distributions of cell culture–derived influenza A virus particles within the Hofmeister series, Eng. Life Sci. 2 (2016) 191–206.

125. H. S. H. Seifert, Tropical Animal Health, 2 ed., Kluwer Academic Publishers, Dordrecht, 1996.

126. P. Steppert, D. Burgstaller, M. Klausberger, A. Tover, E. Berger, A. Jungbauer, Quantification and characterization of virus-like particles by size-exclusion

chromatography and nanoparticle tracking analysis, J Chromatogr A 1487 (2017) 89–99.

127. B. Kalbfuss, A. Knöchlein, T. Kröber, U. Reichl, Monitoring influenza virus content in vaccine production: Precise assays for the quantitation of hemagglutination and neuraminidase activity, Biologicals 36 (2008) 145–161.

128. J. M. Wood, G. C. Schild, R. W. Newman, V. Seagroatt, An improved single-radial-immunodiffusion technique for the assay of influenza haemagglutinin antigen: Application for potency determinations of inactivated whole virus and subunit vaccines, Journal of Biological Standardization 5 (1977) 237–247.

129. L. Opitz, S. Lehmann, U. Reichl, M. W. Wolff, Sulfated membrane adsorbers for economic pseudo-affinity capture of influenza virus particles, Biotechnol. Bioeng. 103 (2009) 1144–1154.

130. Y. Genzel, U. Reichl, Vaccine Production, in: R. Pörtner (Ed.), Animal Cell Biotechnology, Humana Press, Totowa, NJ, 2007, pp. 457–473.

131. H.-G. Bae, A. Nitsche, A. Teichmann, S. S. Biel, M. Niedrig, Detection of yellow fever virus: a comparison of quantitative real-time PCR and plaque assay, J Virol Methods 110 (2003) 185–191.

132. A. T. de Madrid, J. S. Porterfield, A simple micro-culture method for the study of group B arboviruses, Bulletin of the World Health Organization 40 (1969) 113–121.

133. A.-K. Herrmann, S. Grosse, K. Börner, C. Kramer, E. Wiedtke, M. Gunkel, D. Grimm, Impact of the Assembly-Activating Protein on Molecular Evolution of Synthetic Adeno-Associated Virus Capsids., Hum Gene Ther 30 (2019) 21–35.

134. D. A. Bejarano, K. Peng, V. Laketa, K. Börner, K. L. Jost, B. Lucic, B. Glass, M. Lusic, B. Müller, H.-G. Kräusslich, HIV-1 nuclear import in macrophages is regulated by CPSF6-capsid interactions at the nuclear pore complex, eLife Sciences 8 (2019) e41800.

135. K. Börner, D. Niopek, G. Cotugno, M. Kaldenbach, T. Pankert, J. Willemsen, X. Zhang, N. Schürmann, S. Mockenhaupt, A. Serva, M.-S. Hiet, E. Wiedtke, M. Castoldi, V. Starkuviene, H. Erfle, D. F. Gilbert, R. Bartenschlager, M. Boutros, M. Binder, K. Streetz, H.-G. Kräusslich, D. Grimm, Robust RNAi enhancement via human Argonaute-2 overexpression from plasmids, viral vectors and cell lines, Nucleic Acids Res. 41 (2013) e199–e199.

136. A. R. Fortuna, F. Taft, L. Villain, M. W. Wolff, U. Reichl, Optimization of cell culture-derived influenza A virus particles purification using sulfated cellulose membrane adsorbers, Eng. Life Sci. 18 (2017) 29–39.

137. D. Vázquez-Ramírez, I. Jordan, V. Sandig, Y. Genzel, U. Reichl, High titer MVA and influenza A virus production using a hybrid fed-batch/perfusion strategy with an ATF system, Appl Microbiol Biotechnol 103 (2019) 3025–3035.

138. D. Huang, W.-J. Peng, Q. Ye, X.-P. Liu, L. Zhao, L. Fan, K. Xia-Hou, H.-J. Jia, J. Luo, L.-T. Zhou, B.-B. Li, S.-L. Wang, W.-T. Xu, Z. Chen, W.-S. Tan, Serum-Free Suspension Culture of MDCK Cells for Production of Influenza H1N1

Vaccines, PLoS ONE 10 (2015) e0141686–11.

139. F. Tapia, I. Jordan, Y. Genzel, U. Reichl, Efficient and stable production of Modified Vaccinia Ankara virus in two-stage semi-continuous and in continuous stirred tank cultivation systems, PLoS ONE 12 (2017) e0182553–17.

140. T. Huber, S. Feast, S. Dimartino, W. Cen, C. Fee, Analysis of the Effect of Processing Conditions on Physical Properties of Thermally Set Cellulose Hydrogels, Materials 12 (2019) 1066–20.

141. M. W. Wolff, C. Siewert, S. Lehmann, S. Post Hansen, R. Djurup, R. Faber, U. Reichl, Capturing of cell culture-derived modified Vaccinia Ankara virus by ion exchange and pseudo-affinity membrane adsorbers, Biotechnol. Bioeng. 105 (2010) 761–769.

142. S. L. R. Ellison, V. J. Barwick, T. J. Duguid Farrant, Practical Statistics for the Analytical Scientist, 2 ed., Royal Society of Chemistry, Cambridge, 2009.

143. S.-P. Tao, J. Zheng, Y. Sun, Grafting zwitterionic polymer onto cryogel surface enhances protein retention in steric exclusion chromatography on cryogel monolith, J Chromatogr A 1389 (2015) 104–111.

144. L. Opitz, J. Hohlweg, U. Reichl, M. W. Wolff, Purification of cell culture-derived influenza virus A/Puerto Rico/8/34 by membrane-based immobilized metal affinity chromatography, J Virol Methods 161 (2009) 312–316.

145. T. Krober, M. W. Wolff, B. Hundt, A. Seidel-Morgenstern, U. Reichl, Continuous purification of influenza virus using simulated moving bed chromatography, J Chromatogr A 1307 (2013) 99–110.

146. T. Weigel, T. Solomaier, S. Wehmeyer, A. Peuker, M. W. Wolff, U. Reichl, A membrane-based purification process for cell culture-derived influenza A virus, Journal of Biotechnology 220 (2016) 12–20.

147. E. Cocucci, J. Meldolesi, Ectosomes and exosomes: shedding the confusion between extracellular vesicles, Trends in Cell Biology 25 (2015) 364–372.

148. J. Meldolesi, Ectosomes and Exosomes-Two Extracellular Vesicles That Differ Only in Some Details, Biochemistry & Molecular Biology Journal 2 (2016) 1–4.

149. B. J. Tauro, D. W. Greening, R. A. Mathias, H. Ji, S. Mathivanan, A. M. Scott, R. J. Simpson, Comparison of ultracentrifugation, density gradient separation, and immunoaffinity capture methods for isolating human colon cancer cell line LIM1863-derived exosomes, Methods 56 (2012) 293–304.

150. K. Junker, J. Heinzelmann, C. Beckham, T. Ochiya, G. Jenster, Extracellular Vesicles and Their Role in Urologic Malignancies, European Urology 70 (2016) 323–331.

151. V. A. Pospelov, S. B. Svetlikova, V. I. Vorob'ev, Nucleosome packing in chromatin as revealed by nuclease digestion, Nucleic Acids Res. 6 (1979) 399–418.

152. P. Gagnon, R. Nian, Y. Yang, Q. Yang, C. L. Lim, Non-immunospecific association of immunoglobulin G with chromatin during elution from protein A

inflates host contamination, aggregate content, and antibody loss, J Chromatogr A 1408 (2015) 151–160.

153. P. Gagnon, R. Nian, L. Tan, J. Cheong, V. Yeo, Y. Yang, H. T. Gan, Chromatin-mediated depression of fractionation performance on electronegative multimodal chromatography media, its prevention, and ramifications for purification of immunoglobulin G, J Chromatogr A 1374 (2014) 145–155.

154. P. Gagnon, R. Nian, J. Lee, L. Tan, S. M. A. Latiff, C. L. Lim, C. Chuah, X. Bi, Y. Yang, W. Zhang, H. T. Gan, Nonspecific interactions of chromatin with immunoglobulin G and protein A, and their impact on purification performance, J Chromatogr A 1340 (2014) 68–78.

155. H. T. Gan, J. Lee, S. M. A. Latiff, C. Chuah, P. Toh, W. Y. Lee, P. Gagnon, Characterization and removal of aggregates formed by nonspecific interaction of IgM monoclonal antibodies with chromatin catabolites during cell culture production, J Chromatogr A 1291 (2013) 33–40.

156. T. Weigel, T. Solomaier, A. Peuker, T. Pathapati, M. W. Wolff, U. Reichl, A flow-through chromatography process for influenza A and B virus purification, J Virol Methods 207 (2014) 45–53.

157. J. J. Wolf, L. Wang, F. Wang, Application of PCR technology in vaccine product development., Expert Review of Vaccines 6 (2007) 547–558.

158. L. Mallet, E. Sarcey, A. Sabouraud, New Analytical Methods for Host Cell Residual DNA testing, in: New Cells for New Vaccines II, Sanofi Pasteur, Wilmington, DE, 2007.

159. Y. Ikeda, S. Iwakiri, T. Yoshimori, Development and characterization of a novel host cell DNA assay using ultra-sensitive fluorescent nucleic acid stain "PicoGreen", Journal of Pharmaceutical and Biomedical Analysis 49 (2009) 997–1002.

160. V. L. Singer, L. J. Jones, S. T. Yue, R. P. Haugland, Characterization of PicoGreen Reagent and Development of a Fluorescence-Based Solution Assay for Double-Stranded DNA Quantitation, Anal. Biochem. 249 (1997) 228–238.

161. C. Tidona, G. Darai (Eds.), The Springer Index of Viruses, 2 ed., Springer, New York, 2011.

162. C. Wang, S. Bai, S.-P. Tao, Y. Sun, Evaluation of steric exclusion chromatography on cryogel column for the separation of serum proteins, J Chromatogr A 1333 (2014) 54–59.

163. Bissinger, Thomas, Reichl, Udo, Genzel, Yvonne, Wu, Yixiao, Liu, Xuping, Tan, Wen-Song, Highly efficient influenza virus production: A MDCK-based high-cell-density process, Vaccine Technology VII (2018).

164. J. Herrera-Rodriguez, A. Signorazzi, M. Holtrop, J. de Vries-Idema, A. Huckriede, Inactivated or damaged? Comparing the effect of inactivation methods on influenza virions to optimize vaccine production, Vaccine 37 (2019) 1630–1637.

165. P. Perrin, S. Morgeaux, Inactivation of DNA by beta-propiolactone., Biologicals 23 (1995) 207–211.

166. T. P. Pato Cunha, Desenvolvimento de um processo de purificação do vírus da febre amarela produzido em células Vero, Ph.D. thesis, Universidade Federal do Rio de Janeiro, 2015.

167. T. P. Monath, Stability of yellow fever vaccine., Dev Biol Stand 87 (1996) 219–225.

168. S. Zhai, R. K. Hansen, R. Taylor, J. N. Skepper, R. Sanches, N. K. H. Slater, Effect of Freezing Rates and Excipients on the Infectivity of a Live Viral Vaccine during Lyophilization, Biotechnol. Prog. 20 (2004) 1113–1120.

169. S. T. Mundle, M. Giel-Moloney, H. Kleanthous, K. V. Pugachev, S. F. Anderson, Preparation of pure, high titer, pseudoinfectious Flavivirus particles by hollow fiber tangential flow filtration and anion exchange chromatography, Vaccine 33 (2015) 4255–4260.

170. N. Vijayasankaran, J. Li, R. Shawley, A. Chen, M. Shiratori, M. Gawlitzek, F. Li, R. Kiss, A. Amanulah, Animal Cell Culture Media, in: M. C. Flickinger (Ed.), Encyclopedia of Industrial Biotechnology, John Wiley & Sons, Inc., Hoboken, 2010, pp. 261–274.

171. D.-S. Choi, Y. S. Gho, Isolation of Extracellular Vesicles for Proteomic Profiling, in: A. Posch (Ed.), Proteomic Profiling, Springer, New York, 2015.

172. T. M. Finn, W. Egan, Vaccine Additives and Manufacturing Residuals in Vaccines Licensed in the United States, in: S. A. Plotkin, W. A. Orenstein, P. A. Offit, K. M. Edwards (Eds.), Plotkin's Vaccines, Elsevier, Philadelphia, 2018, pp. 75–83.e2.

173. T. P. Pato, M. C. O. Souza, D. A. Mattos, E. Caride, D. F. Ferreira, L. P. Gaspar, M. S. Freire, L. R. Castilho, Purification of yellow fever virus produced in Vero cells for inactivated vaccine manufacture, Vaccine 37 (2019) 3214–3220.

174. A. Polson, A. Keen, C. Sinclair-Smith, I. G. Furminger, Polyethylene glycol purification of influenza virus with respect to aggregation and antigenicity., The Journal of Hygiene 70 (1972) 255–265.

175. B. A. Piras, J. E. Drury, C. L. Morton, Y. Spence, T. D. Lockey, A. C. Nathwani, A. M. Davidoff, M. M. Meagher, Distribution of AAV8 particles in cell lysates and culture media changes with time and is dependent on the recombinant vector, Mol Ther Methods Clin Dev 3 (2016) 16015.

176. W. Nakai, T. Yoshida, D. Diez, Y. Miyatake, T. Nishibu, N. Imawaka, K. Naruse, Y. Sadamura, R. Hanayama, A novel affinity-based method for the isolation of highly purified extracellular vesicles, Sci. Rep. 6 (2016) 33935–11.

177. H. G. Lamparski, A. Metha-Damani, J.-Y. Yao, S. Patel, D.-H. Hsu, C. Ruegg, J.-B. Le Pecq, Production and characterization of clinical grade exosomes derived from dendritic cells., J. Immunol. Methods 270 (2002) 211–226.

178. R. Stranska, L. Gysbrechts, J. Wouters, P. Vermeersch, K. Bloch, D. Dierickx, G. Andrei, R. Snoeck, Comparison of membrane affinity-based method with

size-exclusion chromatography for isolation of exosome-like vesicles from human plasma, Journal of Translational Medicine 16 (2018) 1–9.

179. B. R. Lentz, J. K. Lee, Poly(ethylene glycol) (PEG)-mediated fusion between pure lipid bilayers: a mechanism in common with viral fusion and secretory vesicle release?, Mol Membr Biol 16 (1999) 279–296.

180. K. O. Evans, B. R. Lentz, Kinetics of Lipid Rearrangements during Poly(ethylene glycol)-Mediated Fusion of Highly Curved Unilamellar Vesicles, Biochemistry 41 (2002) 1241–1249.

181. W. Lim, H.-S. Kim, Exosomes as Therapeutic Vehicles for Cancer, Tissue Engineering and Regenerative Medicine (2019) 1–11.

182. K. Pachler, T. Lener, D. Streif, Z. A. Dunai, A. Desgeorges, M. Feichtner, M. Öller, K. Schallmoser, E. Rohde, M. Gimona, A Good Manufacturing Practice–grade standard protocol for exclusively human mesenchymal stromal cell–derived extracellular vesicles, Cytotherapy 19 (2017) 458–472.

183. V. R. Minciacchi, M. R. Freeman, D. Di Vizio, Extracellular Vesicles in Cancer: Exosomes, Microvesicles and the Emerging Role of Large Oncosomes, Seminars in Cell and Developmental Biology 40 (2015) 41–51.

184. J. Costa, M. Gatermann, M. Nimtz, S. Kandzia, M. Glatzel, H. S. Conradt, N-Glycosylation of Extracellular Vesicles from HEK-293 and Glioma Cell Lines, Anal. Chem. 90 (2018) 7871–7879.

185. M. W. Wolff, U. Reichl, Downstream processing: From egg to cell culture-derived influenza virus particles, Chem Eng Technol 31 (2008) 846–857.

186. I. L. Shulgin, E. Ruckenstein, Preferential hydration and solubility of proteins in aqueous solutions of polyethylene glycol, Biophys Chem 120 (2006) 188–198.

187. H.-X. Zhou, G. Rivas, A. P. Minton, Macromolecular Crowding and Confinement: Biochemical, Biophysical, and Potential Physiological Consequences, Annu. Rev. Biophys. 37 (2008) 375–397.

188. E. Hindle, G. M. Findlay, The Electrical Charge of Yellow-Fever Virus, British journal of experimental pathology 11 (1930) 134–136.

189. A. Levanova, M. M. Poranen, Application of steric exclusion chromatography on monoliths for separation and purification of RNA molecules, J Chromatogr A 1574 (2018) 50–59.

190. J. T. Lis, R. Schleif, Size fractionation of double-stranded DNA by precipitation with polyethylene glycol, Nucleic Acids Res. 2 (1975) 383–390.

191. R. Ghosh, Principles of Bioseparations Engineering, World Scientific Publishing Co. Pte. Ltd., Toh Tuck Link, 2006.

192. S. Broeders, I. Huber, L. Grohmann, G. Berben, I. Taverniers, M. Mazzara, N. Roosens, D. Morisset, Guidelines for validation of qualitative real-time PCR methods, Trends in Food Science & Technology 37 (2014) 115–126.

193. T. Gu, Chromatography, radial flow, in: M. C. Flickinger (Ed.), Encyclopedia of Industrial Biotechnology, John Wiley & Sons, Inc., Hoboken, 2010, pp. 1630–1641.

194. C. Fee, 3D-printed porous bed structures, Current Opinion in Chemical Engineering 18 (2017) 10–15.

195. C. Fee, S. Nawada, S. Dimartino, 3D printed porous media columns with fine control of column packing morphology, J Chromatogr A 1333 (2014) 18–24.

196. G. Kaur, J. Grewal, K. Jyoti, U. K. Jain, R. Chandra, J. Madan, Oral controlled and sustained drug delivery systems: Concepts, advances, preclinical, and clinical status, in: A. M. Grumezescu (Ed.), Drug Targeting and Stimuli Sensitive Drug Delivery Systems, William Andrew Publishing, 2018, pp. 567–626.

197. M. T. Holtzapple, Cellulose, in: B. Caballero (Ed.), Encyclopedia of food sciences and nutrition, Academic Press, Oxford, 2003, pp. 998–1007.

198. T. Heinze, T. Liebert, 4.2 Chemical characteristics of cellulose acetate, Macromol. Symp. 208 (2004) 167–238.

199. T. Arakawa, The mechanism of increased elution volume of proteins by polyethylene glycol, Anal. Biochem. 144 (1985) 267–268.

200. Jungbauer, Alois, Chromatographic media for bioseparation, J Chromatogr A 1065 (2005) 3–12.

201. X. Lu, D. Zhao, G. Ma, Z. Su, Polyethylene glycol increases purification and recovery, alters retention behavior in flow-through chromatography of hemoglobin, J Chromatogr A 1059 (2004) 233–237.

202. P. Gagnon, Purification tools for monoclonal antibodies, Validated Biosystems, Tucson, AZ, 1995.

203. P. Gagnon, Improved antibody aggregate removal by hydroxyapatite chromatography in the presence of polyethylene glycol., J. Immunol. Methods 336 (2008) 222–228.

204. T. Arakawa, P. Gagnon, Excluded Cosolvent in Chromatography, J Pharm Sci 107 (2018) 2297–2305.

Supplementary Figures

The following process diagrams were made with the kind assistance from Masoud Babakhani at the Max-Planck-Institute Magdeburg.
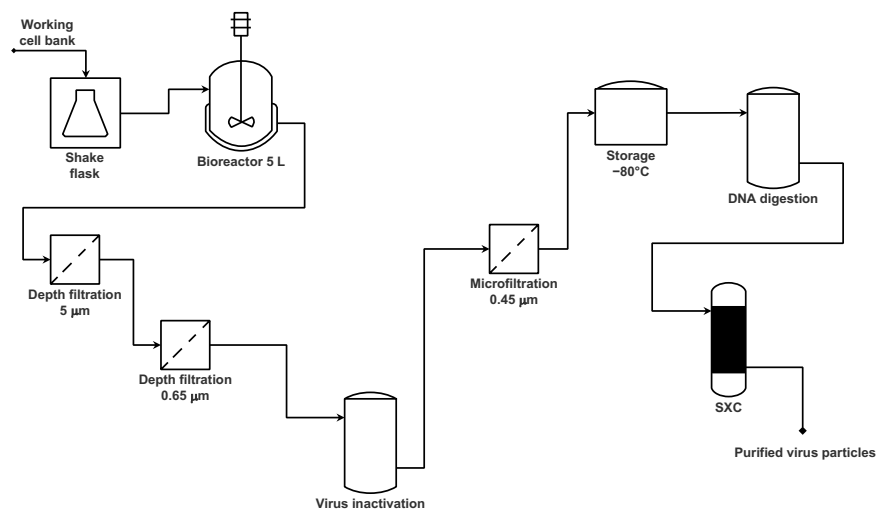

Figure A.1. Process diagram for the production of influenza virus A/Puerto Rico/8/34 H1N1 in a 5 L stirred tank reactor with MDCK$_{sus}$ cells in SMIF8 chemically-defined medium. The results from this process were published in Ref. [122].
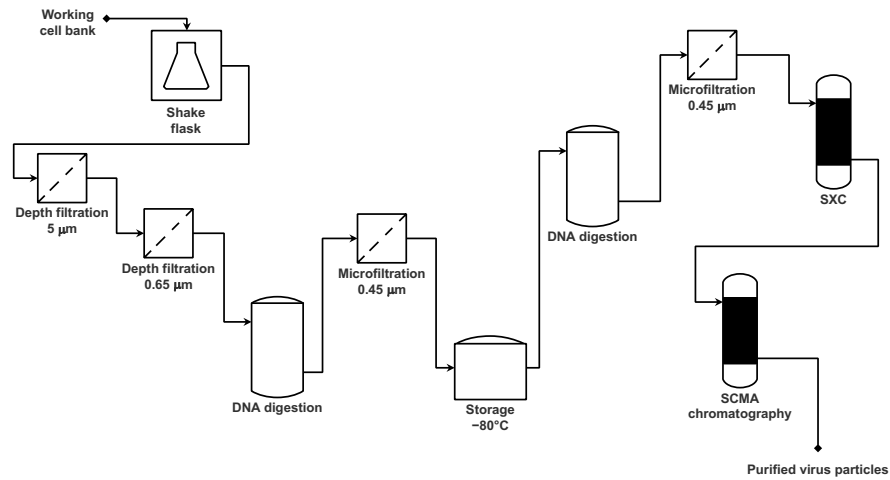
Figure A.2. Process diagram for the production of influenza virus strains A/Puerto Rico/8/34 H1N1, A/Switzerland/9715293/2013 H3N2, and B/Phuket/3073/2013 (Yamagata) in shaker flasks with MDCK$_{sus}$ cells in SMIF8 chemically-defined medium. This was the first iteration of the process.
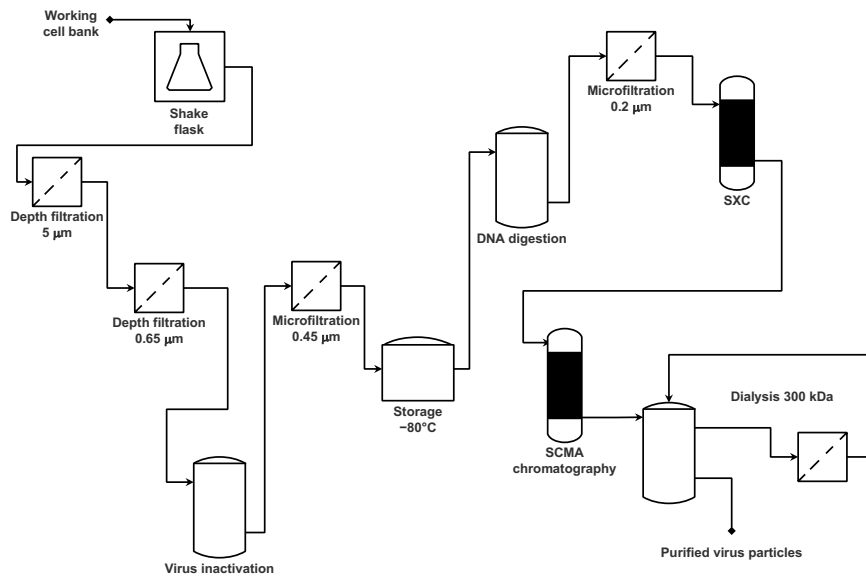

Figure A.3. Process diagram for the production of influenza virus strains A/Puerto Rico/8/34 H1N1, A/Switzerland/9715293/2013 H3N2, and B/Phuket/3073/2013 (Yamagata) in shaker flasks with MDCK$_{sus}$ cells in SMIF8 chemically-defined medium. This was the second iteration of the process (0.2 µm filtration step before SXC) from the first workflow in Figure A.2.
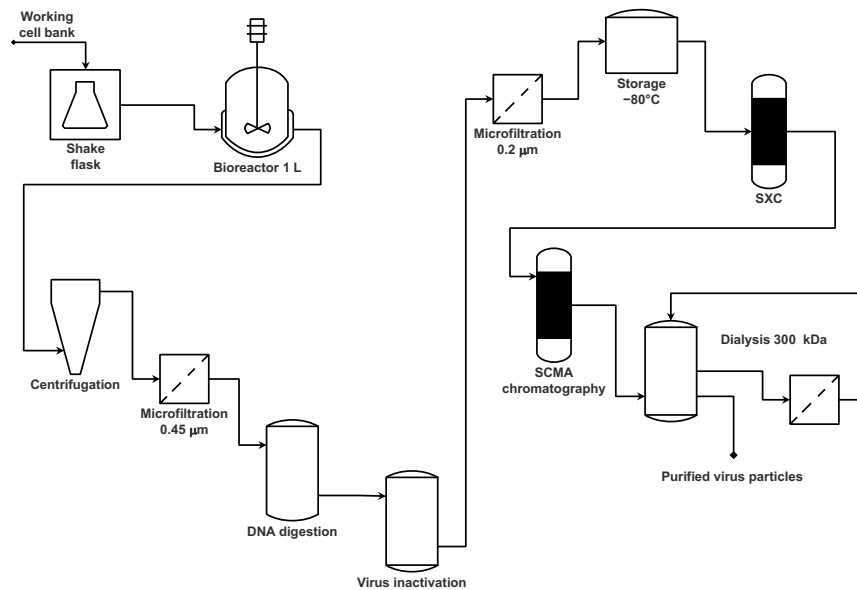
Figure A.4. Process diagram for the production of influenza virus A/Puerto Rico/8/34 H1N1 in a 1 L stirred tank reactor with MDCK$_{sus}$ cells in Xeno™ chemically-defined medium. The SCMA step was found to be not necessary but is pictured here as a polishing option.
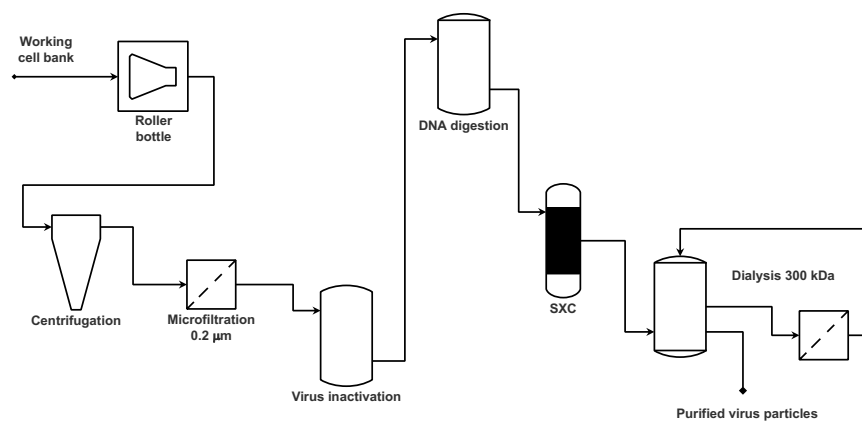

Figure A.5. Process diagram for the production of yellow fever virus (strain 17D) in either T-flasks or roller bottles (pictured here) with adherent Vero cells in OPTI-MEM serum-free medium.
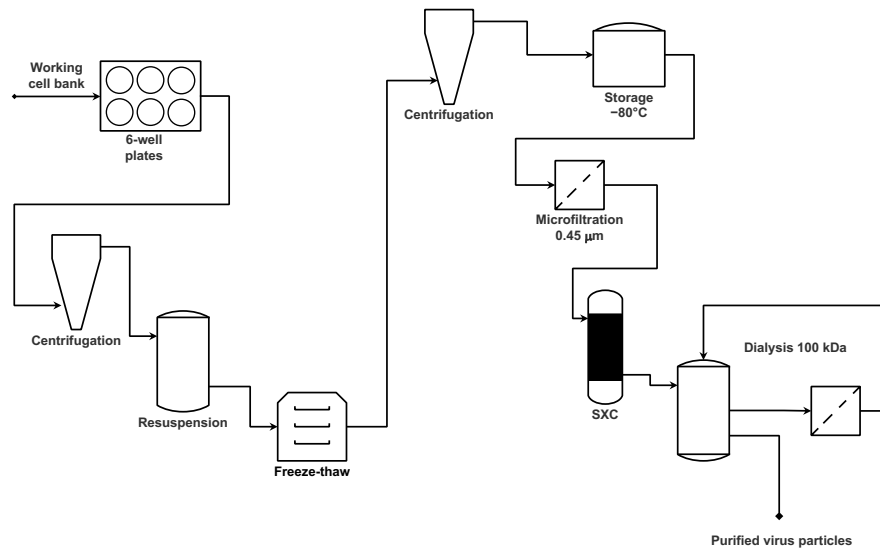
Figure A.6. Process diagram for the production of several adeno-associated virus serotypes and variants in 6-well plates with adherent HEK cells in Dulbecco's Modified Eagle Medium.